The radial wrist as a morphological and functional unit in extant African apes and humans

Olivia Laureijs

A thesis presented to Lakehead University

in partial fulfillment of the requirements of

Master of Science in Archaeological Science

Thunder Bay, Ontario, Canada, 2025

Table of contents

Acknowledgements

I am grateful to everyone who made this project possible by providing support and guidance over the past two years. A sincere thank you to Dr. Matt Tocheri for your invaluable mentorship and encouragement throughout my research journey. You have equipped me with so many skills essential for researching, academic writing, and critical thinking in general. This project would not have been possible without your help both in the classroom and the lab.

I would like to thank Dr. Ryan Knigge for helping me with three-dimensional geometric morphometrics and R coding, Dr. Tamara Varney for serving on my committee, as well as Jessica Zachariasz, Anneliese Eber, Sarah Friesen, and my other lab mates for your advice on everything from scholarship applications to data analysis. I would also like to thank Dr. Matt Tocheri, Dr. Scott Hamilton, Dr. Deborah Merrett, and Dr. Jessica Metcalfe for being exceptional educators and delivering courses that gave me the knowledge and skills to complete this project. Special thanks to Jennifer McKee and the rest of the Lakehead University's Anthropology Department for providing excellent student assistance and always promptly answering my many questions.

For access to the 3D surface models used in this project, I would like to thank Dr. Matt Tocheri and Dr. Caley Orr as well as the museum and zoo collections where these bones were originally acquired from. I also thank the Social Sciences and Humanities Research Council of Canada (CGS-M award to Olivia Laureijs) and the Lakehead University Ontario Graduate Scholarship committee for funding this research.

Finally, I would like to thank my family and friends for their unwavering support over the past two years. Their belief in me has been a constant source of motivation, and I am incredibly fortunate to have such a supportive network.

List of figures

List of tables

Abstract

Previous research has identified multiple aspects of carpal (i.e., wrist bones) morphology in *Homo sapiens* (humans) and some fossil hominin species that may reflect adaptations to the habitual use and manufacture of stone tools, particularly among bones from the radial side of the wrist (i.e., the, trapezium, trapezoid, scaphoid, and capitate). Using three-dimensional (3D) surface models of radial-side carpals and 3D geometric morphometrics (3DGM), this study aims to quantify the shape variation of this anatomical region among extant African apes and humans. Extending on previous studies that have typically quantified carpal morphology by studying each bone individually and in isolation from each other, this study marks the first time where these four radial-side carpals are quantitatively analyzed together as articulated units. Based on previous descriptions as well as qualitative and quantitative analyses, *Pan troglodytes* (chimpanzees), *Pan paniscus* (bonobos), and *Gorilla gorilla gorilla* (western lowland gorillas) wrists were predicted to display features that facilitate radioulnar stability and proximodistally-directed loading, which would be more efficient for locomotor behaviours. Conversely, human wrists were predicted to display features that facilitate proximodistal stability and radioulnarly-directed loading, which would be more efficient for manual dextrous behaviours. Results showed that the combined shapes of these carpal bones, as well as their sizes and orientations relative to each other, vary considerably between the African ape and human samples. The African ape wrists showed, as predicted, a complex of features that provides biomechanical advantages for withstanding and distributing forces directed proximodistally during knuckle walking and other locomotor behaviours. In contrast, the human wrists displayed a complex of features that appears to provide biomechanical advantages for withstanding and distributing large forces directed radioulnarly during human-like power and precision grips.

Introduction and Background

The wrist is pivotal in transferring loads between the hand and the forearm, as well as providing mobility and stability for locomotor and manipulative tasks involving the forelimb. As such, carpal (i.e., wrist bone) anatomy is often a compelling indicator of adaptations to locomotion and manual dexterity among primates (Lewis, 1989; Marzke et al., 1992; Napier, 1960). Marked variation in carpal morphology among extant African apes (chimpanzees, bonobos, and gorillas) and *Homo sapiens* (humans) has been documented qualitatively (Kivell and Begun, 2007; Lewis, 1969, 1973, 1977, 1989; Lewis et al., 1970; Marzke 1971; Marzke et al., 1992, 1998; Marzke and Marzke, 1987; Marzke and Shackley, 1986; Napier 1960; Sarmiento, 1988; Tuttle, 1967) and quantitatively (Almecija et al., 2015; Corrucini, 1978; Kivell et al., 2011, 2013, 2015; Kivell and Begun, 2009; Kivell and Schmitt, 2009; Marzke et al., 2010; Niewoehner et al., 1997; Orr et al., 2013; Tocheri, 2007; Tocheri et al., 2003, 2005, 2007; Wuthrich et al., 2019). The differences in wrist morphology between humans and their closest living relatives likely reflect the evolutionary shift during hominin evolution from using the hand principally for bearing the weight of the body during locomotor behaviours to regularly gripping and manipulating objects (e.g., tools). Thus, further detailed studies of carpal bones have the potential to provide critically important details about wrist function and the origins and persistence of stone tool manufacture in human evolution. In this study, I aim to quantify the shape variation of multiple carpal bones from the radial side of the wrist (i.e., the trapezium, trapezoid, scaphoid, and capitate) among extant African apes and humans (Figure 1). Previous studies have identified multiple features of this anatomical region that are distinct in humans and may reflect adaptations to the habitual use and manufacture of stone tools (Kivell et al., 2023; Tocheri et al., 2008). However, previous research has typically quantified these features by

studying each carpal bone individually and in isolation from each other. Using three-dimensional (3D) surface models of radial-side carpals and 3D geometric morphometrics (3DGM), I aim to provide the first study wherein these four radial-side carpals are quantitatively analyzed together as articulated units.

Wrist anatomy

The wrist is a complex anatomical region composed of the distal radius and ulna, the carpals, and the proximal bases of the metacarpals (Figure 2). African apes and humans have eight carpals arranged into two rows (Berger, 1996; Eschweiler et al., 2022; Kijima and Viegas, 2009; Lewis, 1989; Lewis et al., 1977; MacConaill, 1941; Napier, 1960, 1962; Sarmiento, 1988). The proximal carpal row includes the scaphoid, lunate, triquetrum, and pisiform, and articulates variably with the distal radius and ulna (i.e., the antebrachiocarpal joint). The distal carpal row includes the trapezium, trapezoid, capitate, and hamate, and articulates proximally with the proximal carpal row (i.e., the midcarpal joints) and distally with the proximal bases of the five metacarpals (i.e., the carpometacarpal joints).

The antebrachiocarpal joint. African apes and humans have a derived antebrachiocarpal joint (Kivell, 2016; Lewis, 1989; Sarmiento 1988). Firstly, the head of the ulna articulates with the sigmoid notch region of the distal radius (i.e., the distal radioulnar joint) in a synovial joint, which facilitates greater wrist mobility by allowing the hand and radius to rotate around the ulna; this ability to pronate and supinate the forearm is important during vertical climbing and suspensory behaviours as well as various manipulative behaviours (Lewis, 1989; Orr et al., 2024). Secondly, the ulnar styloid process is reduced such that it has variable contact with the proximal carpal row. In *Pan*, a semilunar meniscus separates the ulna from the pisiform while partial stylotriquetral contact is retained (Lewis, 1989; Sarmiento, 1988). In *Homo* and

Gorilla, the stylotriquetral contact is absent and a triangular fibrocartilage complex completely separates the ulna from the pisiform and triquetrum. The triangular fibrocartilage is a load-bearing surface that transmits weight from the ulnar head to the triquetrum (Lewis, 1989; Sarmiento, 1985, 1988). Contrary to previous assumptions, the reduced ulnar styloid process does not facilitate ulnar deviation of the wrist but instead may reduce stress on the ulnar side of the wrist or represent a byproduct of morphology that increased the ability to pronate and supinate the forearm (Orr et al., 2024).

The midcarpal joints. The midcarpal joints in African apes and humans contribute to moving the hand in relation to the forearm long bones, distribute forces directed across the wrist, and provide stability in the extended wrist postures assumed during various locomotor and manipulative behaviours (Corruccini, 1978; Kivell and Schmitt, 2009; Richmond et al., 2001; Tuttle, 1967). African apes have a larger trapezoid-scaphoid joint, which would experience large shear stresses during knuckle walking (Tocheri, 2007). In contrast, humans have a larger trapezium-scaphoid joint, which extends further onto the scaphoid tubercle and likely facilitates forces directed along the first metacarpal (MC1) and radial lip of the second metacarpal (MC2) base to the trapezium, then to the scaphoid and finally to the capitate (Marzke et al., 1992; Tocheri, 2007). In the African ape-human clade, the centrale is fused to the scaphoid whereas in other primates it is a separate bone that is interposed between the trapezium, trapezoid, scaphoid, and capitate (Kivell and Begun, 2007; Lewis, 1989). Fusion of the centrale to the scaphoid likely decreases mobility of the midcarpal joint in extension as well as the shear stress and ligament strain experienced when the wrist undergoes compression during knuckle walking (Orr, 2018). In humans, the scaphoid-capitate joint is more open distally due to reduction of bone along the distal border (Tocheri, 2007). This morphology combined with a larger palmarly-placed

trapezoid-capitate joint creates a larger articular surface for the capitate that may reduce compressive and shear stresses when the thumb is flexed during various precision-pinch type grips (Tocheri, 2007).

The antebrachiocarpal and midcarpal joints have a suite of additional features that may limit wrist extension but are variably present in African apes and humans. For example, the distal radius has a dorsal ridge, which has been suggested to limit extension at the radiocarpal joint (Kivell and Schmitt, 2009; Orr, 2005; Richmond et al., 2001; Tuttle, 1967), but a more recent study found that radioscaphoid range of motion is not related to this feature among primates (Orr, 2017). *Pan* also has pronounced dorsal ridges on the capitate and hamate and together these may limit extension of the proximal carpal row on the distal carpal row (Kivell and Schmitt, 2009), while a well-developed hamate distal concavity may limit extension specifically at the triquetrohamate joint (Kivell and Schmitt, 2009). Compared to humans, the capitate neck is radioulnarly narrow (i.e., is waisted) in African apes, creating a distal concavity (Kivell and Schmitt, 2009; Lewis, 1973, 1989; Richmond et al., 2001). Furthermore, the scaphoid facet on the capitate has expanded distally onto the concave portion of the capitate neck such that the joint is concavoconvex. When the wrist is extended, the centrale portion of the scaphoid fits into the waisted neck of the capitate to limit intercarpal movement and stabilize the capitate-scaphoid joint (Lewis, 1973, 1989; McHenry, 1983; Richmond, 2006; Richmond et al., 2001; Tuttle, 1967). These features are clearest in *Pan* but may be absent or not as strongly developed in *Gorilla* (Kivell and Schmitt, 2009). Accordingly, *Gorilla* displays higher ranges of motion in wrist extension compared to those of *Pan*, although the exact amount of mobility that occurs at each of the joints is not yet known (Orr, 2017; Tuttle, 1967). Kivell and Schmitt (2009) proposed that gorillas may compensate for this apparent lack of extension-limiting features via adopting a

more columnar wrist posture during knuckle walking (i.e., where the forearm, carpal joints, and hand are aligned). Meanwhile, the extension-limiting features in *Pan* may reflect extended wrist postures used on arboreal substrates (Kivell and Schmitt, 2009). However, more recent kinematic studies show that *Pan* and gorillas have similar wrist angles during quadrupedal locomotion (Finestone et al., 2018). Additionally, contrary to previous assumptions, the wrist in *Pan* is only slightly extended during knuckle walking leaving little room for gorillas to be less extended (or more columnar) (Thompson, 2020).

The intercarpal joints. The intercarpal articulations of the distal carpal row have features that may reduce compressive and shear stress from radioulnarly directed forces transmitted from the MC1 to the trapezium, trapezoid, and capitate during strong precision-pinch type grips (Lewis, 1989; Marzke et al., 1992; Tocheri, 2007; Tocheri et al., 2003, 2005). The African ape trapezoid is wedge-shaped with a broad dorsal aspect and tapered palmar aspect. The trapezium is shifted palmarly in front of the trapezoid such that the trapezium, trapezoid, and capitate form a curved carpal arch (Lewis, 1989; Tocheri, 2007). This morphology disposes the thumb to oppose the fingers when the fingers and thumb are flexed, which is important given the reduced mobility of the African ape first carpometacarpal joint (Tocheri, 2007). Conversely, the human trapezoid is 'boot-shaped' with a palmar nonarticular area that is broad and rectangular in shape (Lewis, 1989; Tocheri, 2007). African apes have a smaller, more dorsally placed capitate-trapezoid joint or often no capitate-trapezoid joint at all in the case of gorillas (Lewis, 1989; Tocheri, 2007). In contrast, the radioulnar breadth of the palmar portion of the human trapezoid shifts the trapezium into a more supinated position such that the trapezium is more aligned with the rest of the distal carpal row. The palmarly larger breadth and height of the trapezoid in humans is accompanied by a larger and more palmarly placed trapezoid-capitate

joint that is oriented more parallel to a relatively large trapezium-trapezoid joint (Lewis, 1989; Marzke et al., 1992; Tocheri, 2007).

The carpometacarpal joints. The distal carpal row in African apes and humans articulates distally with the bases of the five metacarpals at the carpometacarpal joints. The first carpometacarpal joint includes the MC1 and the trapezium and is saddle-shaped, which allows flexion-extension to occur in a dorsopalmar direction and abduction-adduction in a radioulnar direction (Napier, 1962; Tocheri, 2007). Although the first carpometacarpal joint has been demonstrated to be a two-axis joint in humans, these axes are not perpendicular to one another and do not cross so pronation-supination (i.e., conjunct rotation) occurs from simultaneous flexion and abduction (Cooney et al., 1994; Hollister et al., 1992; Hollister and Giurintano, 1995). Rotation of the MC1 is important for opposition of the thumb and is achieved through the coordination of various muscles that move the thumb at the first carpometacarpal joint (Cooney et al., 1994). In humans, the abductor pollicis brevis and the opponens pollicis act to flex and abduct the MC1 while the flexor pollicis brevis contributes primarily to flexion (Cooney et al., 1994). The first carpometacarpal joint in African apes is more curved and has a smaller surface area that likely reduces mobility but increases stability in terms of joint dislocation (Tocheri, 2007). In humans, this joint is relatively flatter and has a larger surface area that is oriented more parallel with the trapezium-scaphoid joint surface, all of which likely contributes to increased mobility as well as reduced compressive and shear stresses during strong contraction of the thumb musculature (Marzke et al., 2010; Tocheri, 2007; Tocheri et al., 2003).

The MC2 articulates proximally with the trapezoid, radially with the trapezium, and ulnarly with the capitate. In African apes, the palmar aspect of the trapezoid is proximodistally tapered and the trapezium-MC2 and capitate-MC2 joints are radioulnarly oriented such that the

MC2 base is positioned between the trapezium and capitate. The base of the MC2 is thus prevented from sliding radioulnarly such that maximum contact is maintained between the mutual articular facets of the second carpometacarpal joint, likely facilitating the distribution of proximodistally directed forces experienced during knuckle walking (Marzke, 1983; Marzke et al., 1992; Tocheri, 2007). The trapezoid-MC2 is larger and more parallel to the radiocarpal joint in African apes, which may also reduce proximodistally directed compressive and shear stresses (Tocheri, 2007). In humans, the MC2 base is not buttressed against the radial side of the capitate because of the proximodistally tall palmar aspect of the trapezoid (Tocheri, 2007). Together with more proximodistal orientations of the trapezium-MC2 and capitate-MC2 joints, this morphology prevents the capitate and trapezium from sliding distally relative to the MC2 base. This ensures that maximum contact is maintained between the mutual articular facets of the trapezium-trapezoid and capitate-trapezoid joints, potentially facilitating radioulnarly directed forces as well as enabling the MC2 base to pronate slightly during various grips (e.g., pad-to-side and three-jaw chuck precision grips) (Marzke, 1983; Marzke et al., 1992; Tocheri, 2007). Additionally, the more proximodistally orientated MC2 facets and larger capitate-MC2 joint in humans enable axial loads experienced during grips to be distributed to the capitate and trapezium as well as the trapezoid (Marzke, 1983, 1997; Marzke et al., 1992).

The third metacarpal (MC3) articulates with the capitate proximally. The MC3 in humans has a styloid process on its dorsoradial corner and is accommodated by the beveled corner on the distal surface of the capitate (Marzke and Marzke, 1987). The styloid process may prevent hyperextension of the MC3 and subluxation of its base when the palmar aspect of the head experiences forces during hammering and digging (Marzke and Marzke, 1987; McHenry, 1983). In African apes, the group of mesenchymal cells that compose the styloid process in humans

instead fuse with the capitate during embryonic development (Marzke and Marzke, 1987). The capitate-MC3 joint in African apes is thus more irregular which may facilitate "close-packing" for wrist stability during knuckle walking (McHenry, 1983). Indeed, the capitate-MC3 joint may have reduced mobility compared to that of other apes and monkeys (Orr, 2017).

The fourth (MC4) and fifth metacarpals (MC5) articulate together with the hamate. Humans have a saddle-shaped hamate-MC5 joint which allows for flexion-extension and pronation-supination of the metacarpal, facilitating cupping of the palm (Marzke, 1983; Marzke et al., 1992; Orr et al., 2013; Ward et al., 1999). The hamate-MC4 joint in humans also allows for some flexion whereas little flexion is possible in African apes (El-Shennawy et al., 2001; Marzke, 1983, Marzke et al., 1992). The hamulus in gorillas and humans primarily projects palmarly and increases the moments of the opponens digiti minimi and flexor digiti minimi muscles, facilitating grips involving the ulnar side of the hand (Ward et al., 1999). In contrast, the hamulus in *Pan* is more distally projecting and restricts flexion at the hamate-MC5 joint (Kivell, 2016; Ward et al., 1999). In African apes, the MC4 facet is larger than the MC5 facet on the hamate. This may accommodate axial stresses on the MC4 during locomotion (Marzke et al., 1992). In humans, the opposite pattern is typically seen where the MC5 facet is larger compared to the MC4 facet, which has been suggested to facilitate axial stress on the MC5 during "squeeze" power grips (Marzke et al., 1992), although more likely reflects reduction of the MC4 facet which increases rotation of the MC5 during flexion (Orr et al., 2013). Similar to the capitate-MC3 joint, the hamate-MC4 and MC5 joints in African apes have interlocking irregularities that limit movement between mutual joint surfaces (Marzke, 1983).

Wrist kinematics

Understanding wrist kinematics is important for forming functional interpretations of carpal morphology. Wrist movement has been defined in terms of three orthogonal axes: the flexion-extension axis (oriented radioulnarly), the radial-ulnar deviation axis (oriented dorsopalmarly), and the pronation-supination axis (oriented proximodistally) (Kobayashi et al., 1997; Palmar et al., 1985; Yalden, 1972). Flexion-extension occurs at the radiocarpal and midcarpal joints (Kaufmann et al., 2006; Orr, 2017, 2018; Sarrafian et al., 1977). The proximal row intercarpal and carpometacarpal joints may also contribute to flexion-extension in anthropoid primates (Orr, 2018). Radial-ulnar deviation occurs mostly at the midcarpal joint, and less so at the radiocarpal joint (Kaufmann et al., 2005; Orr et al., 2024). Pronation-supination occurs due to movement of the radius around the ulna (Yalden, 1972). Many occupational, daily, and sporting tasks require movements along the flexion-extension and radioulnar axes simultaneously in oblique planes of motion. Wrist movement from an extended/radially-deviated position to a flexed/ulnarly-deviated position is termed the "dart thrower's motion" (Crisco et al., 2005; Moojen et al., 2003; Palmer et al., 1985; Rohde et al., 2010). The presence of the dart thrower's motion in activities involving tool use, throwing, and clubbing suggest it may have been evolutionarily advantageous (Young, 2003; Williams et al., 2014; Wolfe et al., 2006). Recent studies on the internal bone structure of various carpals suggest that humans and Neandertals regularly loaded the midcarpal joint along the oblique path of the dart thrower's motion, whereas extant great apes and other fossil hominins loaded their wrist in different ways (Bird et al., 2021, 2022, 2024).

At a finer level, wrist movement occurs due to a combination of rotations and translations of individual carpal bones (Moojen et al., 2002). Various carpal kinematic models have been

developed to explain carpal kinematics and theorize the degree and direction of motion of each carpal bone during different wrist motions. The screw-clamp model was first proposed by MacConaill (1941) and separates the wrist into three functional units: the scaphoid, the lunate and triquetrum, and the hamate, capitate, and trapezoid. During extension, the centrale portion of the scaphoid engages with the capitate waist, and the capitate and scaphoid move together upon the lunate (Kaufmann et al., 2006; MacConaill, 1941; Orr, 2017). An extension moment from muscle contraction or ground reaction forces acts on the distal carpal row, creating torque that is transferred first to the scaphoid (Orr, 2017). The scaphoid acts as the link to the distal carpal row and transfers the torque to the rest of the proximal carpal row (Orr, 2017). The scaphoid rotates the most and the lunate the least along the flexion-extension axis so the proximal carpal row joints (i.e., the scapholunate and lunotriquetral joints) have higher ranges of motion (Kaufmann et al., 2006; Kobayashi et al., 1997; Moojen et al., 2002; Orr, 2017). The hamate rotates with the capitate, and the proximal surface formed by these bones creates a male screw surface (MacConaill, 1941). The female screw surface created by the triquetrum and lunate locks into the male screw surface, and the triquetrum pins the lunate against the scaphoid (MacConaill, 1941). The overall result is that the carpal rows are screwed together in a close-packed, maximally congruent position during extension.

Wrist movement is controlled by the shape of the carpals in conjunction with ligaments and muscles. Extrinsic ligaments connect the distal forearm to the carpals while intrinsic ligaments connect the carpals to each other, and together these function to guide and restrain carpal movement (Berger, 2001; Eschweiler et al., 2022; Kijima and Viegas, 2009; Mayfield et al., 1976). Carpals in the distal row are bound tightly to each other by strong intrinsic ligaments, such that it moves as a single unit (Kijima and Viegas, 2009; Moojen et al., 2002). In contrast,

the proximal carpal row allows for significant movement between adjacent bones and acts as an intercalated segment between the radius and the distal carpal row (Berger, 1996; Landsmeer, 1961; Ruby et al., 1988). Wrist movement is initiated by muscles in the forearm that insert into the distal carpal row or the metacarpal bases (Eschweiler et al., 2022; Kijima and Viegas, 2009). Motion initiated at the distal carpal row causes extrinsic ligaments crossing the midcarpal joint to become taut and applies force to the proximal carpal row (Eschweiler et al., 2022).

Hand use and function

Extant African apes and humans use their hands for manipulating objects with both prehensile and nonprehensile methods. Nonprehensile hand use involves using the hand or digits to push or lift an object without grasping whereas prehensile hand use involves grasping an object between two or more digits or between one or more digits and the palm (Kivell et al., 2023; Napier, 1956). Manual grasping is used for both manipulation (e.g., feeding, grooming, tool use) and, in the case of African apes, arboreal locomotion. Napier (1956) classified grips into two forms: power and precision. During a power grip, the object is held by the thumb, flexed fingers, and palm for strength. During a precision grip, the object is held between the thumb and fingers away from the palm for fine control. However, later studies on manual grasping during locomotor and manipulative behaviours in chimpanzees and humans observed that many grips had elements of both power and precision grips (Marzke and Shackley, 1986; Marzke and Wullstein, 1996). An extended classification of grips was developed based on the involvement and relative position of the thumb, fingers, and palm (Marzke and Shackley, 1986; Marzke and Wullstein, 1996). The type of grip used depends on the shape and size of the object, as well as the intended usage. Humans also perform precision handling, which translates or rotates the

object through movements at the carpometacarpal, metacarpophalangeal, and interphalangeal joints of the thumb and fingers involved in the grip (Landsmeer, 1962; Marzke, 1997).

Various studies have aimed to elucidate how grips relate to the effective and economical manipulation of tools in African apes and humans (Kivell et al., 2023; Marzke et al., 1992; Marzke and Marzke, 1987; Marzke and Shackley, 1986; Marzke and Wullstein, 1996; Schick et al., 1999; Toth et al., 1993; Williams et al., 2012, 2014; Williams-Hatala et al., 2018, 2021). The replication and use of Oldowan tools appear to involve three main grips: the pad-to-side grip between the thumb and index finger, the 3-jaw chuck ("baseball") grip, and the cradle pinch grip with the thumb and four finger pads (Marzke et al., 1998; Marzke and Shackley, 1986). Studies of modern pastoralists during butchering with stone tools have shown common grips include pad-to-side grips between the thumb pad and radial side of the third digit with the pad of the second digit on top of the tool (i.e., three-jaw chuck pad-to-side) and grips between the pad of the thumb and the sides of the third to fifth digits and the palm, with the second digit extended along the top of the tool (i.e., buttressed five-jaw chuck with active palm) (Key et al., 2018). The strong precision grips used in these studies facilitate the control of preforms, hammerstones, and hand-held tools, as well as maximize the exposed surface area of the object that can be struck with a hammerstone or used for cutting, hammering, or digging (Marzke, 1997; Marzke and Shackley, 1986). Although stone tools can be made and used with power grips, it likely causes muscle fatigue and repetitive stress in hand joints, as well as increases the risk for hand injuries due to the increased surface area of the tool in contact with the hand (Marzke, 1997).

A captive bonobo ("Kanzi") was able to produce sharp-edged cutting tools using various methods, although finished products indicated a lower degree of skill compared to tools from Early stone age assemblages (Schick et al., 1999; Toth et al., 1993). Although force and precision

during hand-held percussion with a hammerstone improved with experience, the amount of force Kanzi produced was low. Rather, Kanzi frequently removed flakes by throwing the cobble against another on the ground or a hard surface, which produced greater force than he could through hard-hammer percussion methods. It was suggested that biomechanical constraints in bonobos presented difficulties in controlling a forceful, well aimed blow with the hammerstone as well as avoiding hitting the fingers holding the stone core (Schick et al., 1999; Toth and Schick, 2009).

There are various differences between extant African ape and human manipulative behaviour that may facilitate the economical and effective manipulation of tools in the latter. Precision grips in African apes are relatively weak when experiencing forces attempting to dislodge the object (e.g., from the mouth during feeding), and may require support from another hand or foot to maintain hold of the object (Marzke and Wullstein, 1996). African apes struggle to perform certain human grips that involve pad-to-pad opposability with the thumb and fingers (e.g., the two-jaw chuck pad-to-pad grip) because the thumb is markedly shorter relative to the fingers (Marzke et al., 2015; Marzke and Wullstein, 1996; Napier, 1960). Rather, these apes perform precision grips using a combination of other surfaces on the fingers and thumb (e.g., tip, dorsal aspect, side), and these grips are generally much weaker than those of humans (Marzke and Wullstein, 1996; Napier, 1960). Finally, African ape grips are static so object orientation must be changed by movements at the wrist, elbow, and shoulder or by putting the object down or picking it up with another body part then gripping it again in the desired orientation (Marzke, 1997; Marzke et al., 2015; Marzke and Wullstein, 1996).

In terms of power grips, chimpanzees grasp cylindrical objects using a variety of diagonal grips, which do not employ the thumb for stabilization or control except in the case where only

the thumb, index finger, are third finger (but not the fourth or fifth fingers) are used in opposition with the thenar region of the palm, making these grips weaker (Marzke et al., 1992; Marzke and Wullstein, 1996). In contrast, humans have a unique "squeeze" grip where cylindrical objects are secured diagonally across the palm between the thumb and thenar region on one side and the palmar surfaces of all four flexed fingers on the other (Marzke et al., 1992). This grip better secures these kinds of objects when using them forcefully as an extension of the arm (e.g., hammering) and the thumb helps to control the direction of the applied force.

During manual grasping, contraction of thenar musculature compresses the base of the MC1 into the trapezium and generates large compression forces at the first carpometacarpal joint, which are then thought to be transmitted radioulnarly through the wrist (Bettinger et al., 1999, 2000; Cooney and Chao, 1977; Garcia-Elias, 1997; Lewis, 1989; Momose et al., 1999; Tocheri, 2007). Relatively high loads are consistently exerted on the thumb during making and using tools (Rolian et al., 2011; Williams-Hatala et al., 2018). Consistent with this, in an experimental study the flexor pollicis longus muscle was recruited during all grips used for tool making and use, and was especially high during activities that exerted force on the thumbs' volar pad such as hammering, cutting, and knapping (Hamrick et al., 1998). In contrast, the flexor pollicis longus activity was lower during activities that mimicked those often used by great apes, namely the manipulation of food items as well as making and using wooden probes (Hamrick et al., 1998). However, another study found that the flexor pollicis longus was not strongly recruited during tool making, although it was during tool-using activities (Marzke et al., 1998). Axial loads may also be experienced in the nonpollical digits. For instance, Williams et al. (2012) found that loads experienced by the second and third digits on the hammer stone hand during Oldowan stone tool making were significantly higher than those experienced by the

thumb. The distribution of pressure in the wrist differs according to behaviour, although hammerstone use during flake production and bone marrow acquisition appears to place the greatest loads on the digits overall (Williams-Hatala, 2018). In addition to compressive forces, the carpometacarpal and intercarpal joints will experience forces from the structures that limit joint movement (e.g., tensile forces from ligaments), shear forces, and bending forces (e.g., the cantilever bending forces on the trapezium) (Bettinger et al., 1999, 2000; Matarazzo, 2013; Sarmiento, 1988; Schuind, 1995).

Various morphological features of the hand have been proposed to facilitate effective precision and power grips during the making and use of stone tools in humans (Marzke et al., 1992; Marzke and Shackley, 1986). These features function to accommodate the thumb, fingers, and/or palm to the object, facilitate forceful ulnar deviation of the wrist during hammering, and/or to distribute the large forces generated by contact between the tool and its target as well as large internal forces from hand muscle contractions (Marzke et al., 1992).

African apes habitually use their wrist to bear body weight during various locomotor behaviours, including knuckle walking and climbing. Locomotor behaviours also depend on the age of the individual. For instance, juvenile African apes more frequently use suspension, climbing/scrambling, and palmigrade quadrupedalism compared to their adult counterparts (Doran, 1992, 1993, 1997). All African apes are predominantly knuckle-walking terrestrial quadrupeds but each species varies in the amount of climbing behaviours they engage in. Mountain gorillas (*G. b. beringei*) tend to climb the least often because they live in high-altitude montane forests with a paucity of fruits available (Doran and McNeilage, 1998; Groves, 1971; Schaller, 1963; Watts, 1984). Western lowland gorillas (*G. g. gorilla*) live in lower altitude rainforests and are more frugivorous, harvesting the majority of plants arboreally, similar to

sympatric chimpanzees (Doran and McNeilage, 1998; Goldsmith, 1996; Remis, 1994, 1997; Tutin and Fernandez, 1993). Generally speaking, chimpanzees and bonobos are more arboreal than gorillas and this likely relates to their dietary focus as ripe-fruit specialists (Doran, 1993, 1997; Doran and Hunt, 1994; Hunt, 1992, 1994; Sarringhaus et al., 2014; Susman, 1984; Susman et al., 1980). Initial studies at Lomako suggested that bonobos were more arboreal than *P. t. verus* (western chimpanzees) at Tai National Forest, and exhibited more frequent suspensory behaviours as well as arboreal locomotor behaviour that closely resembled that of 2–5-year-old chimpanzees (Doran, 1992, 1993, 1996; Doran and Hunt, 1994). However, these findings may have been the result of a lack of habituation to human observers. More recent studies at Lui Kotale have shown that habituated bonobos spend 56% of the time terrestrially and 44% arboreally (Ramos, 2014), which is comparable to that of adult *P. t. schweinfurthii* (eastern chimpanzees) at Mahale Mountains and Gombe Stream National Parks and western chimpanzees (Doran, 1996; Doran and Hunt 1994). Furthermore, bonobos were observed to engage in less suspensory behaviours than reported for western and eastern chimpanzees (Doran, 1996; Hunt, 1991, 1992; Ramos, 2014). The frequencies of some arboreal locomotor behaviours in bonobos were similar to that reported in infant and juvenile chimpanzees, consistent with initial observations (Doran, 1992; Ramos, 2014). For example, the frequency of climbing and scrambling relative to all arboreal locomotor behaviours for Lui Kotale bonobos was similar to that of western chimpanzee infants aged 0–6 months (Ramos, 2014).

Different locomotor behaviours are associated with a range of hand postures and loading. During knuckle walking, the interphalangeal joints are flexed such that the dorsum of the middle phalanges contacts the substrate (Sarmiento, 1988; Tuttle, 1969). The palm and proximal phalanges do not contact the substrate and the metacarpophalangeal joints are in a neutral

position or extended position. The wrist can be fully pronated (i.e., palm facing posteriorly or "palm-back") or semipronated (i.e., palm facing medially or "palm-in") hand postures (Inouye, 1994; Matarazzo, 2013; Thompson, 2020; Tuttle, 1967, 1969). Ground reaction forces will be transmitted from the middle phalanges to the proximal phalanges, metacarpals, carpals, then into the forearm (Matarazzo, 2013; Sarmiento, 1988; Wunderlich and Jungers, 2009). Indeed, studies on trabecular bone suggest that the metacarpal heads experience compressive joint reaction forces at the metacarpophalangeal joints (Tsegai et al., 2013; Zeininger et al., 2011). Thus, the wrist experiences proximodistally directed compression forces as well as shear forces and those that limit joint movement (Matarazzo, 2013; Sarmiento, 1988). In some knuckle-walking postures, African apes contact the ground with their ulnar digits then transfer their weight to their radial digits, which would also produce shear stress (Matarazzo, 2013; Richmond et al., 2001).

Suspensory locomotion among African apes includes various power grips, depending on the size and orientation of the supporting substrate. On horizontal supports, apes often use a transverse hook grip with the fingers flexed around the substrate and the thumb adducted or opposed to the fingers (Marzke and Wullstein, 1996; Sarmiento, 1988). The wrist may be flexed or neutral and the distal palm may contact the substrate on large diameter supports (Marzke and Wullstein, 1996; Sarmiento, 1988). On large vertical supports, apes often use power grips with the flexed fingers and palm grasping the substrate and the thumb adducted or abducted (Neufuss et al., 2017; Sarmiento, 1988). When the thumb is abducted, the thenar area is used to exert counterpressure so the MC1 may experience forceful loading (Neufuss et al., 2017). On medium vertical supports, apes often use diagonal power grips with the object held diagonally across the flexed fingers and palm (the second and third digits moderately flexed, the fourth and fifth digits more flexed) and the thumb held in line with the long axis of the support or opposed to the

fingers (Marzke et al., 1992; Marzke and Wullstein, 1996; Neufuss et al., 2017). When the thumb is opposed it may experience large loads (Neufuss et al., 2017). During suspensory behaviours, the articular ends of the phalanges experience compression from joint reaction forces (Richmond, 2007). Muscles pull the midshaft palmarly, compressing the phalanges dorsally and tensing them palmarly, strains which are reduced by greater phalangeal curvature (Richmond, 2007). The wrist experiences a net tensile force, although compressive forces also occur when joints reach their limit of movement or when muscles apply forces (Preuschoft and Weinmann, 1973; Sarmiento, 1985, 1988).

Quantifying carpal morphology

Previous qualitative analyses of carpal variation among human and nonhuman primates have identified multiple features that vary between and among taxa, and many of these act as morphological correlates for particular locomotor and/or manipulative behaviours (Kivell and Begun, 2007; Lewis, 1969, 1973, 1977, 1989; Lewis et al., 1970; Marzke, 1971; Marzke et al., 1992, 1998; Marzke and Marzke, 1987; Marzke and Shackley, 1986; Napier, 1960; Sarmiento, 1988; Tuttle, 1967). These qualitative studies often used wet (e.g., formalin-fixed or dissecting room cadavers), dry ligamentous or osteological preparations, and individual bones or casts. Radiographs were also sometimes used to visualize the articulated carpals in various wrist positions or during locomotor behaviour (Lewis, 1969, 1977; Lewis et al., 1970; Tuttle, 1967). Detailed descriptions of visual observations (e.g., size of bones, articulations, soft tissue and bony features) were generated and, in some cases, scoring systems were used to determine the frequencies of certain morphological features in a sample (Kivell and Schmitt, 2009; Lewis, 1989; Marzke et al., 1994). For instance, Kivell and Schmitt (2009) scored knuckle-walking features as “present” or “absent” to determine their frequencies among hominoids and

cercopithecoids. Qualitative descriptions and analyses remain an important part of studying morphology and are often used in conjunction with various quantitative techniques (Kivell et al., 2011). However, qualitative data have various limitations that are mostly related to difficulties in capturing the full ranges of carpal variation that can exist within and between species (Marzke and Marzke, 2000; Tocheri et al., 2005).

Attempts to quantify previously identified qualitative aspects of carpal anatomy are important for reliably establishing if and how carpal shapes and features vary among primates. However, carpals have complex shapes and articulations, which together make adequately capturing this morphology by quantitative measurements extremely challenging (Almécija et al., 2015; Hawks et al., 2017; Kivell et al., 2015; Marzke et al., 2010; Orr et al., 2013; Tocheri et al., 2003, 2005, 2007). Morphometrics is the quantitative analysis of biological shape variation, where shape is the geometry of an object independent of scale, location, and orientation (Rohlf, 1990). Carpal studies have often relied on traditional morphometrics, namely linear distances, ratios, and/or angles (Corrucini, 1978; Kivell et al., 2011, 2013; Kivell and Begun, 2009; Kivell and Schmitt, 2009; Niewoehner et al., 1997). Linear distances can be measured directly on the bone and have the benefit of being independent of location and orientation, often only requiring the removal of size by using a ratio (Rohlf, 1990; Slice, 2005). Angles are naturally independent of location, orientation, and size. However, traditional morphometrics have various limitations, the main one being the loss of aspects of shape because the geometric relationships between different measurements are not preserved (Adams et al., 2004). Additionally, linear distances may be defined in ways such as maximum or minimum dimensions of a bone or feature and this adds complications if one is interested in assessing homology (i.e., similarity due to shared ancestry) (Adams et al., 2004).

3D modeling techniques have shown considerable promise in recent years by successfully quantifying carpal morphology among closely related primate taxa (Almecija et al., 2015; Kivell et al., 2015; Marzke et al., 2010; Orr et al., 2013; Tocheri, 2007; Tocheri et al., 2003, 2005, 2007). Some of the earliest attempts at 3D analyses used stereophotogrammetry, which involved the photography of a surface from multiple angles and was used to create 3D models of the first carpometacarpal joint surfaces (Ateshian, 1992; Marzke et al., 2010). From these models, the surface areas and curvatures of the articular surfaces were calculated (Ateshian, 1992; Marzke et al., 2010). Subsequently, research shifted toward using laser or computed tomography (CT) scanning as these data acquisition methods have advantages for capturing 3D data of entire bones (Marzke and Marzke, 2000) and to date have been used to study the morphology of various carpals (Almecija et al., 2015; Hawks et al., 2017; Kivell et al., 2015; Marzke et al., 2010; Orr et al., 2013; Tocheri, 2007; Tocheri et al., 2003, 2005, 2007; Wuthrich et al., 2019). In some of these studies, individually scanned bones were segmented into articular and nonarticular areas and various measurements were calculated, such as the relative surface areas of joints (i.e., % of total bone surface area), angles between articular surfaces, and curvatures of articular surfaces. These variables were then examined either univariately or combined for multivariate analyses. Additionally, variables from multiple bones were combined in multivariate analyses to study different bone combinations. For instance, Kivell et al. (2015) performed a multivariate analysis of the scaphoid, trapezium, and trapezoid together, and another of the capitate and hamate together by combining each bone's angles, relative areas, and curvatures.

More recently, researchers have CT scanned intact cadaver forearms in various positions throughout the wrist’s full range of motion, from which they produced 3D models of the entire

wrist along with the radius, ulna, and five metacarpals (Orr et al., 2010). Subsequent studies have used these intact 3D models to measure various properties, including carpal volumes, the triquetrohamate joint angle, the dorsal lunatocapitate articular arc, and ulnar styloid projection (Orr, 2017; Orr et al., 2024). Although these various approaches using 3D laser or CT-scanned models have enabled the collection of various measurements (e.g., surface areas, bone volumes, surface curvatures) beyond more straightforward linear distances and angles, much like traditional morphometrics these measures do not necessarily preserve the geometric relationships that exist between these various measurements. The field of geometric morphometrics (GM) has grown and developed over the past few decades in response to these specific kinds of limitations (Gunz and Mitteroecker, 2013).

Using either 2D or 3D landmarks (i.e., x, y or x, y, z coordinates), GM captures the size, orientation, and shape of objects with the ability to remove size and orientation such that only variation in shape remains (Adams et al., 2004; Rohlf and Marcus, 1993). Traditional landmarks are defined as discrete locations on an object, such as the points where three structures meet or the local curvature maxima (Bookstein, 1992; Slice, 2005). Alternatively, ordered sets of landmarks (i.e., semilandmarks) can be placed along curves or outlines or along surfaces (Slice, 2005). Landmarks are collected directly from objects using digitizing equipment (e.g., a MicroScribe) or from 2D and 3D digital images or models (Gunz and Mitteroecker, 2013) and subsequently analyzed using a variety of statistical techniques. GM also enables the visualization of shape variation via deformation grids and deformed surface models (i.e., warped surface models), which is particularly beneficial for interpreting results when working with highly multivariate data (Gunz and Mitteroecker, 2013). In many ways, GM appears well suited as a method to quantify the complex shapes of carpals as well as for detecting and quantitatively

describing shape differences among closely related taxa (Adams et al., 2004; Almecija et al., 2015; Monteiro et al., 2000, 2002; Rohlf and Marcus, 1993; Zelditch et al., 2004).

Although 3DGM has been used extensively in various fields, particularly in paleoanthropology and biological anthropology (Baab and McNulty, 2009; Friess, 2010; Rein, 2019; Rein and Harvati, 2014), its use on carpals in primates has thus far been limited to studies of the trapezium, capitate, hamate, and triquetrum (Almécija et al., 2015; Bardo et al., 2020; Daver et al., 2014; Niewohner et al., 2005; Vanhoof et al., 2021, 2024; Wuthrich et al., 2019). In most of these studies, with the exception of those on the first carpometacarpal joint (Bardo et al., 2020; Niewohner et al., 2005), sets of discrete landmarks were used to study the surface morphology of the actual bones or 3D surface models. These analyses have shown considerable success in quantitatively capturing the complexities of carpal shape variation that exists among primate taxa, and demonstrate the potential of GM for further research on primate wrists.

Objectives

In this study, 3DGM is used to further quantitatively evaluate radial-side carpal morphology among extant western lowland gorillas, chimpanzees, bonobos, and humans, and represents the first time that digitally articulated sets of carpals are analyzed together as morphological and functional units. Previous studies using 3DGM and/or 3D models have typically quantified wrist morphology by studying each carpal bone or joint individually and in isolation from each other using sets of discrete landmarks or measurements (Almécija et al., 2015; Bardo et al., 2020; Daver et al., 2014; Hawks et al., 2017; Kivell et al., 2015; Marzke et al., 2010; Orr et al., 2013; Rein, 2019; Rein and Harvati, 2014; Tocheri, 2007; Tocheri et al., 2003, 2005, 2007; Vanhoof et al., 2021, 2024; Wuthrich et al., 2019). However, carpal shape is highly complex and there is generally a lack of landmarks that are both easily defined and

homologous, which provides specific challenges for methods like 3DGM. To overcome this challenge, this study will use semilandmark patches placed on the articular facets of each carpal instead of discrete landmarks because these surfaces are arguably homologous among African apes and humans even though any given point on these surfaces may not be. Semilandmark patches are *n* x *m* grids of relatively evenly spaced landmarks that can be placed on homologous surfaces to capture denser, more comprehensive shape information (Bardua et al., 2019; Gunz et al., 2005). Furthermore, the increased density of landmarks will allow for more accurate visualization of shape variation using surface warps.

The first objective of this study is to demonstrate that collecting 3D data from wrists of intact cadaver arms can inform the process of manually articulating 3D models of bones scanned from previously macerated skeletal specimens. Some previous studies combined shape variables from different carpals for statistical analysis (Hawks et al., 2017; Kivell et al., 2015), however, these data still essentially reflect the shape features of individual bones (e.g., the surface area of the facets on the trapezoid relative to the total surface area of the trapezoid) rather than the anatomical region as a whole.

The second objective of this study is to use the sets of articulated carpals to test previous ideas about how radial wrist shape varies among African apes and humans while also exploring if they may vary in additional ways that have yet to be discovered. African apes use their hands to support their body weight during locomotor behaviours such as knuckle walking and climbing, whereas humans habitually use their hands for gripping and manipulating objects (e.g., tools). During knuckle walking, ground reaction forces are transmitted proximally through the wrist (Matarazzo, 2013; Sarmiento, 1988; Wunderlich and Jungers, 2009). In contrast, during manual grasping, contraction of thenar musculature generates forces that must be distributed radioulnarly

across the wrist (Cooney and Chao, 1977; Lewis, 1989). My predictions follow those of previous studies (e.g., Lewis, 1989; Tocheri, 2007) that carpal morphology in African apes will facilitate proximodistally directed forces while stabilizing the carpus radioulnarly. Conversely, carpal morphology in humans will facilitate radioulnarly directed forces while stabilizing the carpus proximodistally, as well as facilitate greater mobility of the MC1 and MC2 bases for manual grasping.

The third objective of this study is to explore and document how radial wrist shape varies among African ape taxa as relatively little about this has been documented by previous quantitative research. African ape taxa vary in body size and weight as well as in their locomotor behavioural repertoires. Gorillas are larger in body weight than chimpanzees, while bonobos tend to be smaller than *P. t. troglodytes* (central chimpanzees) but similar or even larger in body weight compared to western and eastern chimpanzees (Coolidge and Shea, 1982; Druelle et al., 2018; Jungers and Susman, 1984; McHenry and Corruccini, 1981; Smith and Jungers, 1997). Although all African apes are primarily terrestrial knuckle walkers, chimpanzees and bonobos are generally considered more arboreal than gorillas (Doran, 1993, 1997; Doran and Hunt, 1994; Hunt, 1992, 1994; Sarringhaus et al., 2014; Susman, 1984; Susman et al., 1980). Furthermore, knuckle-walking postures and pressure distributions may differ between African ape species (Inouye, 1994; Kivell and Schmitt, 2009; Matarazzo, 2013; Tuttle, 1967; Wunderlich and Jungers, 2009) and their radial-side carpal morphology may reflect some or all of the above-mentioned variation among these taxa.

Methods

Samples

The 3D surface models used in this study were generated from laser and medical CT scans of wrist bones derived from either previously macerated skeletons (provided by Dr. Matt Tocheri) or intact cadaver upper limbs (provided by Dr. Caley Orr). The complete study sample consisted of 57 trapeziums, 57 trapezoids, 57 scaphoids, and 32 capitates from 7 western lowland gorillas, 21 chimpanzees, 5 bonobos, and 24 humans (Table 1). All bones were analyzed as belonging to the right side of the body so left-side bones were reflected in Geomagic Studio (Geomagic, 2013) prior to data collection.

Articulating the carpals

The wrists of six individuals (5 chimpanzees and 1 western gorilla) in the sample were acquired from medical CT scans of intact cadaver limbs. These limbs were scanned with the wrist in a neutral posture (i.e., neither flexed nor extended) and the articulated radial wrist bones of these individuals were then used as visual references for digitally articulating into a similar neutral posture the capitate, scaphoid, trapezium, and trapezoid of the remaining sample wherein the bones of each individual had been separately laser scanned. All manual articulations were conducted digitally in Geomagic Studio software. Once manually articulated, the individual bones were exported in their new coordinate space as separate 3D models (henceforth referred to here as articulated sets). To examine the potential effects of variation in the manual articulation process, articulations of 5 chimpanzee and 2 human individuals were carried out independently by two observers (one by OL and the other by Dr. Tocheri).

Landmarks

Three-dimensional semilandmark patches were manually placed on the articulated radial carpus models using the "patches" option in Stratovan Checkpoint version 2024.08.01:44 (Stratovan Corporation, 2024). Each patch had 16 movable semilandmarks along the edges and 1 movable semilandmark in the center. For each patch, a subset of edge semilandmarks that were homologous and easily locatable (e.g., points where three structures meet, maxima of curvature, etc.) were used as anchors to place the patches. The other edge semilandmarks were spaced evenly between these anchor landmarks along the edges of the articular facet. The center semilandmark was placed such that the other semilandmarks were evenly spaced on the surface.

The trapezium, trapezoid, and scaphoid were each given a total of 324 landmarks spread equally across four 9 x 9 patches (Tables 2–4). For the trapezium, a patch was placed on each of the MC1, trapezoid, MC2, and scaphoid facets (Figure 3). For the trapezoid, a patch was placed on each of the scaphoid and trapezium facets along with the radial and ulnar portions of the MC2 facet (Figure 4). For the scaphoid, a patch was placed on each of the scaphoid, lunate, trapezium-trapezoid, and radius facets (Figure 5). The capitate was given a total of 532 landmarks (Table 5). A higher density 17 x 17 patch was placed on the scaphoid-lunate facet since it is a complex surface. Lower density 9 x 9 patches were placed on the MC2, MC3, and hamate facets (Figure 6). A patch was not placed on either the trapezoid facet of the capitate or the capitate facet of the trapezoid because these facets are often absent in gorillas. The articular and nonarticular areas of each bone model had been digitally segmented for previous research (e.g., Tocheri, 2007; Tocheri et al., 2007) using Geomagic Studio software. These segmentations were used as visual references for placing patches on the radial carpus models.

The landmark data was exported as x, y, z coordinates from Stratovan Checkpoint (Stratovan Corporation, 2024). The landmark matrix for each articulated radial carpus model was combined with other landmark matrices belonging to the same specimen, creating a new matrix containing the landmarks on all four (or three in cases where the capitate is missing) carpals (Figures 7 and 8).

Sliding

Semilandmarks are slid to reduce statistical artefacts that arise due to the initial arbitrary placement of semilandmarks. Sliding is performed to either reduce the shape differences between each specimen and the average shape in the sample by minimizing the Procrustes distances, or by minimizing the bending energy of a thin-plate spline deformation (Bardua et al., 2019; Gunz and Mitteroecker, 2013). When minimizing bending energy, all of the semilandmarks are slid together and are influenced by traditional landmarks (Gunz and Mitteroecker, 2013). When minimising Procrustes distances, the semilandmarks are slid separately and sliding is not influenced by other landmarks and semilandmarks. Thus, when using Procrustes distances, curve semilandmarks can slide past the endpoints of the curve or other semilandmarks. Both the bending energy and Procrustes distance methods yield comparable results if shape variation is small and semilandmarks do not need to slide much. However, the minimizing bending energy method yields better results if shape variation is larger (Gunz and Mitteroecker, 2013).

In this study, semilandmarks were slid to minimize the bending energy of a thin-plate spline deformation using the function *slider3d()* in the R package *Morpho* (Schlager, 2017). The stepsize parameter, which limits the amount that curve and surface semilandmarks can move, was set to 0.7 because the default (1) resulted in some curve semilandmarks deviating from their defined curves. The landmark data were organized into types of landmarks for the sliding

process. Edge semilandmarks were designated as landmarks that do not slide. Semilandmarks within patch interiors were designated as surface semilandmarks that can slide along their tangent planes. After each iteration of the sliding process, the semilandmarks were projected back onto the surface to avoid the problem of them "falling off" the actual bone surface (Gunz et al., 2005; Gunz and Mitteroecker, 2013; Schlager, 2017).

Shape analysis

After sliding, all landmarks underwent a generalised Procrustes analysis (GPA) and subsequent principal component analysis (PCA) using the function *procSym()* in the R package *Morpho* (Schlager, 2017). The *procSym()* function returns an array of GPA superimposed coordinates of the translated, scaled, and rotated landmark configurations for each specimen. Thus, the only variation that remains is due to shape differences. The *procSym()* function then performs a PCA on the array of GPA superimposed coordinates (i.e., the shape data) and returns a matrix of principal component (PC) scores. The PC scores were plotted using the function *ggplot()* in the R package *ggplot2* (Wickham, 2016). Because all four selected carpal bones were not available for all individuals included in the sample, four analyses were done using differing combinations of articulated carpals and taxa: a four-bone (trapezium, trapezoid, scaphoid, and capitate) analysis, a three-bone (trapezium, trapezoid, and scaphoid) analysis, a four-bone analysis with African apes only, and a three-bone analysis with African apes only.

For the four-bone analysis, Euclidean distances were calculated to compare the PC score distances across all PCs and along PC1 only between each set of carpals articulated by OL and Dr. Tocheri, and between each chimpanzee, human, and chimpanzee-human pair. Euclidean distances were calculated using the function *dist()* in the R package *stats* (R Core Team, 2024).

Shape changes along each PC were visualised using 3D point clouds and warped 3D surface models. Point clouds representing the landmark coordinates of -1 and +1 standard deviations of each PC were generated using *plotRefToTarget()* (method = points) in the R package geomorph version 4.0.4 (Adams et al., 2025; Baken et al., 2021). Warped 3D surface models were generated by warping the 3D surface model of the mean specimen across all PCs to a theoretical mean shape as defined by the set of mean landmark coordinates using the function *warpRefMesh()* in *geomorph* (Adams et al., 2025; Baken et al., 2021). The resulting mean 3D mesh was then warped to the landmark coordinates of -1 and +1 standard deviations of each PC axis using *plotRefToTarget()* (method = surface). For the three-bone analysis of African apes only, the centroid sizes of the articulated wrists were also plotted against PC1 to examine potential size-related shape changes using a linear regression line, calculated using *geom_smooth()* in the R package *ggplot2* (Wickham, 2016).

Results

Euclidean distances

The Euclidean distances between each human and chimpanzee wrist manually articulated by a different observer (one by OL and the other by Dr. Tocheri) were small in comparison to the Euclidean distances between individuals within each species across all PCs and especially for PC1 (Figure 9). For example, the mean and total range of variation for the Euclidean distances between all possible pairs of chimpanzee individuals across all PCs were 0.16 and 0.11–0.22, respectively, whereas those between each chimpanzee articulated in duplicate were 0.10 and 0.09–0.13, respectively. Similarly, the mean and total range of variation for the Euclidean distances between all possible pairs of human individuals across all PCs were 0.20 and

0.17–0.24, respectively, whereas those between each human articulated in duplicate were 0.11 and 0.10–0.11, respectively.

African apes and humans

The four-bone (trapezium, trapezoid, scaphoid, and capitate) and three-bone (trapezium, trapezoid, and scaphoid) PCAs resulted in clear separation of African apes and humans along PC1, which explained 26.9% and 33% of the variance, respectively (Figures 10 and 11). The shape differences that best explained the observed separation along PC1 were essentially identical in each of these analyses and are thus described together below along with any shape differences that were specific to only one of the analyses. The warps for the four-bone and three-bone analyses were generated from two different chimpanzees, USNM 220064 (Figure 12) and USNM 23697 (Figure 13), respectively, as these individuals were identified as closest in shape to the calculated mean shapes of the total samples across all PCs combined. The variation detected by the warps along PC1 essentially reflect African ape versus human morphology.

The trapezium. African apes clustered negatively along PC1 because the trapezia were positioned palmarly and more in front of the trapezoid, resulting in a deeper carpal tunnel (Figure 14). In contrast, humans clustered positively along PC1 because the trapezia were positioned radially due to the radioulnar expansion of the palmar aspect of the trapezoid. As a result, the trapezium in humans was more in line with the rest of the distal carpal row and the carpal tunnel was shallower. The trapezium was radioulnarly narrower and similar in size to the trapezoid in African apes, whereas this bone was wider and larger relative to the trapezoid in humans (Figures 15 and 16).

The trapezium and its MC1 articular facet. African apes clustered negatively along PC1 because the MC1 facets were smaller (Figures 17 and 18). The MC1 facets were also more

curved radioulnarly and dorsopalmarly as well as oriented less parallel to the scaphoid facet of the trapezium (Figures 15, 16, 19, and 20). In contrast, humans clustered positively along PC1 because the MC1 facets were larger and flatter in both directions as well as orientated more parallel to the scaphoid facet of the trapezium.

The trapezium and its MC2 articular facet. African apes clustered negatively along PC1 because the MC2 facet was smaller and more radioulnarly oriented (Figures 15, 16, 19, and 20). In contrast, humans clustered positively along PC1 because the MC2 facet was larger and more proximodistally oriented.

The trapezium and its trapezoid articular facet. African apes clustered negatively along PC1 because the trapezoid facet was flatter and dorsopalmarly narrower (Figures 15, 16, 19, and 20). In contrast, humans clustered positively along PC1 because the trapezoid facet was more curved and wider. The three-bone analysis also detected differences in trapezoid facet height. The trapezoid facet was proximodistally taller in African apes, whereas this facet was shorter in humans (Figure 16).

The trapezium and its scaphoid articular facet. African apes clustered negatively along PC1 because the scaphoid facet was smaller, whereas humans clustered positively along this axis because the scaphoid facet was larger (Figures 15 and 16).

The trapezoid. African apes clustered negatively along PC1 because the trapezoids were "wedge-shaped" with a narrower palmar aspect (Figures 21 and 22). The MC2 and scaphoid facets were less parallel to each other (Figure 23). Additionally, the space for the capitate facet on the radial side of the bone was smaller and less parallel to the trapezium facet (Figure 23). In contrast, humans clustered positively along PC1 because the trapezoids were "boot-shaped" with an radioulnarly and proximodistally expanded palmar aspect (Figures 21 and 22). The MC2 and

scaphoid facets were more parallel to each other while the space for the capitate facet was larger and more parallel to the trapezium facet (Figure 23).

The trapezoid and its radial and ulnar MC2 articular facets. African apes clustered negatively along PC1 because the palmar portions of the radial and ulnar MC2 facets were tilted proximally, corresponding with the narrower palmar aspect of the trapezoid (Figures 21 and 22). In contrast, humans clustered positively along PC1 because the palmar portions of the radial and ulnar MC2 facets were shifted distally, corresponding with the expanded palmar aspect of the trapezoid. In African apes the MC2 joint is more wedge-shaped whereas in humans the ulnar MC2 facet has shifted further distally relative to the radial MC2 facet, resulting in a more saddle-shaped MC2 joint (Figures 21 and 22).

The trapezoid and its trapezium articular facet. African apes clustered negatively along PC1 because the trapezium facet was flatter whereas humans clustered positively along this axis because the trapezium facet was more curved (Figures 15 and 16). The three-bone analysis also detected differences in trapezium facet height. The dorsal portion of the trapezoid facet was proximodistally taller in African apes whereas the dorsal portion of this facet is shorter in humans (Figure 16).

The trapezoid and its scaphoid articular facet. African apes clustered negatively along PC1 because the scaphoid facet was more triangular and larger (Figures 15 and 16). In contrast, humans clustered positively along PC1 because the scaphoid facet was more rectangular and smaller.

The scaphoid. African apes clustered negatively along PC1 because the scaphoids were proximodistally taller and large relative to the other radial-side carpals (Figures 19 and 20). In contrast, humans clustered positively along PC1 because the scaphoids were shorter and more

similar in size to the other radial-side carpals. The three-bone analysis also detected differences in scaphoid thickness. African apes clustered negatively along PC1 because the scaphoids were dorsopalmarly thinner whereas humans clustered positively along this axis because the scaphoids were thicker (Figure 20).

The scaphoid and its capitate articular facet. African apes clustered negatively along PC1 because the capitate facet is proximodistally taller whereas humans clustered positively along this axis because the capitate facet is shorter (Figure 21 and 23).

The scaphoid and its trapezium-trapezoid articular facet. African apes clustered negatively along PC1 because the trapezium-trapezoid facet has more space on the scaphoid body due to the increase of bone along its distoulnar edge, corresponding with increased surface area for the trapezoid (Figures 15, 16, 21, and 22). The trapezium-trapezoid facet does not extend as far onto the tubercle in African apes, corresponding with decreased surface area for the trapezium respectively (Figures 15 and 16). In contrast, humans clustered positively along PC1 because the trapezoid-trapezium facet has less space on the scaphoid body due to reduced bone along its distoulnar edge, corresponding with decreased surface area for the trapezoid (Figures 15, 16, 21, and 22). The trapezium-trapezoid facet extends radially onto the tubercle in humans, corresponding with increased surface area for the trapezium respectively (Figures 15 and 16).

The scaphoid and its radius articular facet. African apes clustered negatively along PC1 because the radius facet was larger and more circular (Figures 15 and 16). In contrast, humans clustered positively along PC1 because the radius facet was smaller and oval-shaped.

The scaphoid and its lunate articular facet. African apes clustered negatively along PC1 because the lunate facet was more dorsopalmarly orientated (Figures 19 and 20). In contrast,

humans clustered positively along PC1 because the lunate facet was more proximodistally orientated.

The capitate. African apes clustered negatively along PC1 because the capitate has a narrower neck, whereas humans clustered positively along this axis because the capitate has a wider neck (Figure 24).

The capitate and its MC2 articular facet. African apes clustered negatively along PC1 because the MC2 facet was typically more radioulnarly oriented and constrained to the palmar portion of the distal capitate (Figures 17 and 21). In contrast, humans clustered positively along PC1 because the MC2 facet was more proximodistally orientated and extends further dorsally along the entire length of the distal capitate.

The capitate and its MC3 articular facet. African apes clustered negatively along PC1 because the MC3 facet was longer (Figure 14) and more irregular (Figure 24). The dorsoradial corner was fused with the ossification centre that composes the MC3 styloid process in humans (Figure 14). In contrast, humans clustered positively along PC1 because the MC3 facet was dorsopalmarly shorter and more smooth, as well as bevelled dorso-radially to accommodate the MC3 styloid process.

The capitate and its hamate articular facet. African apes clustered negatively along PC1 because the hamate facet was more curved whereas humans clustered positively along this axis because the hamate facet was flatter (Figure 24).

Pan *versus* Gorilla

Along PC1 of the four-bone analysis, which explained 14.7% of the total variance, bonobos clustered negatively whereas gorillas clustered positively (Figure 25). A chimpanzee drove the variation at the negative extreme along PC1, although most chimpanzees seemed to

span the axis, overlapping with both bonobos and gorillas. Along PC1 of the three-bone analysis, which explained 14.9% of the total variance, there was better separation among taxa with *Pan* clustering negatively and gorillas clustering positively (Figure 26). The warps for the four-bone and three-bone analyses were generated from two chimpanzee individuals, USNM 220062 (Figure 27) and USNM 220063 (Figure 28), respectively, as these individuals were identified as closest in shape to the calculated mean shapes of the total samples across all PCs combined. For both analyses, a chimpanzee drove the variation at the negative extreme along PC1 while a gorilla drove the variation at the positive extreme. The shape differences that best explained the observed separation along PC1 were essentially identical in each of these analyses and are thus described together below along with any shape differences that were specific to only one of the analyses.

The trapezium. *Pan* clustered negatively along PC1 because the trapezia were radioulnarly narrower and had less nonarticular area between the MC1 and trapezoid facets (Figures 29 and 30). In contrast, gorillas clustered positively along PC1 because the trapezia were radioulnarly wider and had more nonarticular area between the MC1 and trapezoid facets.

The trapezium and its MC1 articular facet. *Pan* clustered negatively along PC1 because the MC1 facet was more curved radioulnarly and dorsopalmarly (Figures 29, 30, 31, and 32). In contrast, gorillas clustered positively along PC1 because the MC1 facet was flatter in both directions. Bonobos were observed to have dorsopalmarly flatter MC1 facets similar to gorillas, although they clustered negatively along PC1 with chimpanzees.

The trapezium and its MC2 articular facet. *Pan* clustered negatively along PC1 because the MC2 facet was proximodistally shorter (Figures 31 and 32). Gorillas clustered positively along PC1 because the MC2 facet was taller.

The trapezium and its trapezoid articular facet. *Pan* clustered negatively along PC1 because the trapezoid facet was proximodistally taller and tilted ulnarly (Figures 29 and 30). In contrast, gorillas clustered positively along PC1 because the trapezoid facet was shorter and less tilted.

The trapezium and its scaphoid articular facet. The three-bone analysis detected differences in the scaphoid facet shape. *Pan* clustered negatively along PC1 because the scaphoid facet was more triangular and radioulnarly narrower dorsally (Figure 30). In contrast, gorillas clustered positively along PC1 the scaphoid facet was more D-shaped and wider dorsally.

The trapezoid. The three-bone analysis detected differences in the trapezoid shape. *Pan* clustered positively along PC1 because the trapezoids were proximodistally taller and radioulnarly narrower (Figure 30). In contrast, gorillas clustered positively along PC1 because the trapezoids were shorter and wider.

The trapezoid and its radial and ulnar MC2 articular facets. *Pan* had a more wedge-shaped MC2 joint surface because the angle between the radial and ulnar MC2 facets were narrower (Figure 33 and 34). In contrast, gorillas had more saddle-shaped MC2 joint surfaces because the angle between the radial and ulnar MC2 facets were wider. The four-bone analysis detected differences in the orientation of the ulnar MC2 facet. *Pan* clustered negatively along PC1 because the ulnar MC2 facet was more radioulnarly orientated, whereas gorillas clustered positively along this axis because ulnar MC2 facet was more proximodistally orientated (Figure 33). The three-bone analysis detected differences in the size of the radial and ulnar MC2 facets. *Pan* clustered negatively along PC1 because the ulnar MC2 facet was radioulnarly narrower and dorsopalmarly shorter while the radial MC2 facet was dorsopalmarly longer (Figures 34 and 35). In contrast, gorillas clustered positively along PC1 because the ulnar MC2

facet was wider and longer while the radial MC2 facet was shorter. Bonobos were observed to have radioulnarly wider ulnar MC2 facets similar to gorillas, although they clustered negatively along PC1 with chimpanzees.

The trapezoid and its trapezium articular facet. *Pan* clustered negatively along PC1 because the trapezium facet was proximodistally taller and tilted ulnarly (Figures 29 and 30). In contrast, gorillas clustered positively along PC1 because the trapezium facet was shorter and less tilted.

The trapezoid and its scaphoid articular facet. The three-bone analysis detected differences in the size of the scaphoid facet. *Pan* clustered negatively along PC1 because the scaphoid facet was dorsopalmarly shorter whereas gorillas clustered positively along this axis because the scaphoid facet was longer (Figure 36).

The scaphoid. *Pan* clusters negatively along PC1 because the scaphoids were dorsopalmarly thinner, whereas gorillas clustered positively along this axis because the scaphoids were thicker (Figures 31 and 32).

The scaphoid and its capitate articular facet. *Pan* clustered negatively along PC1 because the capitate facet was larger and more oval-shaped, whereas gorillas clustered positively along PC1 because the capitate facet was smaller and more circular (Figures 33 and 36).

The scaphoid and its radius articular facet. The three-bone analysis detected differences in the radius facet morphology. *Pan* clustered negatively along PC1 because the radius facet had a scaphoid beak, while gorillas clustered positively along PC1 because the radius facet lacked a scaphoid beak (Figure 30).

The capitate. *Pan* clustered negatively along PC1 because the capitates were proximodistally taller, whereas gorillas clustered positively along PC1 because the capitates were shorter (Figure 37).

The capitate and its MC2 articular facet. *Pan* clustered negatively along PC1 because the MC2 facet was proximodistally taller (Figure 33), corresponding to a taller capitate overall. In contrast, Gorillas clustered positively along PC1 because the MC2 facet was shorter, corresponding to a shorter capitate overall.

The capitate and its MC3 articular facet. *Pan* clustered negatively along PC1 because the MC3 facet was dorsopalmarly shorter (Figure 38). In contrast, gorillas clustered positively along PC1 because the MC3 facet was longer.

The capitate and its hamate articular facet. *Pan* clustered negatively along PC1 because the hamate facet was proximodistally taller, corresponding to a taller capitate overall (Figure 37). In contrast, gorillas clustered positively along PC1 because the hamate facet was shorter, corresponding to a shorter capitate overall.

Chimpanzees versus gorillas and bonobos

Along PC2 of the four-bone analysis, which explained 10.7% of the total variance, chimpanzees clustered negatively whereas gorillas and bonobos clustered positively (Figure 25). A chimpanzee drove the variation at the negative extreme along PC2 while a gorilla drove the variation at the positive extreme. The warps in this analysis were generated from a chimpanzee, USNM 220062 (Figure 27). Most of the variation detected by the warps along PC2 reflect chimpanzee versus gorilla morphology, although some features gorillas and bonobos share to the exclusion of chimpanzees.

The trapezium. Chimpanzees clustered negatively along PC2 because the trapezia were radioulnarly narrower compared to gorillas who clustered positively along this axis (Figure 39). Based on visual inspection of the specimens, bonobos had narrower trapeziums similar to chimpanzees, although they clustered positively with gorillas along PC2.

The trapezium and its MC1 articular facet. Chimpanzees clustered negatively along PC2 because the radial portion of the MC1 facet was more dorsopalmarly curved, whereas gorillas and bonobos clustered positively along this axis because the MC1 facet was flatter (Figure 40).

The trapezium and its MC2 articular facet. Chimpanzees clustered negatively along PC2 because the MC2 facet was smaller, whereas gorillas clustered positively along this axis because the MC2 facet was larger (Figure 40). Based on visual inspection of the specimens, bonobos had smaller MC2 facets similar to chimpanzees, although they clustered positively with gorillas along PC2.

The trapezium and its trapezoid articular facet. Chimpanzees clustered negatively along PC2 because the trapezoid facet was proximodistally taller and its distal portion was tilted ulnarly (Figure 39). In contrast, gorillas clustered positively along PC2 because the trapezoid facet was shorter and less tilted. Based on visual inspection of the specimens, bonobos had taller and more tilted trapezoid facets similar to chimpanzees, although they clustered positively with gorillas along PC2. The trapezoid facet was also dorsopalmarly narrower in chimpanzees, whereas this facet was wider in gorillas and bonobos (Figure 40).

The trapezium and its scaphoid articular facet. Chimpanzees clustered negatively along PC1 because the scaphoid facet was more triangular and narrower dorsally. In contrast, gorillas clustered positively along PC2 because the scaphoid facet was more D-shaped and wider

dorsally (Figure 39). Bonobos clustered positively along PC2 although, based on visual inspection of the specimens, had variable scaphoid facet widths.

The trapezoid. Chimpanzees clustered negatively along PC2 because the trapezoids were proximodistally taller and radioulnarly narrower (Figure 39). In contrast, gorillas clustered positively along PC2 because the trapezoids were shorter and wider. Based on visual inspection of the specimens, bonobos had taller, narrower trapezoids similar to chimpanzees, although they clustered positively with gorillas along PC2.

The trapezoid and its radial and ulnar MC2 articular facets. Chimpanzees clustered negatively along PC2 because the ulnar MC2 facet was radioulnarly narrower (Figure 41). In contrast, gorillas and bonobos clustered positively along PC2 because the ulnar MC2 facet was wider. Chimpanzees had dorsopalmarly longer radial MC2 facets while gorillas had shorter radial MC2 facets (Figure 42). Chimpanzees also had a more wedge-shaped MC2 joint surface because the angle between the radial and ulnar MC2 facets was narrower (Figure 41). In contrast, gorillas had a more saddle-shaped MC2 joint surface because the angle between the radial and ulnar MC2 facets was wider. Based on visual inspection of the specimens, bonobos had variable radial MC2 facet lengths and more wedge-shaped MC2 joint surfaces, although clustered positively with gorillas along PC2.

The trapezoid and its trapezium articular facet. Chimpanzees clustered negatively along PC2 because the trapezium facet was proximodistally taller and its distal portion was tilted ulnarly (Figure 39). In contrast, gorillas clustered positively along PC2 because the trapezium facet was shorter and less tilted. Based on visual inspection of the specimens, bonobos had taller and more tilted MC2 facets similar to chimpanzees, although they clustered positively with gorillas along PC2.

The scaphoid. The scaphoid is very similar in its overall shape along PC2.

The scaphoid and its capitate facet. Chimpanzees clustered negatively along PC2 because the capitate facet was proximodistally taller (Figure 41). In contrast, gorillas clustered positively along PC2 because the capitate facet was shorter. Based on visual inspection of the specimens, bonobos had taller capitate facets, although they clustered positively with gorillas along PC2.

The scaphoid and its radius articular facet. Chimpanzees clustered negatively along PC2 because the radius facet had a scaphoid beak whereas gorillas clustered positively along this axis because the radius facet lacked a scaphoid beak (Figure 39). Based on visual inspection of the specimens, the scaphoid beak in bonobos was variable in presence and prominence, and they clustered positively with gorillas along PC2.

The capitate. Chimpanzees clustered negatively along PC2 because the capitates were proximodistally taller whereas gorillas clustered positively along this axis because the capitates were shorter (Figure 43). Based on visual inspection of the specimens, capitate height was observed to be quite variable within taxa and bonobos had taller capitate similar to chimpanzees, although they clustered positively with gorillas.

The capitate and its MC2 articular facet. Chimpanzees clustered negatively along PC2 because the MC2 facet was proximodistally taller, corresponding to a taller capitate overall (Figure 41). In contrast, gorillas clustered positively along PC2 because the MC2 facet was shorter, corresponding to a shorter capitate overall. Based on visual inspection of the specimens, bonobos had taller MC2 facets similar to chimpanzees, although they clustered positively with gorillas.

The capitate and its hamate articular facet. Chimpanzees clustered negatively along PC2 because the hamate facet was proximodistally taller, corresponding to a taller capitate overall (Figure 43). In contrast, gorillas and bonobos clustered positively along PC2 because the hamate facet was shorter, corresponding to a shorter capitate overall. Based on visual inspection of the specimens, bonobos had taller hamate facets similar to chimpanzees, although they clustered positively with gorillas.

The capitate and its scaphoid articular facet. Chimpanzees clustered negatively along PC2 because the distodorsal portion of the scaphoid facet extends more radially, corresponding with a dorsal ridge on the capitate (Figure 43). In contrast, gorillas clustered positively along PC2 because the distodorsal portion of the scaphoid facet did not extend as far radially, corresponding with lack of a dorsal ridge on the capitate. Based on visual inspection of the specimens, most bonobos were observed to have a well-developed dorsal ridge on their capitate, although they clustered positively with gorillas along PC2.

Bonobos versus chimpanzees

Along PC3 of the three-bone analysis, which explained 8.8% of the total variance, bonobos clustered negatively while chimpanzees clustered positively, although there was significant overlap between both groups (Figure 26). A bonobo drove the variation at the negative extreme while a chimpanzee drove the variation at the positive extreme along PC3 whereas gorillas clustered near zero along PC3. The warps in this analysis were generated from a chimpanzee, USNM 220063 (Figure 28). The variation detected by the warps along PC3 reflect bonobo versus chimpanzee morphology.

The trapezium. Bonobos clustered more negatively along PC3 because the trapezia were radioulnarly narrower whereas chimpanzees clustered more positively along this axis because the trapezia were wider (Figure 44).

The trapezium and its MC1 articular facet. Bonobos clustered more negatively along PC3 because the MC1 facet was radioulnarly more curved and dorsopalmarly wider, as well as more radioulnarly orientated (Figures 44 and 45). In contrast, chimpanzees clustered more positively along PC3 because the MC1 facet was flatter and narrower, as well as more proximodistally orientated.

The trapezium and its trapezoid articular facet. Bonobos clustered negatively along PC3 because the trapezoid facet was proximodistally taller and its distal portion was tilted ulnarly (Figure 44). In contrast, chimpanzees clustered positively along PC3 because the trapezoid facet was shorter and less tilted.

The trapezoid. Bonobos clustered negatively along PC3 because the trapezoids had a narrower palmar aspect whereas chimpanzees clustered positively along this axis because the trapezoids had a broader palmar aspect (Figure 46). Variation in the palmar aspect of the trapezoid corresponded with changes in the ulnar MC2 facet morphology.

The trapezoid and its radial and ulnar MC2 articular facets. Bonobos clustered negatively along PC3 because the ulnar MC2 facet was radioulnarly wider and more radioulnarly orientated (Figure 46). In contrast, chimpanzees clustered positively along PC3 because the ulnar MC2 facet was narrower and more proximodistally orientated. The radial MC2 facets of bonobos that clustered negatively along PC3 were radioulnarly narrower while the radial facets of chimpanzees that clustered positively along this axis were wider (Figure 47).

The trapezoid and its trapezium articular facet. Bonobos clustered negatively along PC3 because the trapezium facet was proximodistally taller and its distal portion was tilted ulnarly (Figure 44). In contrast, chimpanzees clustered positively along PC3 because the trapezium facet was shorter and less tilted.

The scaphoid. Bonobos clustered more negatively along PC3 because their scaphoids were dorsopalmarly thinner, while chimpanzees clustered more positively along this axis because their scaphoids were thicker (Figure 45). Furthermore, the scaphoids of bonobos that clustered more negatively along PC3 were proximodistally taller while the scaphoids of chimpanzees that clustered positively along this axis were shorter (Figure 45).

The scaphoid and its capitate articular facet. Bonobos clustered negatively along PC1 because the capitate facet was proximodistally taller (Figure 48). In contrast, some chimpanzees clustered positively along PC1 because the capitate facet was shorter.

Centroid sizes

The plot of centroid sizes of the articulated wrists against PC1 (Figure 49) shows that gorillas have larger centroid sizes and cluster positively along PC1, while *Pan* has smaller centroid sizes and clusters negatively along PC1. There appears to be no relationship between size versus PC1 within any of the taxa. For instance, one of the gorilla females is similar in centroid size to those of *Pan* but clusters positively along PC1 with gorillas.

Discussion

The main aim of this study was to quantify the morphology of the radial-side carpals in extant African apes and humans, with a focus on how shape variation may relate to known differences in hand use. Based on the results of previous studies (e.g., Lewis, 1989; Marzke, 1971, 1992, 1997; Tocheri, 2007; Tocheri et al., 2003, 2005, 2007), humans were predicted to

have carpal morphology that a) stabilizes the trapezium, trapezoid, and capitate from sliding proximodistally relative to each other and the second metacarpal base, and b) facilitates the distribution of radioulnarly directed forces generated by the power and precision grips employed during tool use and manufacture. In contrast, African apes were predicted to have carpal morphology that a) stabilizes the second metacarpal base from sliding radioulnarly relative to the trapezium, trapezoid, and capitate, and b) facilitates the distribution of proximodistally directed forces generated when the hand is weight-bearing during locomotor behaviours (Doran, 1997; Sarmiento, 1998; Tuttle, 1967).

Overall, the 3DGM results recovered all of the shape differences between humans and African apes in the radial wrist region that have been identified by previous research focused on single-bone analyses (e.g., Marzke, 1997; Tocheri, 2007; Tocheri et al., 2008) in addition to revealing several previously unidentified features that also appear to be distinct in humans (Table 6). Moreover, several ways in which the wrists of chimpanzees, bonobos, and western lowland gorillas differ from one another were also identified. Analyzing the radial wrist as an articulated set of four or three bones rather than a single bone at a time provided several advantages over previous attempts to quantify this region of the wrist. First and foremost, it has provided a clearer picture about how all of the distinctive features in humans vary in combination with each other while showing how the shapes of these bones contribute to the shape of the radial wrist as a whole. For example, the warps along PC1 help to highlight the shape changes that are required to essentially 'transform' the radial wrist of an African ape into that of a human and vice versa. This results not only in a detailed picture of how each bone is changing shape by itself but also how they are all changing shape and position relative to each other. Recall that these warps are generated by calculating the mean shape of the entire sample—which in this case resulted in a

shape most similar to a chimpanzee individual (USNM 220064 for the four-bone analysis and USNM 236971 for the three-bone analysis) (Figures 12 and 13)—and then modifying this shape to reflect the changes that occur along PC1. Second, although previous work has been successful at documenting human radial wrist anatomy relative to that of great apes, this has not led to a deep understanding of how radial wrist anatomy in great ape species varies from each other. Thus, this study marks the first time wherein the more subtle differences in overall radial wrist anatomy among African ape taxa have been successfully captured quantitatively.

Manual articulation of separately scanned 3D models of carpal bones

The initial aim of this study was to demonstrate that 3D data from wrists of intact cadaver arms, which are articulated together as in life, can inform the process of manually articulating 3D models of bones scanned separately from previously macerated skeletal specimens. In all analyses, the manually articulated sets of carpal bones for *Pan* and *Gorilla* clustered reasonably close to the articulated wrists of the five chimpanzee and one gorilla cadaver arms, respectively (Figures 10, 11, 25, and 26). These results suggest that manually articulating these separately scanned 3D models did not significantly alter the overall radial wrist morphology to the extent that individuals did not resemble other conspecifics. However, the total range of variation observed among the manually articulated sets was generally greater than that of the intact cadaver wrists. Further research that includes either a larger sample of scanned cadaver wrists or a sample of scanned cadaver wrists that are subsequently macerated, scanned, and manually articulated is required to observe if ranges of variation are due to slight errors in the process of manual articulating 3D models or perhaps reflect some inherent property of the intact cadaver wrist sample (e.g., individuals raised in captive settings).

Examination of the potential variation introduced by different observers carrying out the manual articulation process also suggests that such variation is small relative to the observed variation observed among other conspecifics. Specifically, the Euclidean distances between each human and chimpanzee wrist manually articulated by a different observer (one by OL and the other by Dr. Tocheri) were small in comparison to those between individuals within each species across all PCs and especially for PC1 (Figure 9). In the former, the two manual articulations for both humans and three of the five chimpanzees were smaller than all other pairwise comparisons whereas the other two chimpanzees fell among the distribution of chimpanzee wrists that showed the most similarity to one another. This demonstrates that the effects of variation in the manual articulation process is relatively small and does not significantly alter the expected wrist morphology for these taxa. It should also be noted that due to technological limitations, the individual wrists articulated by different observers also had to be landmarked separately. Thus, slight differences in the landmarking of these duplicate attempts probably accounts for at least part of the observed Euclidean distances between these repeated measures. Developing a method that would prevent the need for separate landmarking (i.e., landmarking specimens prior to articulation rather than after) would better reveal the effects of variation in the articulation process alone.

Overall, manually articulating separately scanned 3D models of carpal bones was successful in terms of producing similar morphometric results to wrists of conspecific individuals, including those of intact cadaver arms. Thus, this approach has great promise as a method for studying the wrist anatomy of extant and extinct primate species.

Extant African ape versus human morphology

The warps along PC1 of the four-bone and three-bone analyses (Figures 10 and 11) showed clear differences in radial-side wrist morphology between African apes and humans. The trapezium in African apes is positioned palmarly, directly anterior to the trapezoid, and the carpal tunnel is deeper (Figure 14). This configuration of the trapezium enables the thumb to oppose the fingers in a neutral position (Marzke, 1992; Marzke et al., 2010) but does not allow for any significant transmission of forces. In contrast, the trapezium in humans is positioned radially on the scaphoid tubercle such that it is more aligned with the rest of the distal carpal row (Table 6). This supinated orientation of the trapezium has been described previously by others and likely facilitates the transmission of forces—generated during forceful thumb use—radioulnarly from the trapezium to the trapezoid and into the capitate (Lewis, 1989; Tocheri, 2007).

As shown in Figures 15 and 16, the trapezium in African apes is relatively smaller with smaller MC1 and scaphoid facets as well as a dorsopalmarly narrower trapezoid facet (Figures 19 and 20). The MC1 and scaphoid facets are less parallel to each other and thus would experience greater shear stress from any forces generated by the thumb. In contrast, the trapezium in humans is relatively larger, with larger MC1 and scaphoid facets as well as a wider trapezoid facet (Figures 15, 16, 19 and 20, Table 6). Stress is defined as force per unit area so these relatively larger articular facets are able to reduce radioulnarly directed compressive stress generated during strong grips (Lewis, 1989; Marzke et al., 1992; Tocheri, 2007). The MC1 and scaphoid facets are also more parallel to each other in humans (Figures 15 and 16, Table 6), which would reduce shear stress from radioulnarly directed forces by reducing the force component that is parallel to the joint surfaces (Tocheri, 2007).

The warps demonstrate that the trapezium-MC1 facet in African apes is radioulnarly and dorsopalmarly more curved (Figures 15, 16, 19, and 20), which would likely increase stability but reduce mobility and the ability to withstand axial forces (Marzke, 1992; Marzke et al., 2010). Reduced thumb mobility may be compensated by the pronated position of the trapezium, which enables the thumb to oppose the fingers in a neutral position (Marzke, 1992; Marzke et al., 2010). Furthermore, the greater dorsopalmar curvature of the first carpometacarpal joint creates a volar beak on the MC1 base, which may stabilize the joint by abutting against the palmar trapezial surface when the metacarpal is slid dorsally on the trapezium (Marzke et al., 2010). The opposite pattern is seen in humans, wherein the trapezium-MC1 facet is radioulnarly and dorsopalmarly flatter (Table 6). This shape difference of this facet was previously quantified by measuring the radius of curvature along the two joint axes (Tocheri, 2007; Marzke et al., 2010). The flatter trapezium-MC1 in humans likely results in increased mobility and an ability to withstand axial forces at the expense of stability (Marzke, 1992; Marzke et al., 2010).

The trapezoid has a narrow palmar aspect in African apes due to the palmar portions of ulnar and radial MC2 facets slanting proximally (Figures 21 and 22). In contrast, the trapezoid has a broad palmar aspect in humans due to the palmar portions of the ulnar MC2 facet, and to a lesser extent the radial MC2 facet, shifting distally (Table 6). The resulting large palmar nonarticular area is the attachment site of the trapeziotrapezoid ligament, which stabilize the trapezium and the first carpometacarpal joint against the cantilever forces that occur during pinch grips by preventing trapezium extension and radial deviation (Bettinger et al., 1999, 2000; Bettinger and Berger, 2001).

The articulated warps demonstrate that the radial and ulnar trapezoid-MC2 facets are more parallel to the scaphoid-radius facet in African apes (Figure 23), which reduces shear stress

from proximodistally directed forces (Tocheri, 2007). Furthermore, the ulnar side of the trapezoid in African apes typically only has space for a capitate articulation dorsally (Figure 23), as seen by a small dorsally located capitate facet in *Pan* and an often absent trapezoid facet in gorillas (Lewis 1989; Tocheri, 2007). Conversely, proximodistal expansion of the palmar aspect in the human trapezoid has resulted in more parallel MC2 and scaphoid facets, which effectively pushes the MC2 distally such that it is no longer buttressed against the radial side of the capitate (Table 6) (Tocheri, 2007). Together with the more proximodistal orientation of the MC2-capitate joint, this morphology prevents the capitate from sliding distally along the MC2 base (Tocheri, 2007). Proximodistal expansion has also resulted in more space on the ulnar side of the bone for articulation with the capitate (Figure 23, Table 6). This supports observations of a larger, palmarly located capitate facet in humans that, in combination with the scaphoid-capitate facet, acts to better distribute radioulnarly directed compressive stress as well as minimise shear stress during grips involving the thumb placed in various positions (Lewis, 1977, 1989; Marzke et al., 1992; Tocheri, 2007). The articulated warps also demonstrate that radioulnar expansion of the palmar aspect in the human trapezoid is indeed accommodated by the supinated position of the trapezium (Figure 14), as discussed above.

Overall, the trapezoid-MC2 facet is less angular in the human trapezoid because the ulnar portion has shifted more distally relative to the radial portion (Figures 21 and 22). This confirms observations by Lewis (1977) that the trapezoid-MC2 joint is more "saddle-shaped" in humans whereas this joint is more "wedge-shaped" in African apes (Table 6). The saddle-shaped joint morphology in humans may facilitate mobility of the index finger, while the African ape morphology likely stabilizes the base of the index finger during locomotion (Lewis 1977).

The articulated carpals confirm that African apes have a larger trapezoid-scaphoid joint (Figures 15 and 16), which likely experiences large shear stresses given that it is not orthogonal to the proximodistal axis (Tocheri, 2007). Fusion of the centrale may have occurred in African apes to accommodate this shear stress (Orr, 2018; Richmond et al., 2001). The opposite pattern occurs in humans wherein the smaller trapezoid-scaphoid facet accommodates the larger trapezium-scaphoid facet (Table 6). Previous studies also documented a relatively larger ulnar portion of the MC2 facet in African ape trapezoids compared to those of humans, again likely acting to reduce compressive stress from proximodistally directed forces (Tocheri, 2007). In this study, the warps did not show any noticeable difference in the sizes of the ulnar portions of MC2 facet (Figure 14, Table 6). However, previous studies (Tocheri, 2007) were evaluating the surface area of the trapezoid-ulnar MC2 facet relative to the total surface area of the trapezoid.

As seen in Figures 19 and 20, the proximodistally taller scaphoid in African apes results in an appreciably larger radius facet (Figures 15 and 16) (Kivell et al., 2013), which almost certainly acts to reduce proximodistally directed compressive stress. In contrast, the scaphoid in humans is shorter (Table 6). In African apes, the scaphoid has increased bone along its distoulnar edge (i.e., the centrale portion of the scaphoid), which results in a larger area for the trapezoid on its distal surface (Figures 15, 16, 21, and 22). The additional bone along the scaphoid's distoulnar edge fits into the waisted neck of the capitate (Figure 21), a mechanism that has been shown to stabilize the midcarpal joint when the wrist is extended during knuckle-walking (Orr, 2017, 2018; Orr et al., 2010). Conversely, in humans the scaphoid has a reduction of bone along its distoulnar edge (Figure 23, Table 6) (Tocheri, 2007).

The warps demonstrate that the capitate neck is radioulnarly thinner in African apes due to a deeply excavated radial surface of the bone and a more curved hamate facet (Figure 24).

This morphology creates a deep concavity that articulates with the centrale portion of the scaphoid (Figure 21) which, as discussed above, likely stabilizes the wrist when it is extended during knuckle-walking. The waisted neck may be derived in African apes as it is absent in other primates, including suspensory Asian apes and other terrestrial quadrupeds (Wuthrich et al., 2019). In contrast, the capitate neck is thicker in humans due to a less excavated radial surface of the bone as well as a flatter hamate facet (Figure 24, Table 6). This morphology may better withstand radioulnarly directed forces being transmitted from the trapezoid to the hamate through the capitate. A thicker neck has been documented previously in humans, although this was primarily attributed to the excavation of bone on the radial side of the bone (Lewis, 1973, 1989).

The capitate-MC3 facet in African apes is dorsopalmarly longer and lacks bevelled dorsoradial corner, as well as a more irregular surface (Figures 14 and 24). The larger MC3 facet may reduce compression stress from proximodistally directed forces while the more irregular MC3 facet quantifies what McHenry (1983) called "cupping," and may facilitate close-packing of the wrist for stability during knuckle walking (Table 6). A recent kinematic study has shown that the capitate-MC3 joint in chimpanzees has a reduced range of motion compared to that of orangutans and monkeys (Orr, 2017). Conversely, the capitate-MC3 facet in humans is dorsopalmarly shorter and has a bevelled dorsoradial corner (Table 6). This confirms previous findings that humans have smaller MC3 facets compared to great apes, as well as bevelled dorsoradial corners to accommodate the MC3 styloid process (Marzke and Marzke, 1987; Orr et al., 2013). The shorter MC3 facet is likely due to fusion of the dorsal ossification center onto the MC3 base, forming the styloid process, rather than the dorsoradial corner of the capitate as it does in apes (Marzke and Marzke, 1987). During power grips, large forces directed to the palmar

aspect of the MC3 head displace the base in a palmar direction (Marzke, 1983; Williams et al., 2012). Thus, the MC3 styloid process may prevent hyperextension of the MC3 as well as sliding and subluxation of its base when the MC3 head experiences external palmar forces, such as those that occur during forceful hammering (Lewis, 1989; Marzke and Marzke, 1987; McHenry, 1983).

The MC2 facets on the trapezium and capitate are more radioulnarly orientated in African apes (Figures 15, 16, 21). This difference in the MC2 facet orientation was previously quantified using joint angles (Tocheri, 2007), and act to stabilize the MC2 during proximodistally directed forces. The flexor carpi radialis inserts into the palmar base of the MC2 (Bishop et al., 1994) and the first dorsal interosseous muscle originates at the dorsal shafts of the MC1 and MC2 (Infatalino and Challis, 2010), and both of these muscles pull the base of the MC2 proximally during grips with neutral or adducted thumb postures (Tocheri, 2007). As shown in the articulated wrist (Figure 21), the more radioulnarly orientated MC2 facets as well as the narrow palmar portion of the trapezoid make it so that contraction of the flexor carpi radialis and first dorsal interosseous muscles pulls the MC2 base proximally in between the trapezium and capitate. This prevents the base of the MC2 from sliding radioulnarly such that maximum contact is maintained between the mutual carpometacarpal joint surfaces, facilitating the distribution of proximodistally directed forces (Marzke, 1983; Marzke et al., 1992; Tocheri, 2007). In contrast, the MC2 facets on the trapezium and capitate are more proximodistally orientated in humans (Figures 15, 16, 21), which act to stabilize the distal carpal row during radioulnarly directed forces (Table 6). The more proximodistally orientated MC2 facets as well as the expanded palmar portion of the trapezoid make it so the MC2 will come down on top of the trapezium and capitate and lock them into place during these grips (Figure 21). This arrangement prevents the

trapezium and capitate from sliding distally relative to the second metacarpal base such that maximum contact is maintained with their mutual articular facets with the trapezoid, facilitating the distribution of radioulnarly directed forces (Marzke, 1983; Marzke et al., 1992; Tocheri, 2007). Since the MC2 base is not lodged between the capitate and trapezium in humans, the MC2 base may also be able to pronate during grips, which would facilitate pad-to-side and three-jaw chuck precision grips (Marzke, 1983, 1997; Marzke et al., 1992).

Variation among African apes

A final aim of this study was to document how radial wrist shape varies among African ape taxa. The warps along PC1 of the four-bone and three-bone analyses for African apes only (Figures 25 and 26) revealed several differences in radial-side wrist morphology between *Pan* and gorillas. Overall, *Pan* have taller and thinner carpals, while gorillas have shorter and stouter carpals. *Pan* has radioulnarly narrower trapeziums with more curved MC1 facets, proximodistally shorter MC2 facets, and proximodistally taller and more tilted trapezoid facets (Figures 29 and 30). In contrast, gorillas have wider trapeziums with flatter MC1 facets, taller MC2 facets, and shorter and less tilted trapezoid facets.

The three-bone analysis also found that *Pan* has radioulnarly narrower scaphoid facets compared to those of gorillas (Figure 30). *Pan* has trapezoids that are proximodistally taller but radioulnarly narrower, with proximodistally taller trapezium facets that are tilted ulnarly (Figure 30). Conversely, gorillas have trapezoids that are shorter but wider, with shorter trapezium facets that are less tilted. In terms of the trapezoid, the four-bone analysis found that *Pan* has more radioulnarly oriented ulnar MC2 facets compared to gorillas (Figure 33). The three-bone analysis also found that *Pan* trapezoids have smaller ulnar MC2 facets and dorsopalmarly shorter scaphoid facets but dorsopalmarly longer radial MC2 facets relative to gorillas (Figures 34, 35,

36). *Pan* has dorsopalmarly thinner scaphoids with larger capitate facets, while gorillas have thicker scaphoids with smaller capitate facets (Figures 31, 32, 33, 36). Finally, *Pan* has proximodistally longer capitates with proximodistally longer MC2 and hamate facets but dorsopalmarly shorter MC3 facets (Figures 33, 37, 38). In contrast, gorillas have shorter capitates with shorter MC2 and hamate facets but longer MC3 facets.

The shorter and stouter carpals in gorillas compared to those in *Pan* may reflect differences in body size and weight. Gorillas are generally larger and heavier than chimpanzees and bonobos (Coolidge and Shea, 1992; Jungers and Susman, 1984). Joint forces are roughly proportional to body mass, although their relative size can differ depending on positional behaviour and joint mobility (Godfrey et al., 1995, 1991; Preuschoft and Weinmann, 1973; Wunderlich and Jungers, 2009). Goldstein and Sylvester (2023) found that the capitate, hamate, lunate, and scaphoid of heavier taxa may be proximodistally shorter and radioulnarly wider than those of lighter taxa to accommodate the higher forelimb loading. Likewise, the gorilla trapezium, trapezoid, scaphoid, and capitate tended to be shorter and wider than the *Pan* carpals in the results of the present study. Similar patterns have been documented in the capitate (Kivell et al., 2013) as well as in other hand elements. For instance, gorilla metacarpals and phalanges are "short and stout" while those of chimpanzees are "long and thin" (Hamrick and Inouye, 1995; Inouye, 1992; Schultz, 1936; Susman, 1979). Figure 49 shows a subtle trend across taxa in the relationship of PC1 scores and centroid sizes (but not within taxa), and this may reflect higher forelimb loading in gorillas, especially large adult males. However, the effects of size on carpal morphology among African ape taxa require further investigation.

According to the warps along PC1 of the three-bone analysis for African apes only, *Pan* has a prominent scaphoid beak on the radius facet whereas this feature is absent in gorillas

(Figure 30). The scaphoid beak has been suggested to limit wrist extension at the radiocarpal joint (Kivell and Schmitt, 2009). Gorillas also often lack a dorsal concavity on their scaphoids as well as a distal concavity and dorsal ridge on their capitates, which may also limit extension (Kivell and Schmitt, 2009). These features were not detected by the warps in this study, perhaps because they are small and subtle and thus may require higher density semilandmark patches to be detected. The warps also failed to detect the less pronounced waisting of the capitate neck observed in gorillas, which has been attributed to filling in of the deep radial excavation that exists in *Pan* (Lewis, 1973). The warps may not have been able to detect this morphology due to the lack of semilandmarks on the nonarticular surface on the radial side of the capitate.

The warps along PC2 of the four-bone analysis for African apes only (Figure 25) detected features that gorillas and bonobos share to the exclusion of chimpanzees. Gorillas and bonobos have trapeziums with dorsopalmarly flatter MC1 facets, radioulnarly wider scaphoid facets, and dorsopalmarly wider trapezoid facets compared to chimpanzees (Figures 39 and 40). The trapezoids of gorillas and bonobos have radioulnarly wider ulnar MC2 facets and dorsopalmarly shorter radial MC2 facets (Figures 41 and 42). Chimpanzees have the opposite pattern wherein the trapezoids have narrower ulnar MC2 facets and longer radial MC2 facets. In gorillas, the scaphoid beak was absent whereas in chimpanzees this feature is prominent (Figure 39). Visual inspections of the specimens showed that some bonobos also have a less prominent or absent scaphoid beak.

The remaining variation seen in the warps along PC2 of the four-bone analysis for African apes only appear to represent morphological differences between gorillas versus *Pan*, rather than between gorillas and bonobos versus chimpanzees. For example, the trapezoid on the right in Figure 39 (representing gorillas and bonobos) is shorter and wider than the trapezoid on

the left (representing chimpanzees), although visual inspection of the specimens show that bonobo trapezoids are actually similar in shape to the latter. This discrepancy is likely because a chimpanzee and gorilla drive the variation negatively and positively, respectively, along PC2. Furthermore, PC2 only represents a small percentage (10.7%) of the total variation in the sample.

The warps along PC3 of the three-bone analysis for African apes only (Figure 26) revealed subtle differences between bonobos and chimpanzees. In general, bonobos have more slender carpals, while chimpanzees have more robust carpals. Bonobos have radioulnarly narrower trapeziums with more radioulnarly curved MC1 facets and proximodistally taller trapezoid facets. In contrast, chimpanzees have wider trapeziums with flatter MC1 facets and shorter trapezoid facets (Figure 44). Bonobo trapezoids have a narrower palmar nonarticular area due to radioulnarly wider and more radioulnarly orientated ulnar MC2 facets (Figure 46). Chimpanzees have the opposite pattern wherein the trapezoids have a broader palmar nonarticular area due to narrower and more proximodistally orientated ulnar MC2 facets. Bonobos also have trapezoids with radioulnarly narrower radial MC2 facets, while in chimpanzees these facets are wider (Figure 47). Bonobo scaphoids are proximodistally taller and dorsopalmarly thinner with proximodistally taller capitate facets (Figures 45 and 48). Conversely, chimpanzee scaphoids are shorter and thicker with shorter capitate facets.

As discussed above, joint forces are roughly proportional to body mass and the carpals of heavier taxa may be more robust to accommodate the higher forelimb loading (Godfrey et al., 1995, 1991; Goldstein and Sylvester, 2023; Preuschoft and Weinmann, 1973; Wunderlich and Jungers, 2009). Thus, the more slender carpals of bonobos could be related to body size and gracility. Bonobo body weight averages are generally smaller than chimpanzees, although ranges overlap considerably (Druelle et al., 2018; McHenry and Corruccini, 1981; Zilhman and Cramer,

1978), and one study observed that bonobos are only smaller than *P. t. troglodytes* (central chimpanzees) but similar or even larger in body weight compared to western and eastern chimpanzees (Smith and Jungers, 1997). Bonobos may also have absolutely and relatively lighter body segments (e.g., head, trunk, upper arm, lower arm, thigh) than chimpanzees (Coolidge and Shea, 1982; Druelle et al., 2018; Zihlman and Cramer, 1978), although when measurements were scaled relative to body mass only the lighter thigh of the bonobo remained statistically significant (Druelle et al., 2018).

Although not all features detected by the warps have a readily apparent function, there is clearly variation in carpal morphology among the African apes. In addition to differences in body size and mass, variation in carpal morphology could be related to differences in the amount of climbing behaviours they engage in. Gorillas are generally less arboreal than chimpanzees and bonobos (Doran, 1993, 1997; Doran and Hunt, 1994; Hunt, 1992, 1994; Sarringhaus et al., 2014; Susman, 1984; Susman et al., 1980). Thus, it would be reasonable to predict that chimpanzee and bonobo wrist morphology may reflect more adaptations to suspension and climbing. Studies comparing hand bone morphology between African apes are limited, although Kralick and Tocheri (2014) found differences in carpal morphology that suggested western gorillas may have a more mobile midcarpal joint and grasping thumb compared to their less arboreal counterparts, the eastern gorillas. Meanwhile, the stout carpals observed in the warps representing gorillas may reflect adaptations to increased terrestriality. In terms of *Pan*, although studies at Lomako reported arboreal travel and suspensory behaviour more frequently in bonobos (Doran, 1992, 1993, 1996; Susman, 1979), more recent studies at Lui Kotale on better habituated bonobo populations observed that they spend similar amounts of time arboreally as western and eastern chimpanzees and are less suspensory (Hunt, 2016; Ramos, 2014). However, the frequency of

some arboreal locomotor behaviours (arboreal quadrupedalism, climbing and scrambling, and suspensory locomotor bouts) were similar to that reported previously in infant and juvenile chimpanzees (Ramos, 2014). Further studies are clearly needed to clarify locomotor behaviours among African apes in order to make appropriate interpretations regarding functional morphology.

Variation in carpal morphology could also be related to biomechanically different forms of knuckle walking among African apes. For instance, gorillas bear weight primarily on the second and third digits while *Pan* bears weight primarily on the third and fourth digits (Matarazzo, 2013; Tuttle, 1967; Wunderlich and Jungers, 2009). *Pan* do not use their fifth digits as much during knuckle walking whereas gorillas distribute weight more evenly across digits two to five, which may occur because gorillas have more evenly aligned digits due to reduced variability in metacarpal and phalangeal lengths (Inouye, 1992, 1994; Matarazzo, 2013; Susman, 1979; Tuttle, 1967). Furthermore, gorillas prefer fully pronated (i.e., palm facing posteriorly or "palm-back") hand postures during knuckle-walking while chimpanzees are more variable, and use both pronated and semipronated (i.e., palm facing medially or "palm-in") hand postures, which can affect digit loading (Inouye, 1994; Matarazzo, 2013; Samuel et al., 2018; Thompson, 2020; Tuttle, 1967, 1969). Kivell and Schmitt (2009) proposed that gorillas may compensate for their lack of extension-limiting features via a more columnar wrist posture during knuckle walking (i.e., where the forearm, carpal joints, and hand are aligned). Meanwhile, the extension-limiting features in *Pan* may reflect extended wrist postures which would lower their center of gravity for better balance on arboreal substrates (Kivell and Schmitt, 2009). Consistent with this hypothesis, larger animals generally use more extended limb postures to align their limbs with ground reaction forces, reducing the forces their muscles must exert to counteract

joint moments, although this pattern was only studied at the elbow and knee joints in primates (Biewener, 1989; Polk, 2004; Polk et al., 2009). However, recent kinematic studies found that wrist posture is similarly columnar (i.e., only slightly extended) during knuckle walking in both *Pan* and gorillas, and failed to detect any significant effect of body mass on forelimb and hindlimb joint angles (Finestone et al., 2018; Thompson, 2020). Similarity in African ape terrestrial walking kinematics may reflect their similar postcranial anatomy and proportions (i.e,, large body, long forelimb, orthograde body plan) (Finestone et al., 2018).

Within *Pan*, bonobos were suggested to have a lower intermembral index and a more pronograde stance when knuckle walking compared to chimpanzees (Coolidge and Shea, 1982; Shea, 1981; Susman, 1979; Zilhman and Cramer, 1978), although recent studies found that absolute and relative lengths of the hindlegs between bonobos and chimpanzees were statistically indistinguishable (Druelle et al., 2018). Although studies on terrestrial substrates are lacking, on arboreal substrates bonobos were observed to use a palm-back posture more frequently than a palm-in posture and the fifth digit nearly always contacted the substrate (Samuel et al., 2018). Furthermore, Samuel et al. (2018) found that bonobos do not have a rolling pattern of contact during knuckle walking as reported in chimpanzees (Matarazzo, 2013; Richmond et al., 2001), so the former may experience less shear stress (Samuel et al., 2018).

Gorillas diverged from the lineage eventually leading to the *Pan-Homo* clade approximately 10 million years ago (Scally et al., 2012; Yoder and Yang, 2000) while chimpanzees and bonobos diverged approximately 1 to 2 Ma (Prüfer et al., 2012). Thus, wrist morphology differences among African apes could also be due to genetic drift, rather than reflect adaptive features.

Conclusions and Recommendations for Future Research

This study has highlighted the potential utility of intact cadaver wrists and manually articulated 3D models to study the wrist as a morphological and functional unit in primates. As predicted, the human wrists displayed a complex of distinct features that appears to provide biomechanical advantages for withstanding and distributing large forces directed radioulnarly during human-like power and precision grips. In contrast, the African ape wrists showed a complex of features that provides biomechanical advantages for withstanding and distributing forces directed proximodistally during knuckle walking and other locomotor behaviours. Additionally, warping the mean articulated wrist shape of the entire sample along various PCs helped to visualize variation that had been described but not quantified by previous morphometric studies on isolated carpals (Kivell et al., 2015; Tocheri, 2007; Tocheri et al., 2005, 2007; Orr et al., 2013; Wuthrich et al., 2019). For instance, the warps showed that expansion of the palmar aspect in human trapezoids has indeed resulted in 'pushing' the trapezium radially onto the scaphoid tubercle into a more supinated position, resulting in a shallower carpal tunnel relative to that of African apes.

Only the articular surfaces of the studied carpal bones were landmarked and as a result, some of the warps looked odd. Applying landmarks or semilandmark curves or patches to nonarticular surfaces (e.g., the scaphoid tubercle) could likely improve the visualization of the shape variation that exists among extant African apes and humans. Nonetheless, this study identified several previously undescribed differences in wrist morphology between *Pan* and *Gorilla* as well as among gorillas, chimpanzees, and bonobos. These differences may be related to variation in body size and weight and/or locomotor behaviour in these taxa.

Expanding the sample size and breadth to include the ulnar-side carpals as well as other primate species and locomotor repertoires would be the goal for future studies. In particular, *Pongo* (i.e., orangutans) is the closest living relative of African apes and humans and is primarily suspensory (Cant, 1987; Thorpe and Crompton, 2006), so could provide important insights about the evolutionary polarity of features that are variable among African apes as well as features that may be adaptively related to arboreal behaviours. Orangutans and other nonhominine primates were not included in this study because their centrale is not fused to the scaphoid. This presents a major difficulty in applying landmarks to that particular surface, which would need to be overcome. Adding mountain gorillas could also help to identify features that may be related to increased levels of terrestriality among African apes. Future studies could also analyze the articulated wrists in different positions, for example, in the extended position used during knuckle walking and making and using tools. A comparative dataset of articulated primate wrists that includes a comprehensive range of species, locomotor repertoires, and wrist postures could be used to study the morphology and function of extant and fossil wrists.

The manually articulated 3D models used in this study may be a useful method to supplement samples of intact wrists in extant species, as well as to study fossil specimens. Different combinations of bones can be analyzed without having to relandmark the entire sample with each new combination, which would be ideal when working with fossils where it is rare that all carpals are preserved. Furthermore, for fossil specimens that are broken, missing landmarks can easily be removed across the entire sample for analysis. Quantifying the wrist morphology of fossil specimens has the potential to help reconstruct the phylogenetic relationships among extinct hominin species while also providing important details about the origins and persistence of stone tool manufacture in human evolution (Corruccini et al., 1975; Kivell, 2015; Kivell et al.,

2011, 2015, 2018; Marzke, 1983, 2013; Marzke and Shackley, 1986; Napier, 1962; Orr et al., 2013; Richmond et al., 2020; Richmond and Strait, 2000; Susman and Creel, 1979; Susman, 1991; Tocheri et al., 2007; Ward et al., 2014). Previous morphometric studies have examined isolated carpals from various fossil hominins, including Neandertals, *Homo naledi*, and *Homo floresiensis* (Kivell et al., 2015; Orr et al., 2013; Tocheri, 2007; Tocheri et al., 2007). Analysis of these carpals as articulated units could potentially support previous observations and reveal new insights on the overall morphology and function of fossil hominin wrists.

Figures

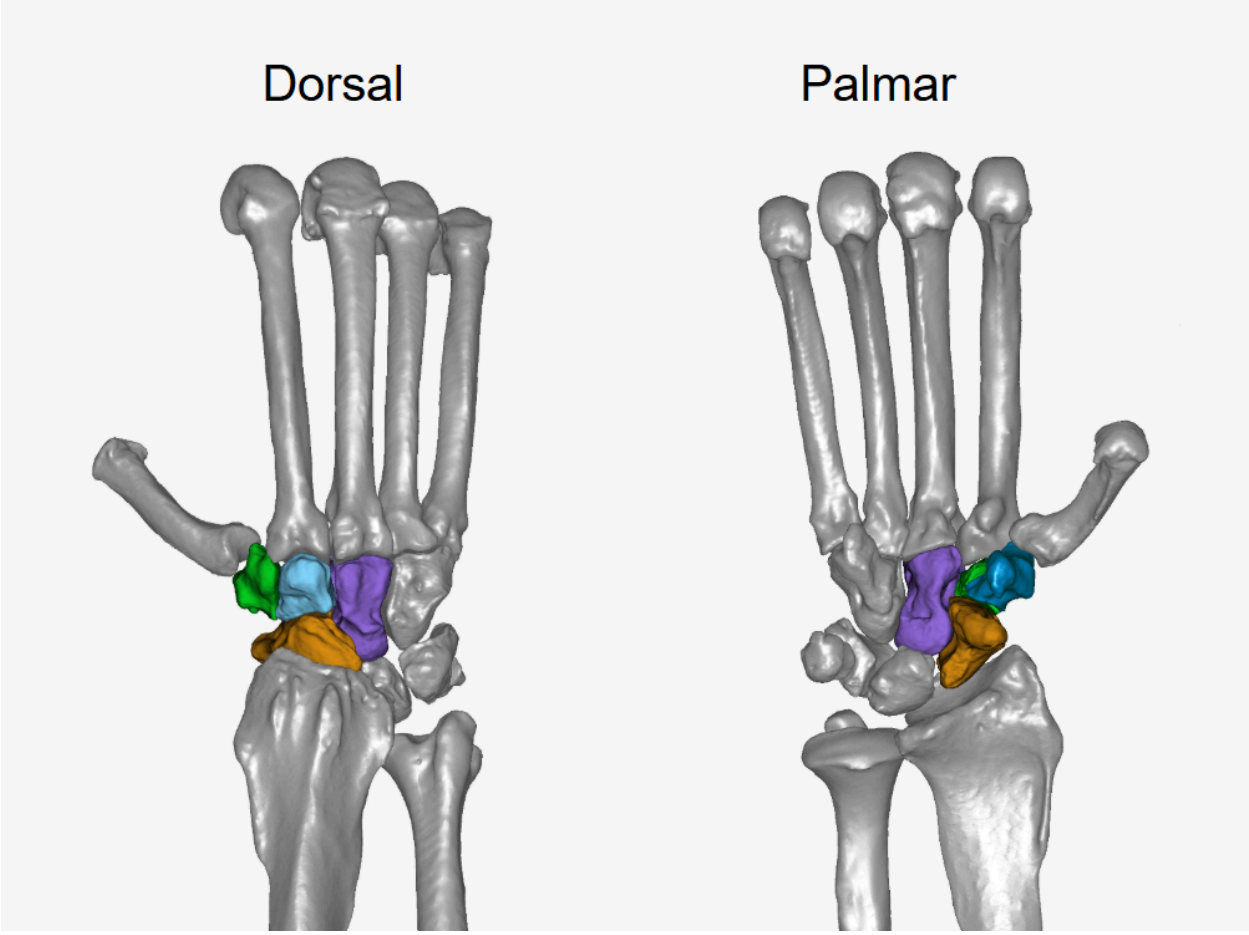

Figure 1. Dorsal and palmar views of a chimpanzee wrist as scanned in an intact cadaver arm. The trapezium (green) articulates ulnarly with the trapezoid and MC2, proximally with the scaphoid, and distally with the MC1. The trapezoid (blue) articulates radially with the trapezium, ulnarly with the capitate, proximally with the scaphoid, and distally with the second metacarpal. The scaphoid (orange) articulates ulnarly with the capitate and lunate, proximally with the radius, and distally with the trapezoid and trapezium. The capitate (purple) articulates radially with the trapezoid, ulnarly with the hamate, distally with the MC2, MC3, and variably the MC4, and proximally with the scaphoid and lunate. (RETURN TO TEXT)

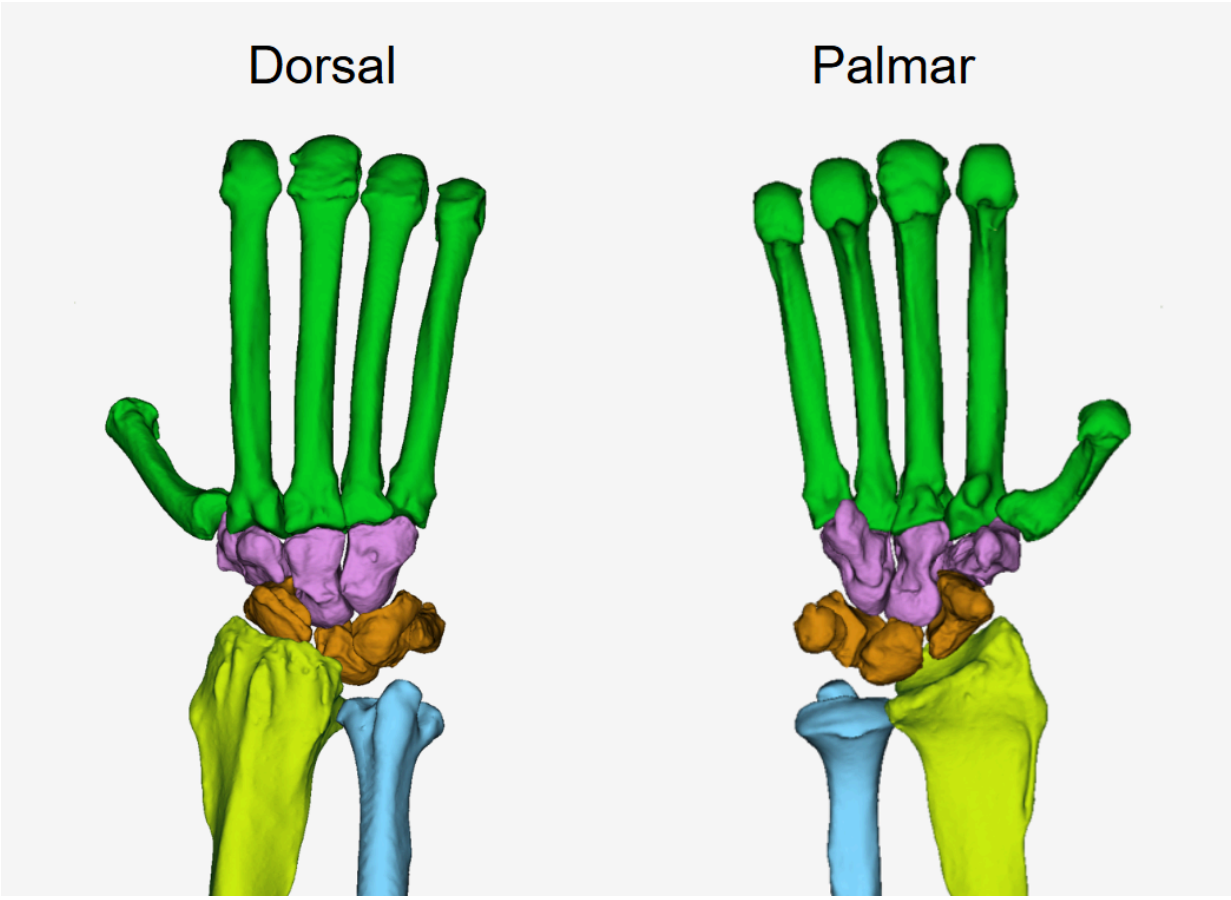

Figure 2. Dorsal and palmar views of a chimpanzee wrist as scanned in an intact cadaver arm (metacarpals, green; distal carpal row, pink; proximal carpal row, orange; radius, yellow; ulna, blue). (RETURN TO TEXT)

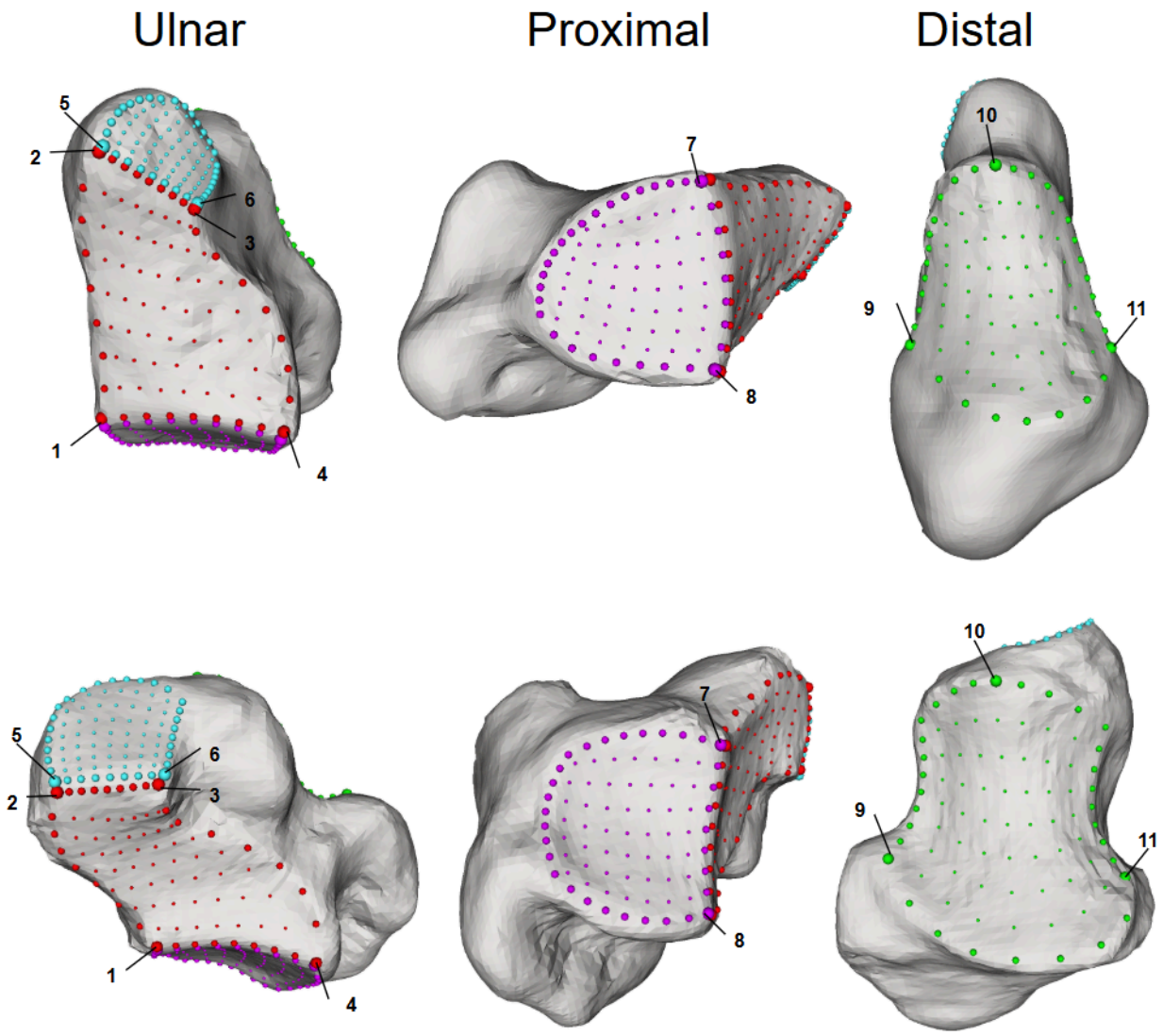

Figure 3. The trapezium of a chimpanzee (top) and human (bottom). Bones are from the same side and scaled approximately to the same size. Four semilandmark patches, used in this study to capture variation in shape and position of the trapezium within the radial wrist, were placed on the articular facets (trapezoid, red; MC2, blue; scaphoid, pink; MC1, green). The large numbered points are anchor landmarks used to place the patches (see Table 2), the medium-sized points along the outlines of each facet are fixed semilandmarks, and the smaller points are surface sliding semilandmarks. (RETURN TO TEXT)

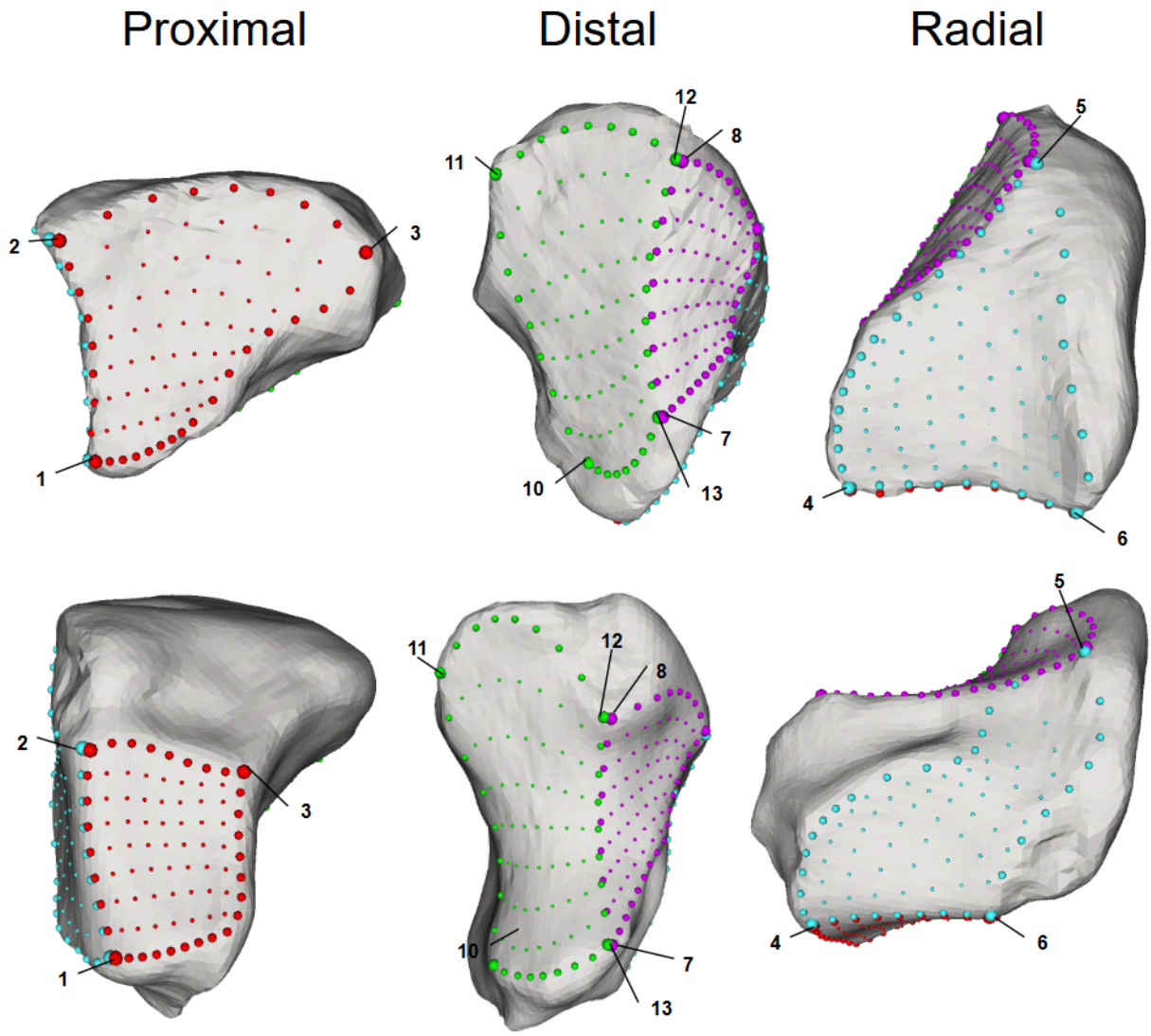

Figure 4. The trapezoid of a chimpanzee (top) and human (bottom). Bones are from the same side and scaled approximately to the same size. Four semilandmark patches, used in this study to capture variation in shape and position of the trapezoid within the radial wrist, were placed on the articular facets (scaphoid, red; radial portion of the MC2, pink; ulnar portion of the MC2, green; trapezium, blue). The large numbered points are anchor landmarks used to place the patches (see Table 3), the medium-sized points along the outlines of each facet are fixed semilandmarks, and the smaller points are surface sliding semilandmarks. (RETURN TO TEXT)

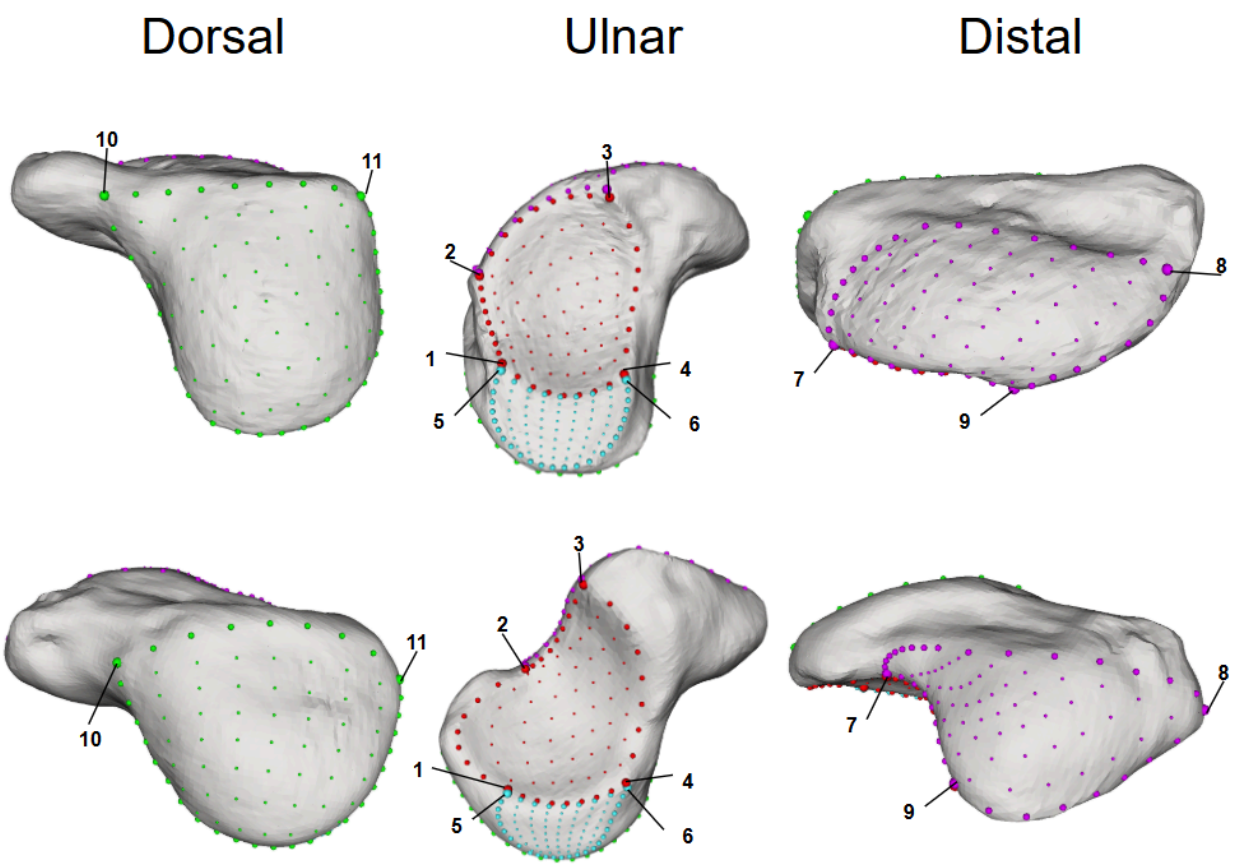

Figure 5. The scaphoid of a chimpanzee (top) and human (bottom). Bones are from the same side and scaled approximately to the same size. Four semilandmark patches, used in this study to capture variation in shape and position of the scaphoid within the radial wrist, were placed on the articular facets (radius, green; capitate, red; lunate, blue; trapezium-trapezoid, pink). The large numbered points are anchor landmarks used to place the patches (see Table 4), the medium-sized points along the outlines of each facet are fixed semilandmarks, and the smaller points are surface sliding semilandmarks. (RETURN TO TEXT)

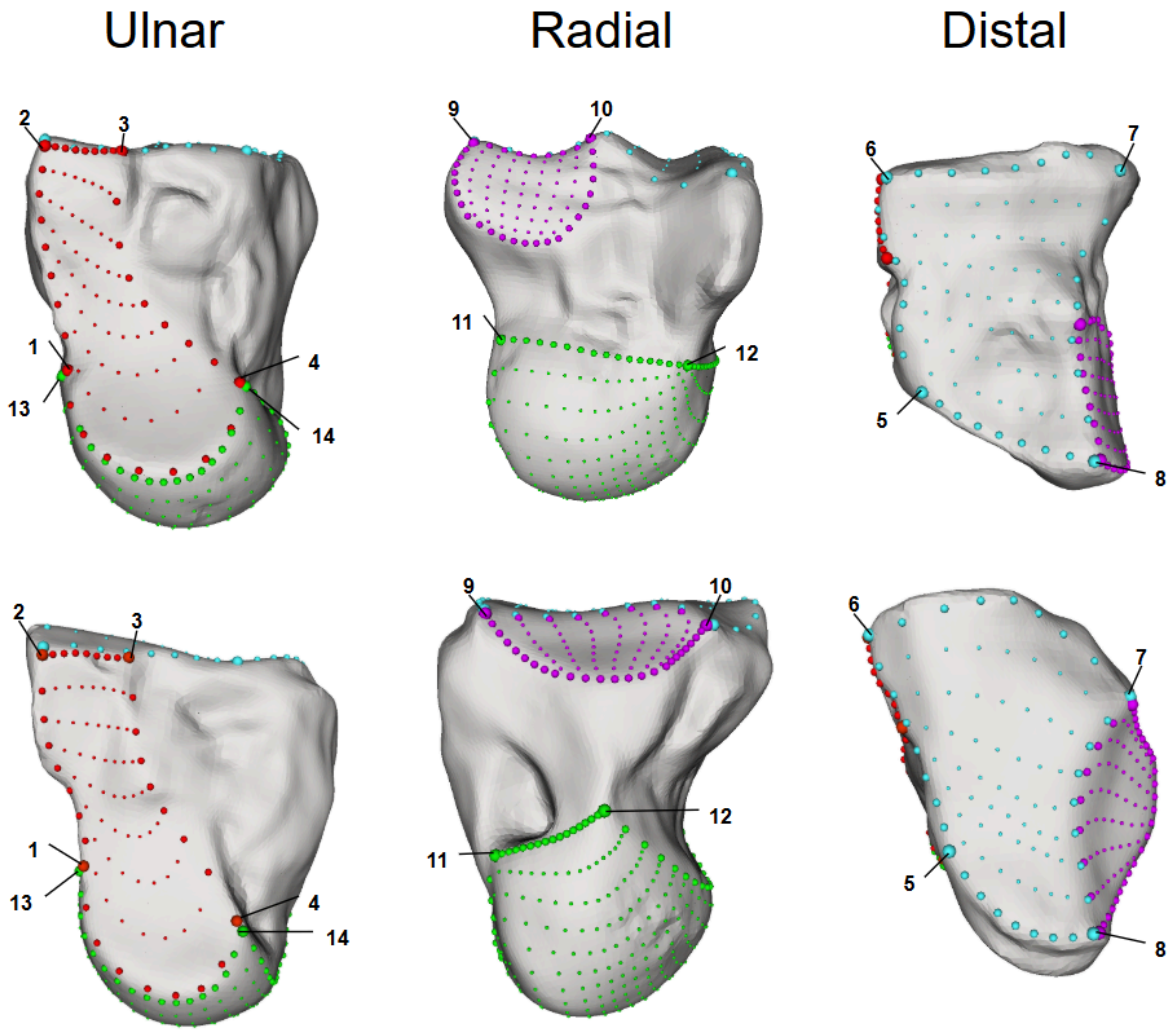

Figure 6. The capitate of a chimpanzee (top) and human (bottom). Bones are from the same side and scaled approximately to the same size. Four semilandmark patches, used in this study to capture variation in shape and position of the capitate within the radial wrist, were placed on the articular facets (hamate, red; MC2, pink; MC3, blue; capitate-lunate, green). The large numbered points are anchor landmarks used to place the patches (see Table 5), the medium-sized points along the outlines of each facet are fixed semilandmarks, and the smaller points are surface sliding semilandmarks. (RETURN TO TEXT)

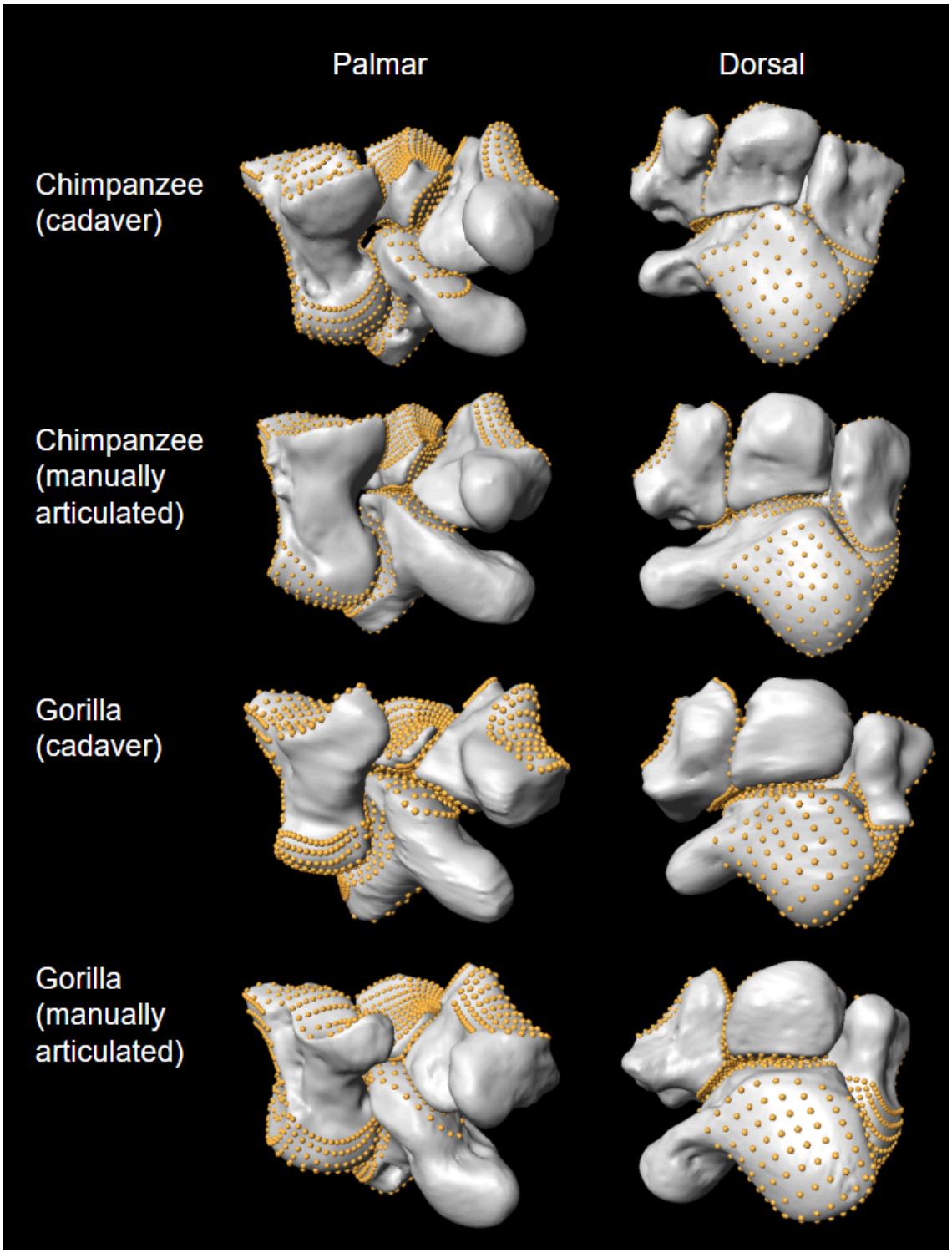

Figure 7. The entire landmark set used in the analyses as shown on the wrist bones of chimpanzees and western lowland gorillas that were CT scanned in articulation in an intact cadaver forearm or manually articulated using separate laser scans of each bone. (RETURN TO TEXT)

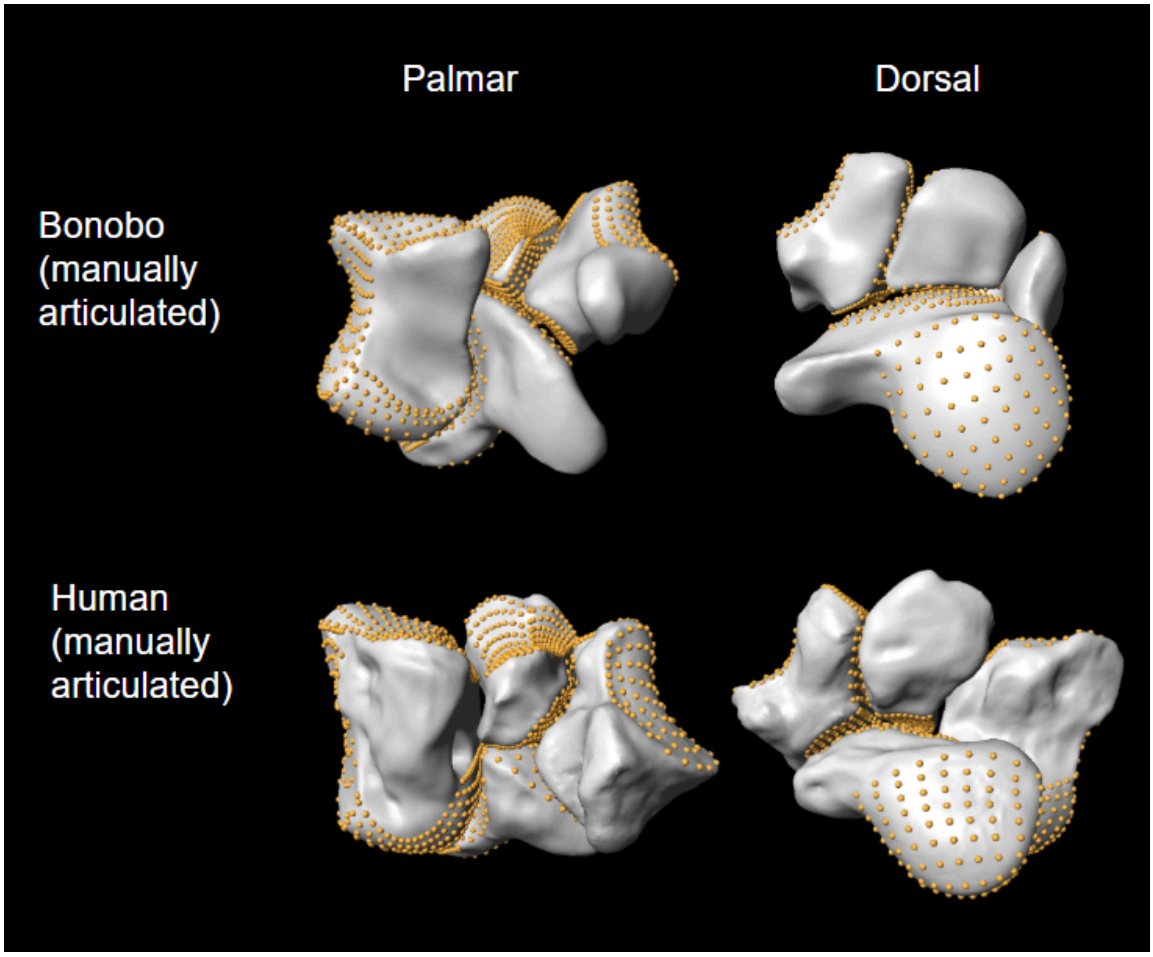

Figure 8. The entire landmark set used in the analyses as shown on the wrist bones of a bonobo and human that were manually articulated using separate laser scans of each bone. (RETURN TO TEXT)

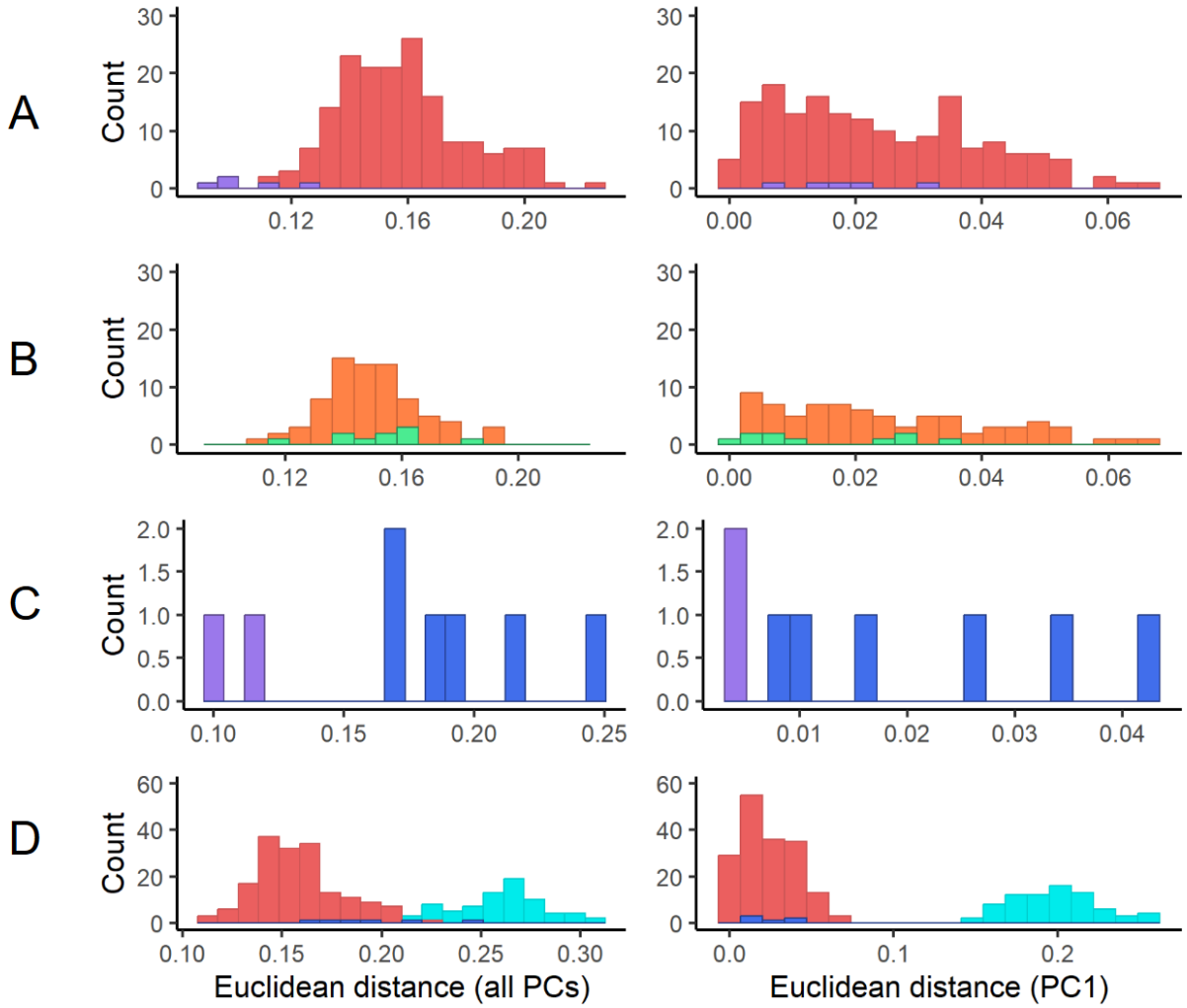

Figure 9. Euclidean distances of all PC scores and PC1 scores for the four-bone analysis. All pairwise distances were calculated A) within the chimpanzee sample (red) and the chimpanzee individuals articulated independently by two observers (purple), B) within the chimpanzee sample from intact cadaver arms (green) and the chimpanzee sample that was manually articulated (orange), C) within the human sample (dark blue) and the human individuals articulated independently by two observers (purple), and D) within the chimpanzee (red) and human (dark blue) samples as well as between the African ape and human samples (light blue). (RETURN TO TEXT) (RETURN TO DISCUSSION)

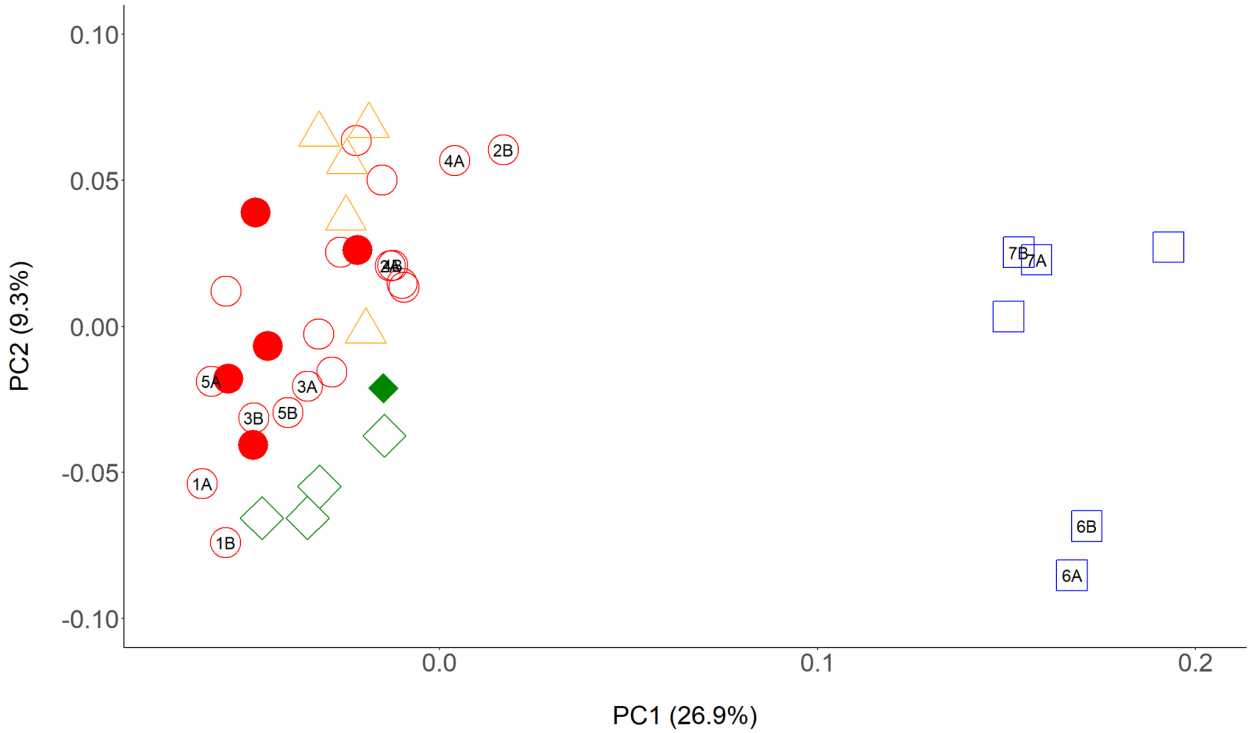

Figure 10. Plot of the principal components (PC1, PC2) generated from landmark data of the articulated trapezium, trapezoid, scaphoid, and capitate (humans = blue squares, chimpanzees = red circles, bonobos = yellow triangles, western gorillas = green diamonds). Closed and open shapes represent intact cadaver and manually articulated specimens, respectively. Symbols with the same number indicate duplicate articulations (A = OL's articulation, B = Dr. Tocheri's articulation). (RETURN TO TEXT) (RETURN TO DISCUSSION)

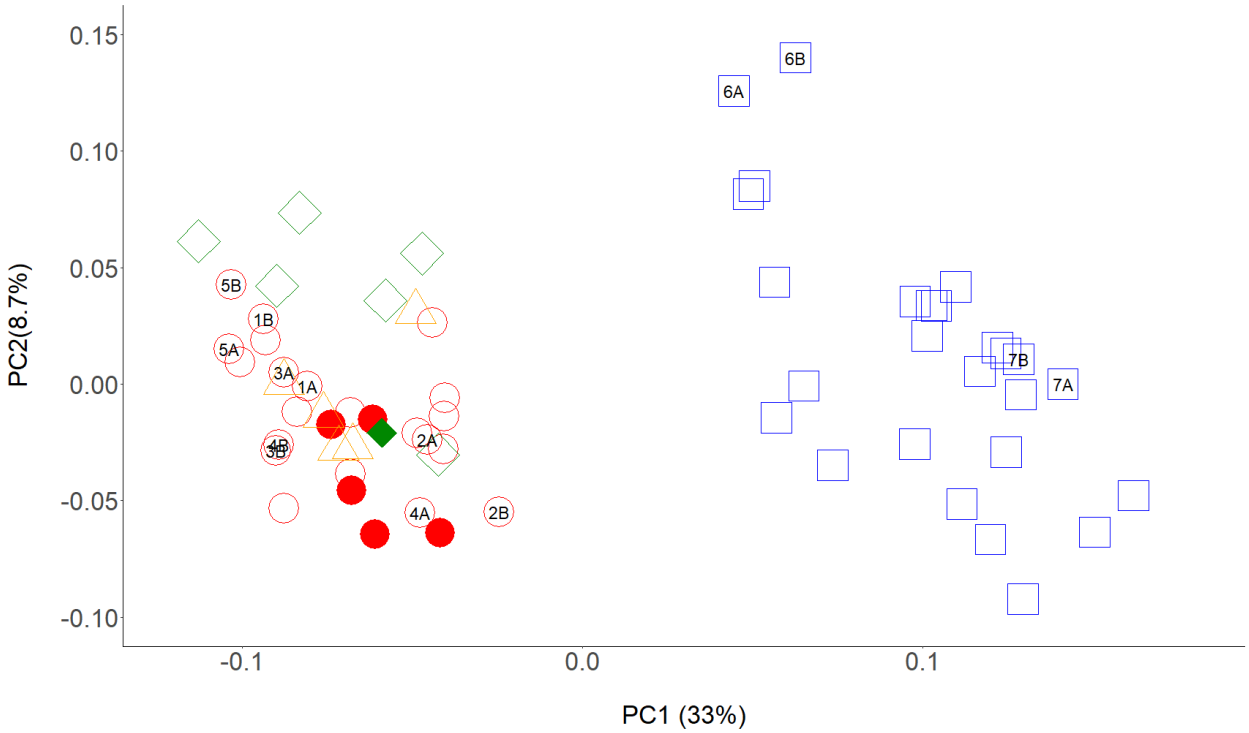

Figure 11. Plot of the principal components (PC1, PC2) generated from landmark data of the articulated trapezium, trapezoid, and scaphoid (humans = blue squares, chimpanzees = red circles, bonobos = yellow triangles, western gorillas = green diamonds). Closed and open shapes represent intact cadaver and manually articulated specimens, respectively. Symbols with the same number indicate duplicate articulations (A = OL's articulation, B = Dr. Tocheri's articulation). (RETURN TO TEXT) (RETURN TO DISCUSSION)

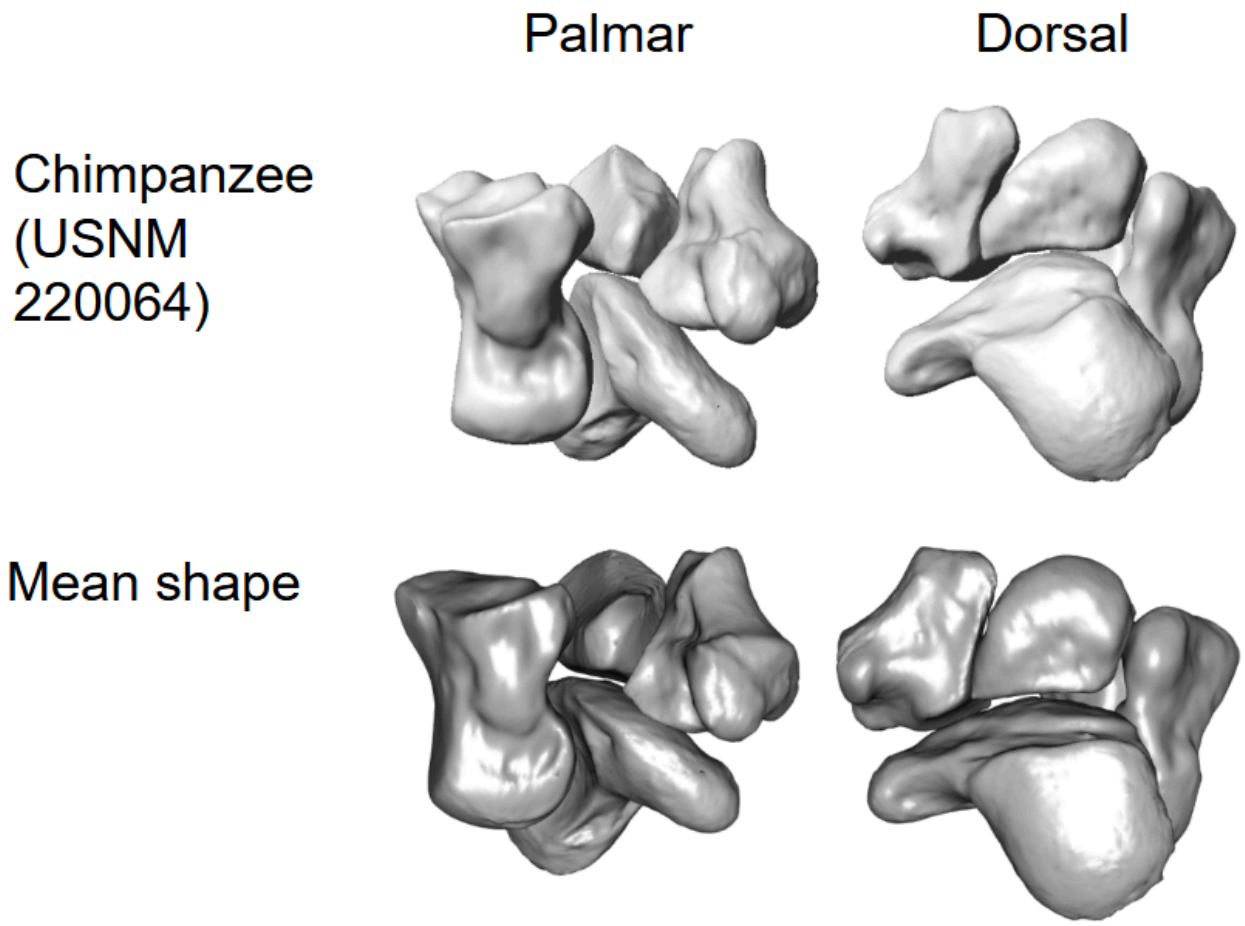

Figure 12. The chimpanzee that is most similar in overall shape to the calculated mean shape of the four-bone analysis. Thus, the mean shape shown here is USNM 220064 warped to the estimated mean landmark configuration across all PCs. (RETURN TO TEXT) (RETURN TO DISCUSSION)

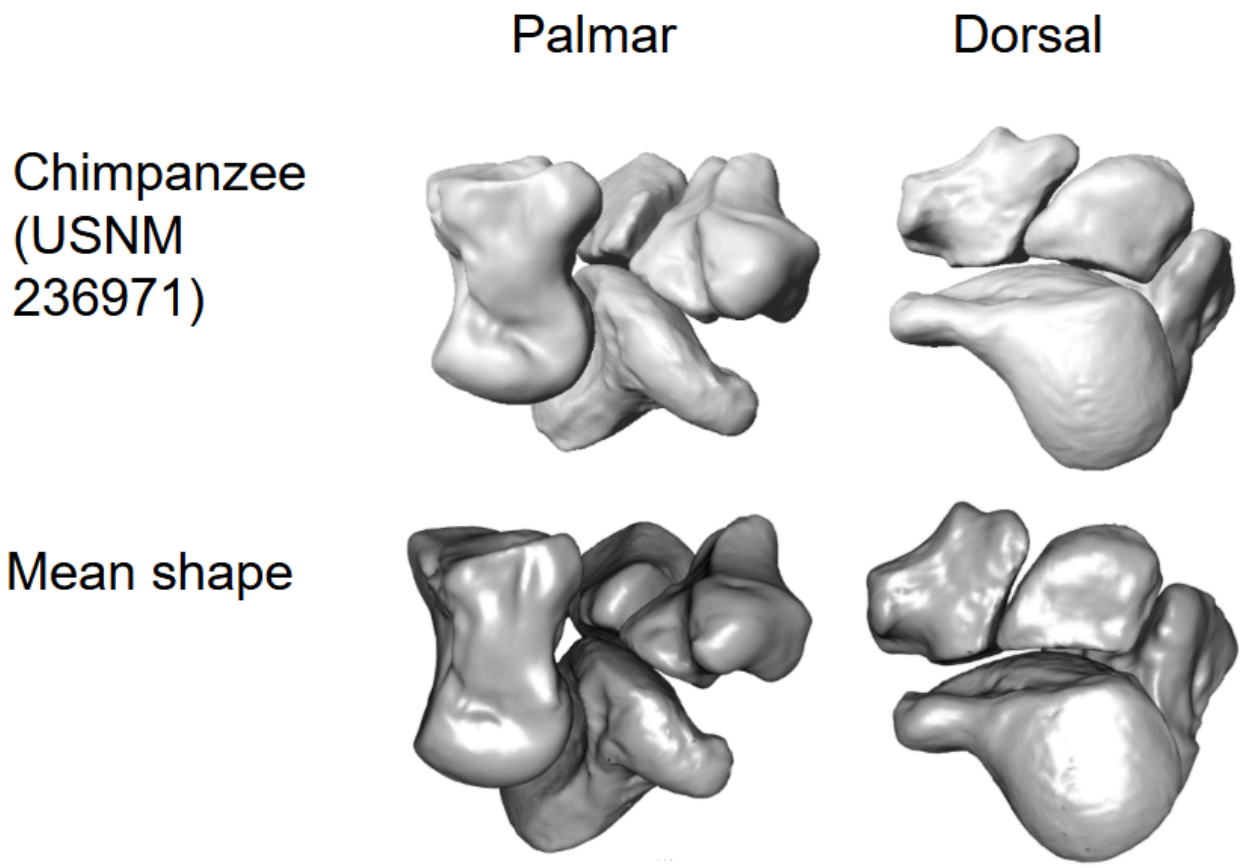

Figure 13. The chimpanzee that is most similar in overall shape to the calculated mean shape of the three-bone analysis. Thus, the mean shape shown here is USNM 236971 warped to the estimated mean landmark configuration across all PCs. (RETURN TO TEXT) (RETURN TO DISCUSSION)

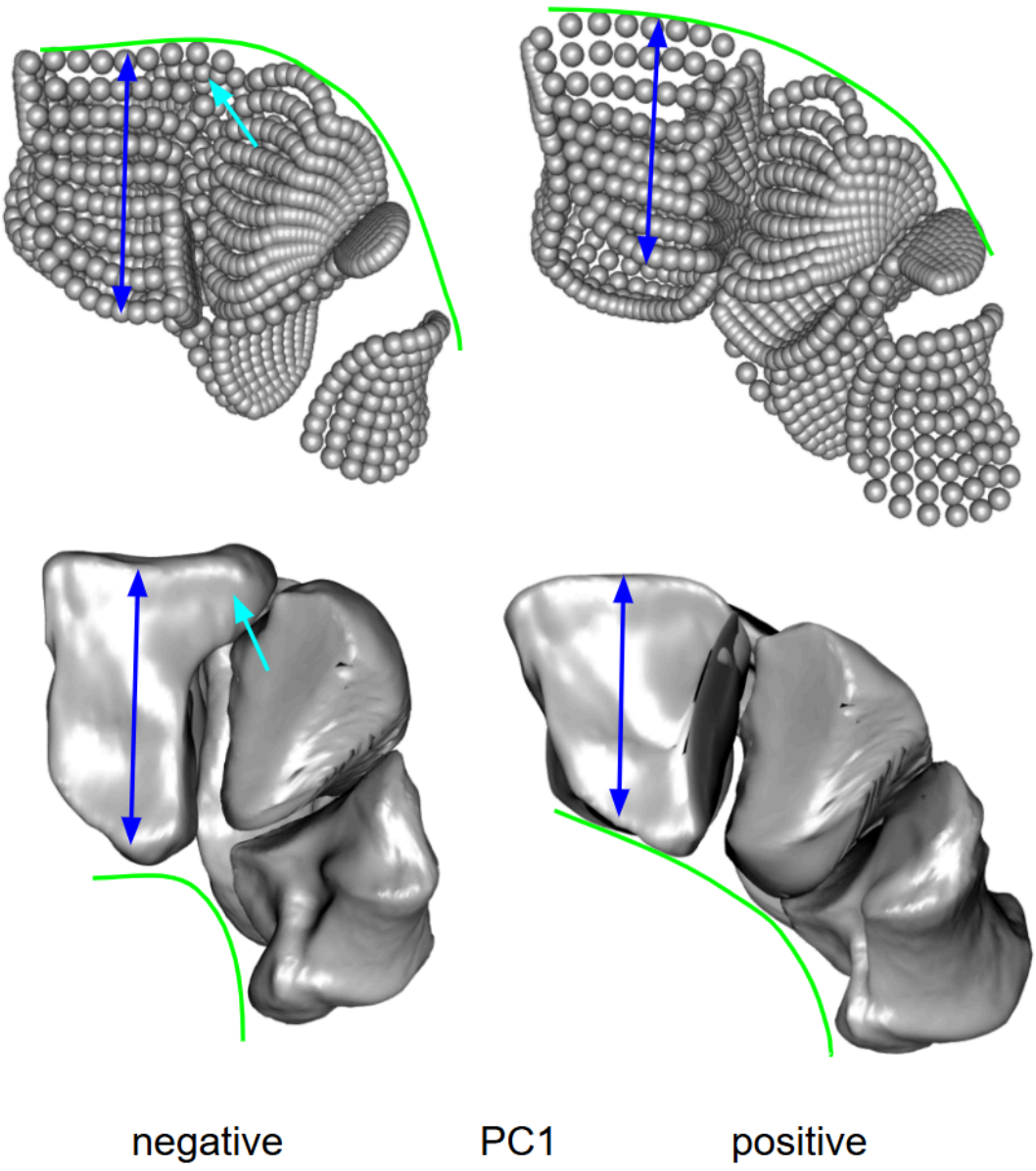

Figure 14. Distal view of the point clouds (top) and surface warps (bottom) along PC1 of the mean shape (see Figure 12) for the four-bone analysis. The annotated features differ at the positive extreme relative to the negative extreme (green, shallower carpal tunnel; light blue, lacks the fused ossification centre on the dorsoradial corner of the capitate-MC3 facet; dark blue, shorter capitate-MC3 facet). (RETURN TO TEXT) (RETURN TO DISCUSSION)

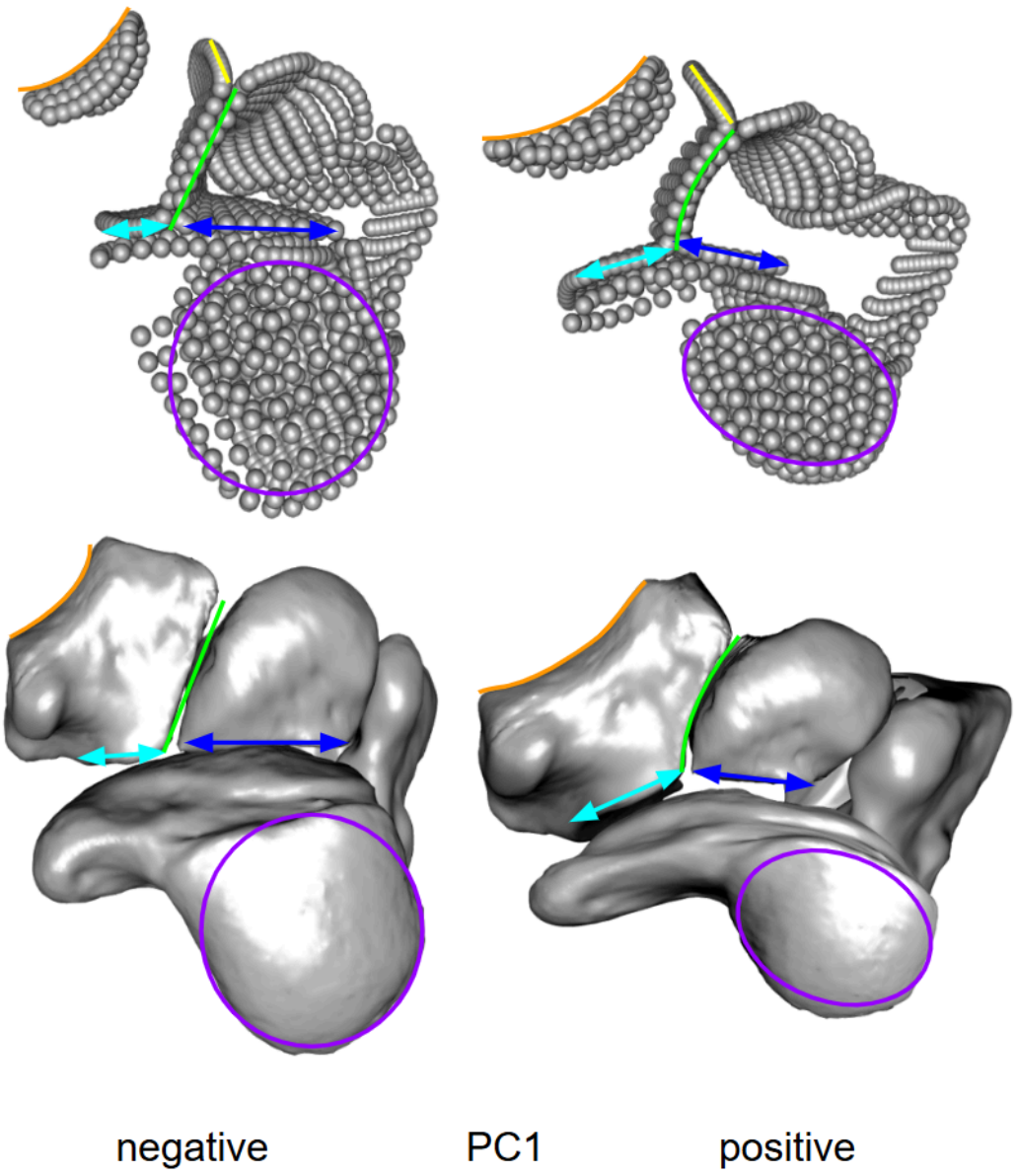

Figure 15. Dorsoradial view of the point clouds (top) and surface warps (bottom) along PC1 of the mean shape (see Figure 12) for the four-bone analysis. The annotated features differ at the positive extreme relative to the negative extreme (orange, flatter trapezium-MC1 facet; yellow, more proximodistally orientated trapezium-MC2 facet; green, more curved trapezium-trapezoid facet; light blue, larger trapezium-scaphoid facet; dark blue, smaller and rectangular trapezoid-scaphoid facet; purple, smaller and oval-shaped scaphoid-radius facet). (RETURN TO TEXT) (RETURN TO DISCUSSION)

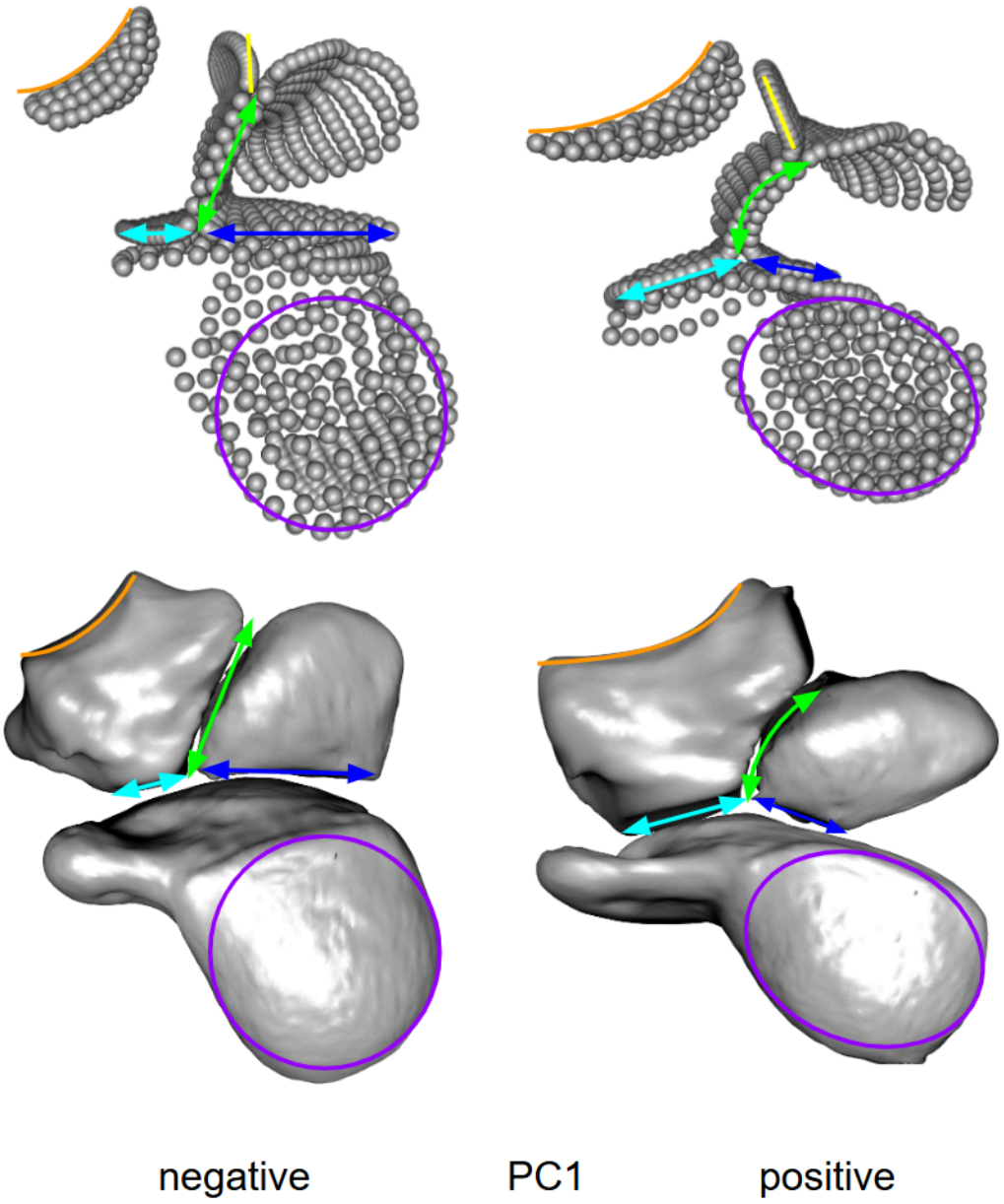

Figure 16. Dorsoradial view of the point clouds (top) and surface warps (bottom) along PC1 of the mean shape (see Figure 13) for the three-bone analysis. The annotated features differ at the positive extreme relative to the negative extreme (orange, flatter trapezium-MC1 facet; yellow, more proximodistally orientated trapezium-MC2 facet; green, shorter and more curved trapezium-trapezoid facet; light blue, larger trapezium-scaphoid facet; dark blue, smaller and rectangular trapezoid-scaphoid facet; purple, smaller and oval-shaped scaphoid-radius facet). (RETURN TO TEXT) (RETURN TO DISCUSSION)

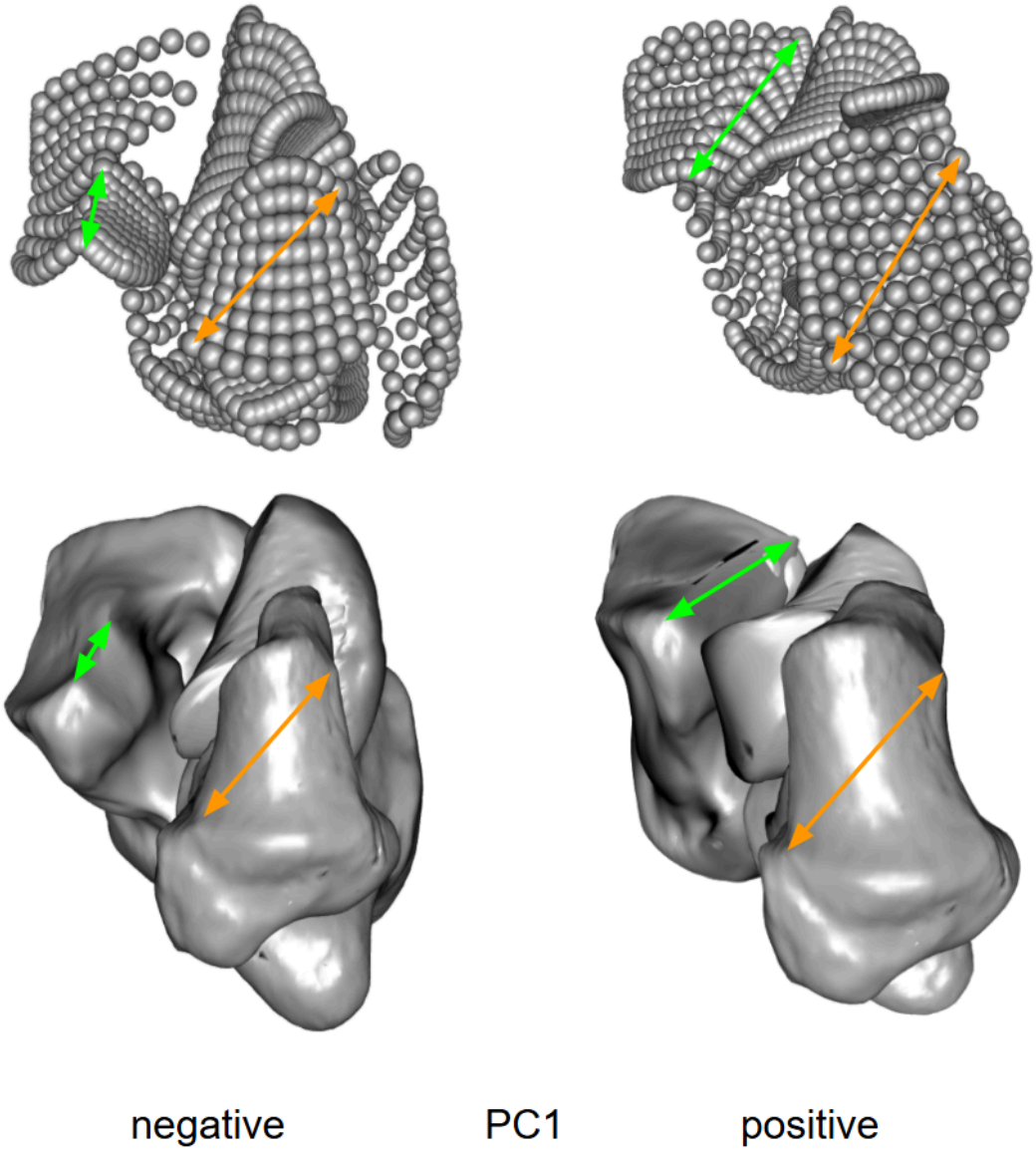

Figure 17. Distoradial view of the point clouds (top) and surface warps (bottom) along PC1 of the mean shape (see Figure 12) for the four-bone analysis. The annotated features differ at the positive extreme relative to the negative extreme (orange; larger MC1 facet; green, longer capitate-MC2 facet). (RETURN TO TEXT) (RETURN TO DISCUSSION)

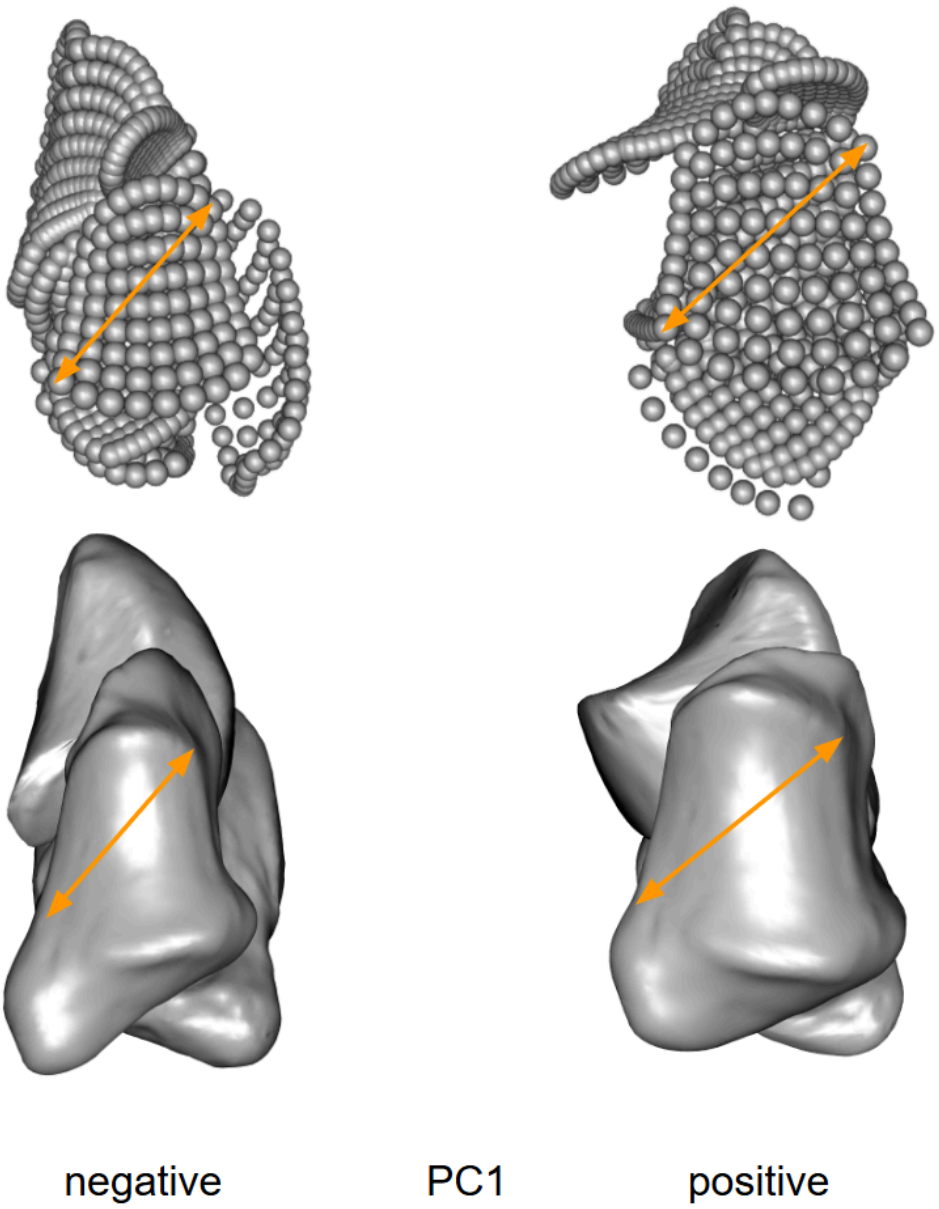

Figure 18. Distoradial view of the point clouds (top) and surface warps (bottom) along PC1 of the mean shape (see Figure 13) for the three-bone analysis. The annotated features differ at the positive extreme relative to the negative extreme (orange, larger MC1 facet). (RETURN TO TEXT) (RETURN TO DISCUSSION)

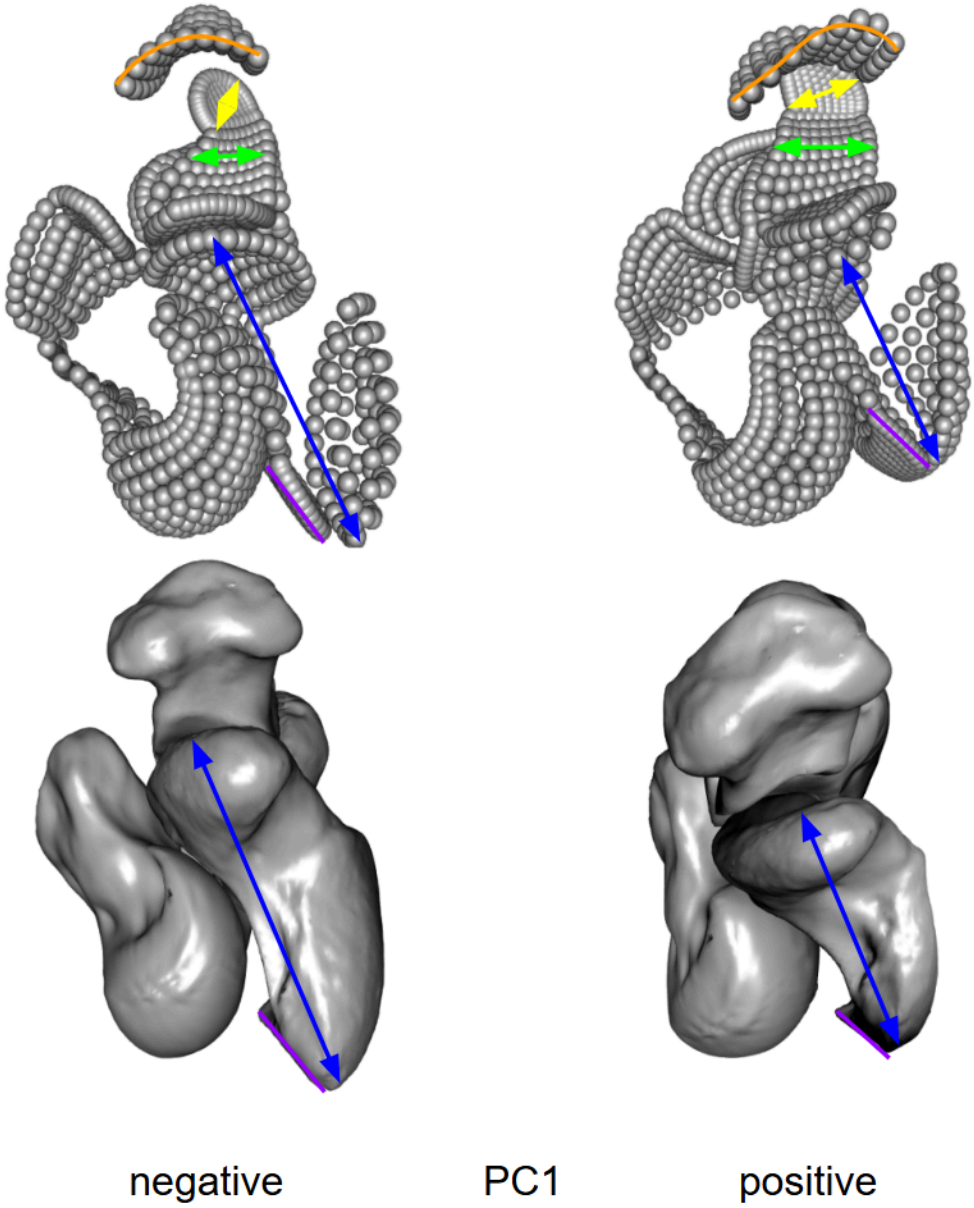

Figure 19. Radial view of the point clouds (top) and surface warps (bottom) along PC1 of the mean shape (see Figure 12) for the four-bone analysis. The annotated features differ at the positive extreme relative to the negative extreme (orange, flatter trapezium-MC1 facet; yellow, larger trapezium-MC2 facet; green, wider trapezium-trapezoid facet; dark blue, shorter scaphoid; purple, more proximodistally orientated scaphoid-lunate facet). (RETURN TO TEXT) (RETURN TO DISCUSSION)

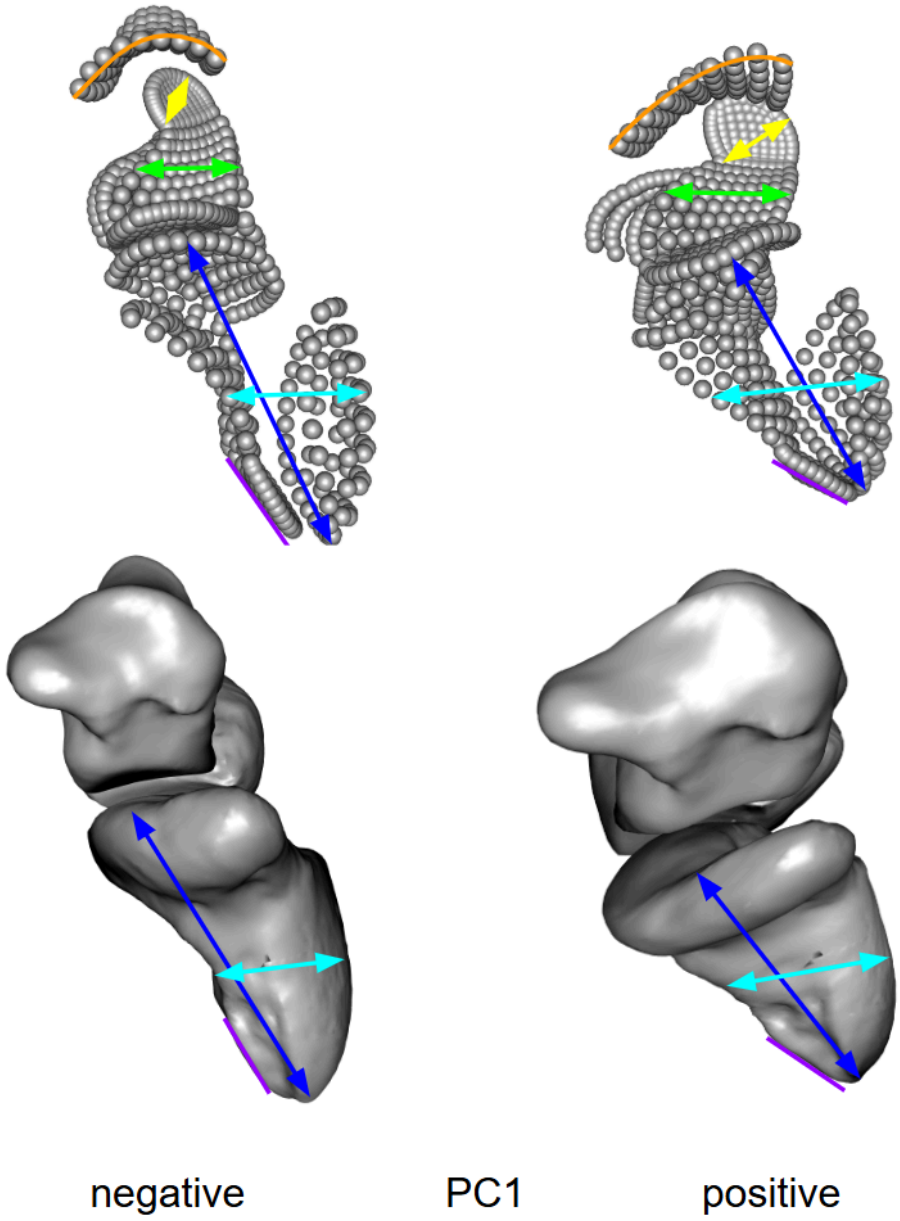

Figure 20. Radial view of the point clouds (top) and surface warps (bottom) along PC1 of the mean shape (see Figure 13) for the three-bone analysis. The annotated features differ at the positive extreme relative to the negative extreme (orange, flatter trapezium-MC1 facet; yellow, larger trapezium-MC2 facet; green, wider trapezium-trapezoid facet; light blue, thicker scaphoid; dark blue, shorter scaphoid; purple, more proximodistally orientated scaphoid-lunate facet). (RETURN TO TEXT) (RETURN TO DISCUSSION)

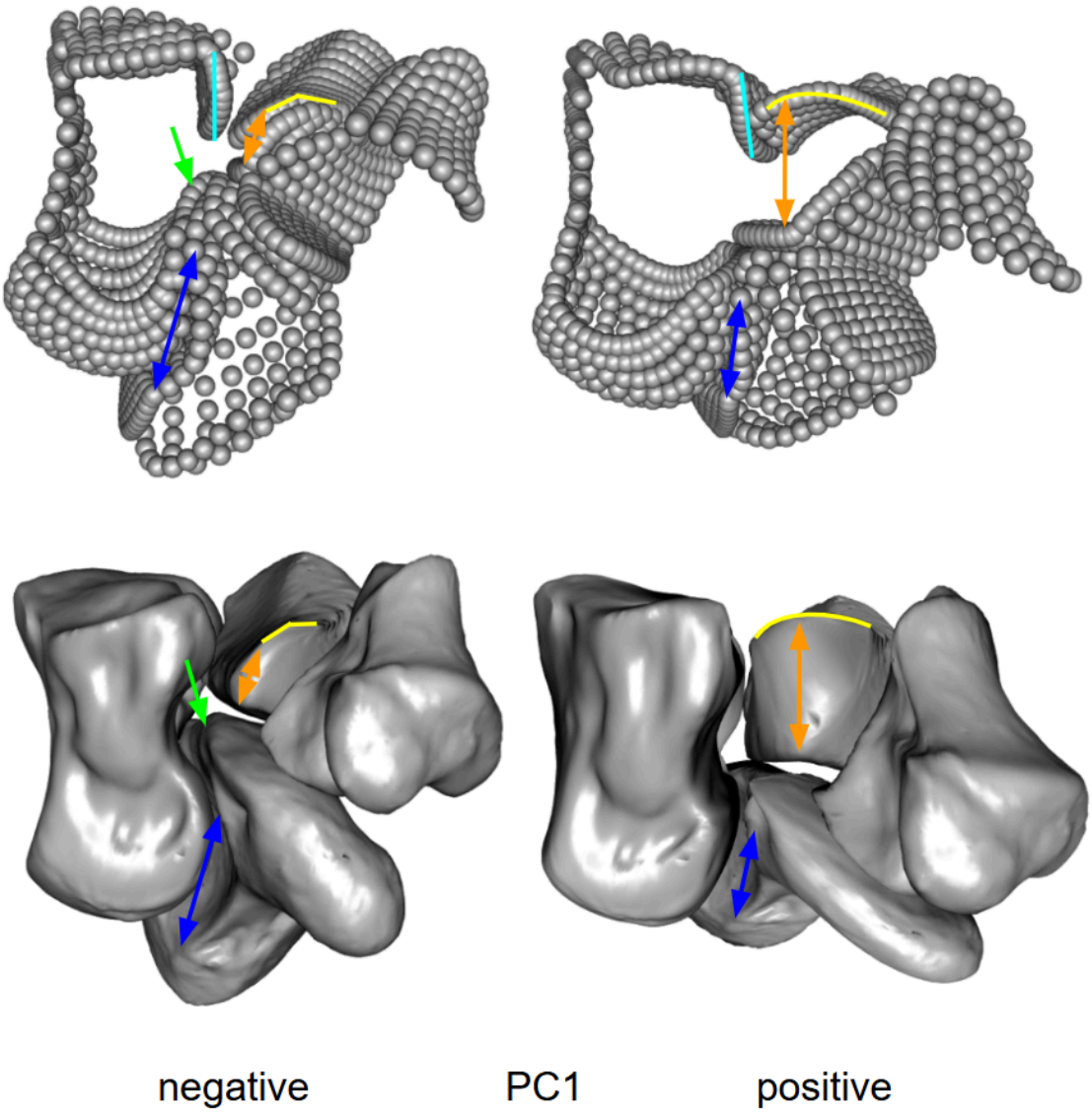

Figure 21. Palmar view of the point clouds (top) and surface warps (bottom) along PC1 of the mean shape (see Figure 12) for the four-bone analysis. The annotated features differ at the positive extreme relative to the negative extreme (orange, expanded palmar aspect of the trapezoid; yellow, saddle-shaped trapezoid-MC2 joint; green, reduction of bone along the distoulnar edge of the scaphoid; light blue, more proximodistally orientated capitate-MC2 facet; dark blue, shorter scaphoid-capitate facet). (RETURN TO TEXT) (RETURN TO DISCUSSION)

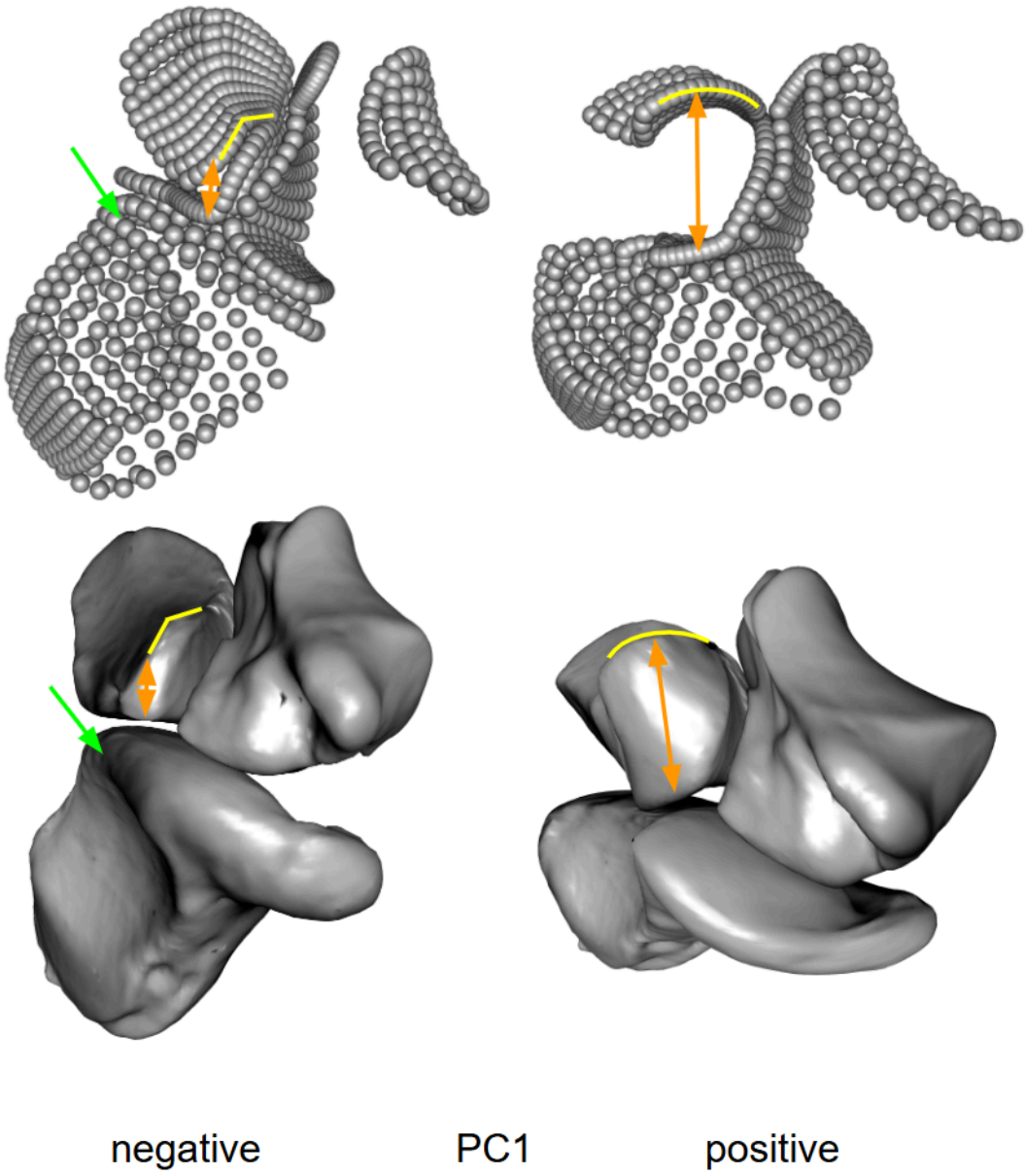

Figure 22. Palmar view of the point clouds (top) and surface warps (bottom) along PC1 of the mean shape (see Figure 13) for the three-bone analysis. The annotated features differ at the positive extreme relative to the negative extreme (orange, expanded palmar aspect of the trapezoid; yellow, saddle-shaped trapezoid-MC2 joint; green, reduction of bone along the distoulnar edge of the scaphoid). (RETURN TO TEXT) (RETURN TO DISCUSSION)

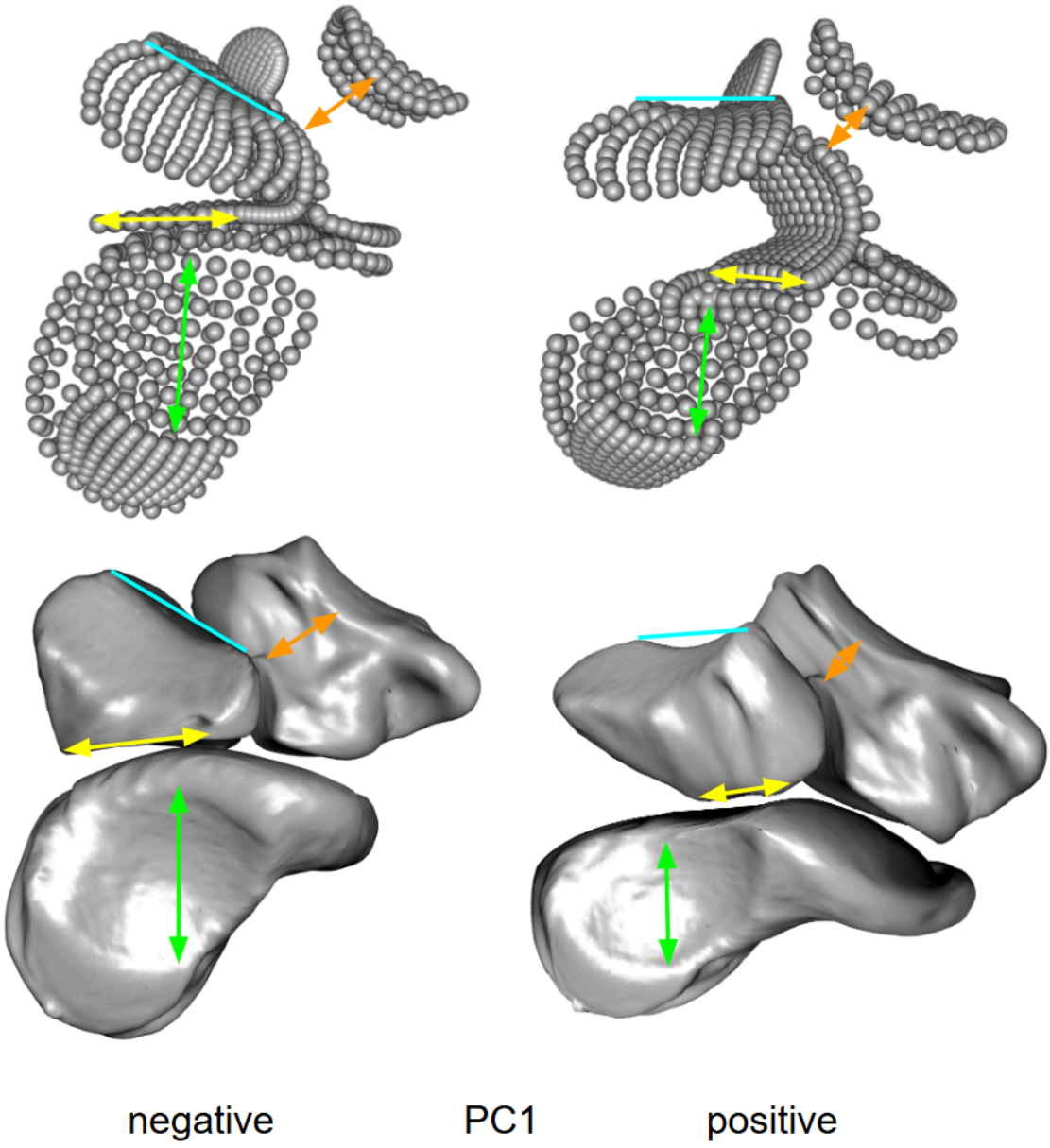

Figure 23. Ulnar view of the point clouds (top) and surface warps (bottom) along PC1 of the mean shape (see Figure 13) for the three-bone analysis. The annotated features differ at the positive extreme relative to the negative extreme (orange, narrower palmar nonarticular surface on the trapezium; yellow, shorter trapezoid-scaphoid facet; green, shorter scaphoid-capitate facet; light blue, trapezoid-MC2 facet more parallel to the trapezoid-scaphoid facet but less parallel to the scaphoid-radius facet). (RETURN TO TEXT) (RETURN TO DISCUSSION)

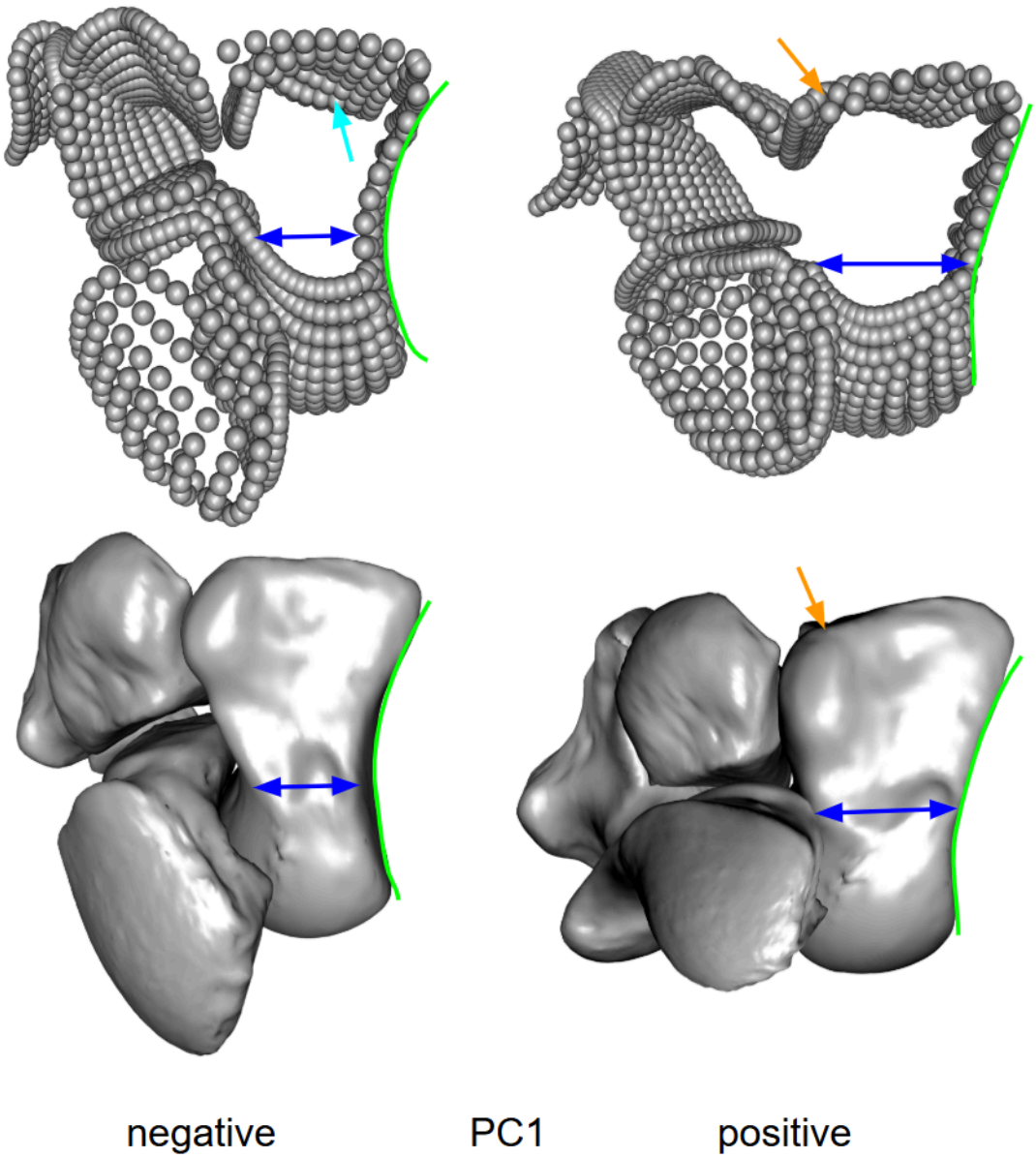

Figure 24. Dorsal view of the point clouds (top) and surface warps (bottom) along PC1 of the mean shape (see Figure 12) for the four-bone analysis. The annotated features differ at the positive extreme relative to the negative extreme (orange, bevelled dorsoradial corner of the capitate-MC3 facet; green, flatter capitate-hamate facet; light blue, less irregular capitate-MC3 facet; dark blue, wider capitate neck). (RETURN TO TEXT) (RETURN TO DISCUSSION)

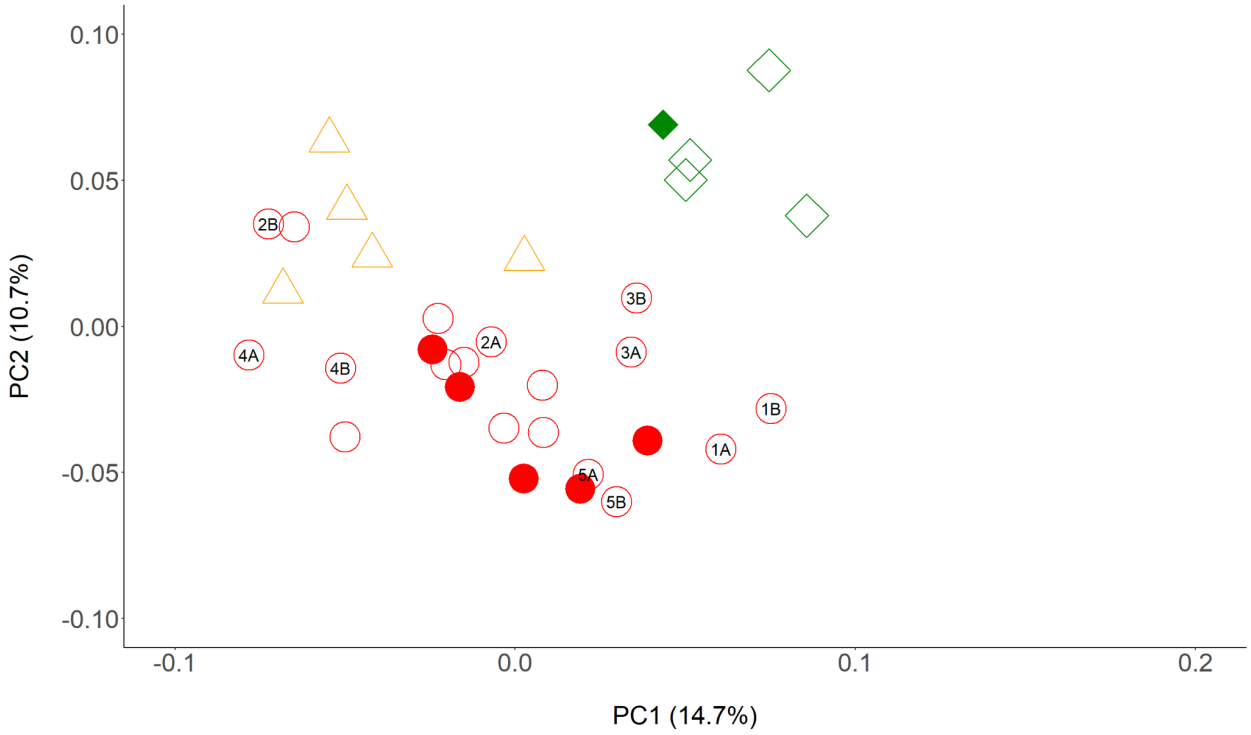

Figure 25. Plot of the principal components (PC1, PC2) generated from landmark data of the articulated trapezium, trapezoid, scaphoid and capitate (chimpanzees = red circles, bonobos = yellow triangles, western gorillas = green diamonds). Closed and open shapes represent intact cadaver and manually articulated specimens, respectively. Symbols with the same number indicate duplicate articulations (A = OL's articulation, B = Dr. Tocheri's articulation). (RETURN TO TEXT) (RETURN TO DISCUSSION)

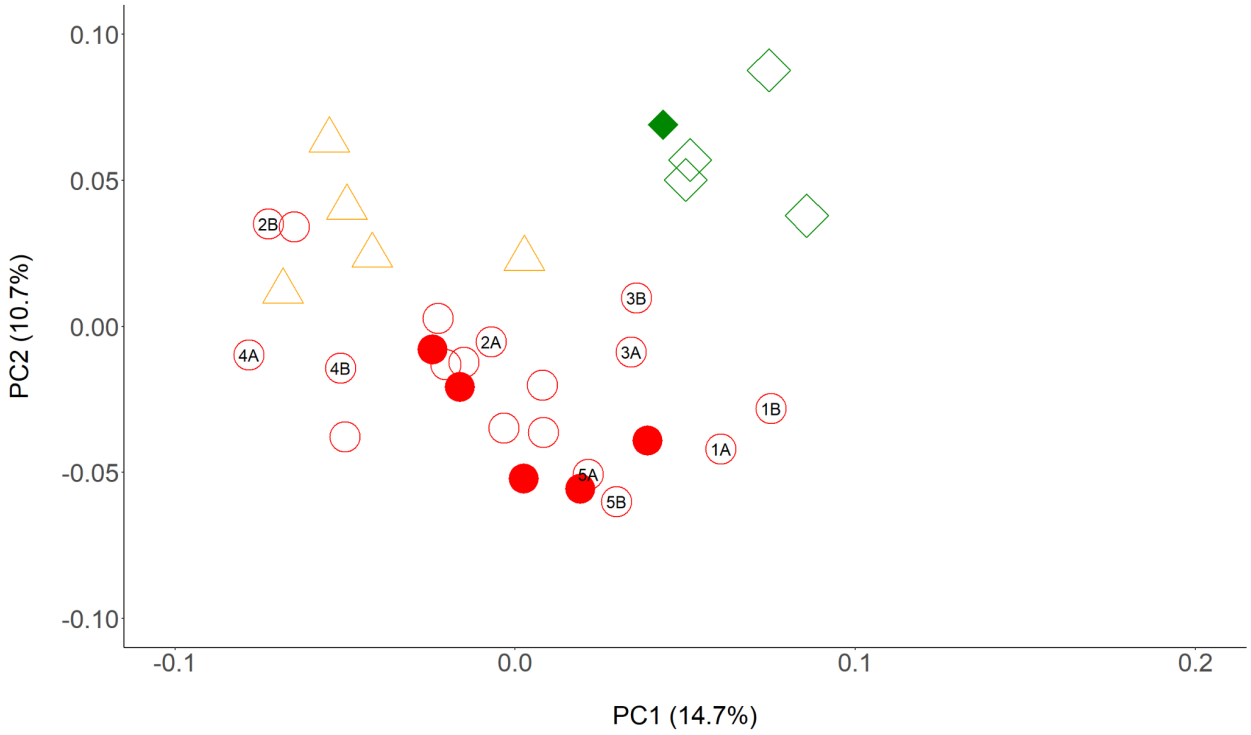

Figure 26. Plot of the principal components (PC1, PC3) generated from landmark data of the articulated trapezium, trapezoid, and scaphoid (chimpanzees = red circles, bonobos = yellow triangles, western gorillas = green diamonds). Closed and open shapes represent intact cadaver and manually articulated specimens, respectively. Symbols with the same number indicate duplicate articulations (A = OL's articulation, B = Dr. Tocheri's articulation). (RETURN TO TEXT) (RETURN TO DISCUSSION)

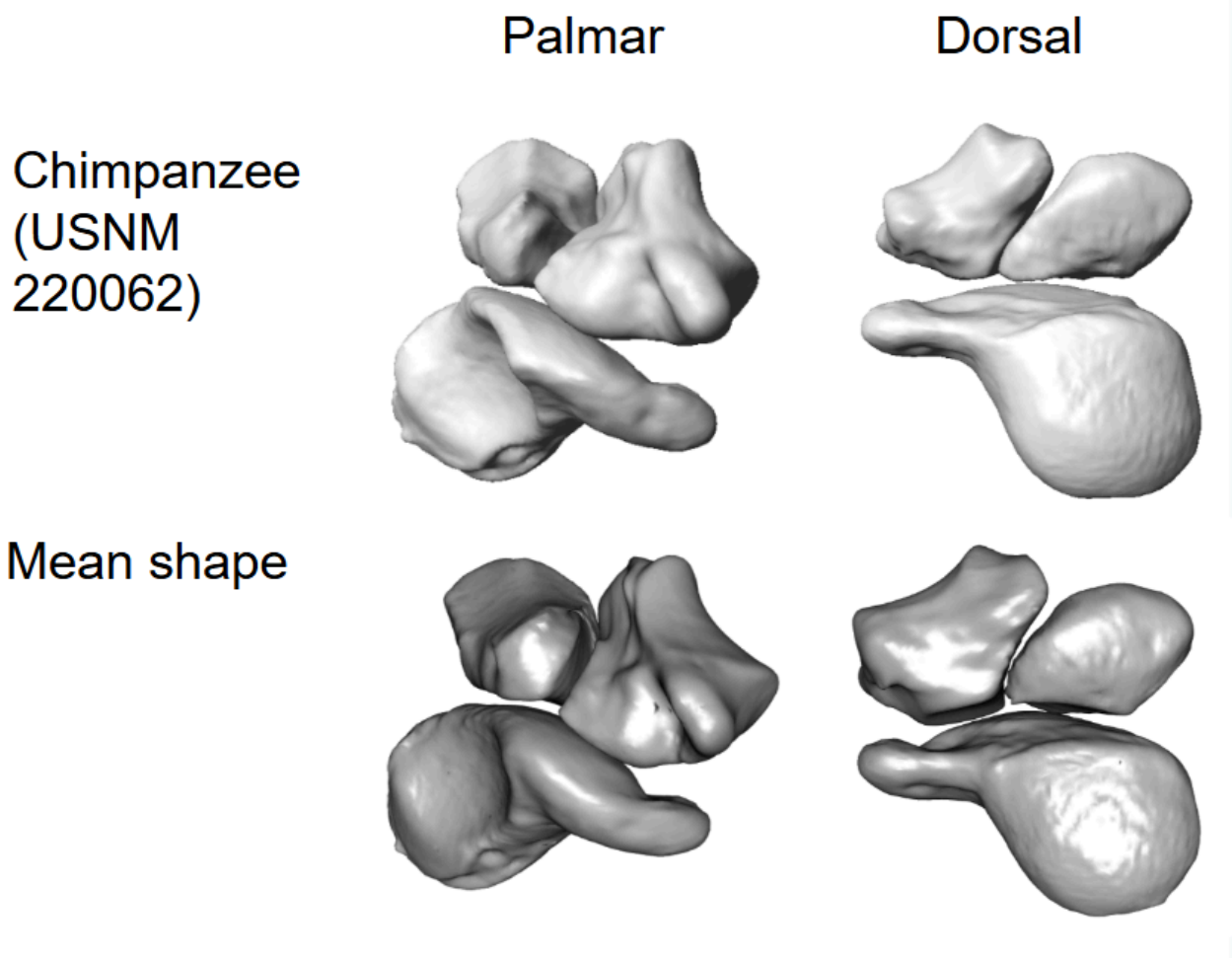

Figure 27. The chimpanzee that is most similar in overall shape to the calculated mean shape of the four-bone analysis of African apes only. Thus, the mean shape shown here is USNM 220062 warped to the estimated mean landmark configuration across all PCs. (RETURN TO TEXT) (RETURN TO DISCUSSION)

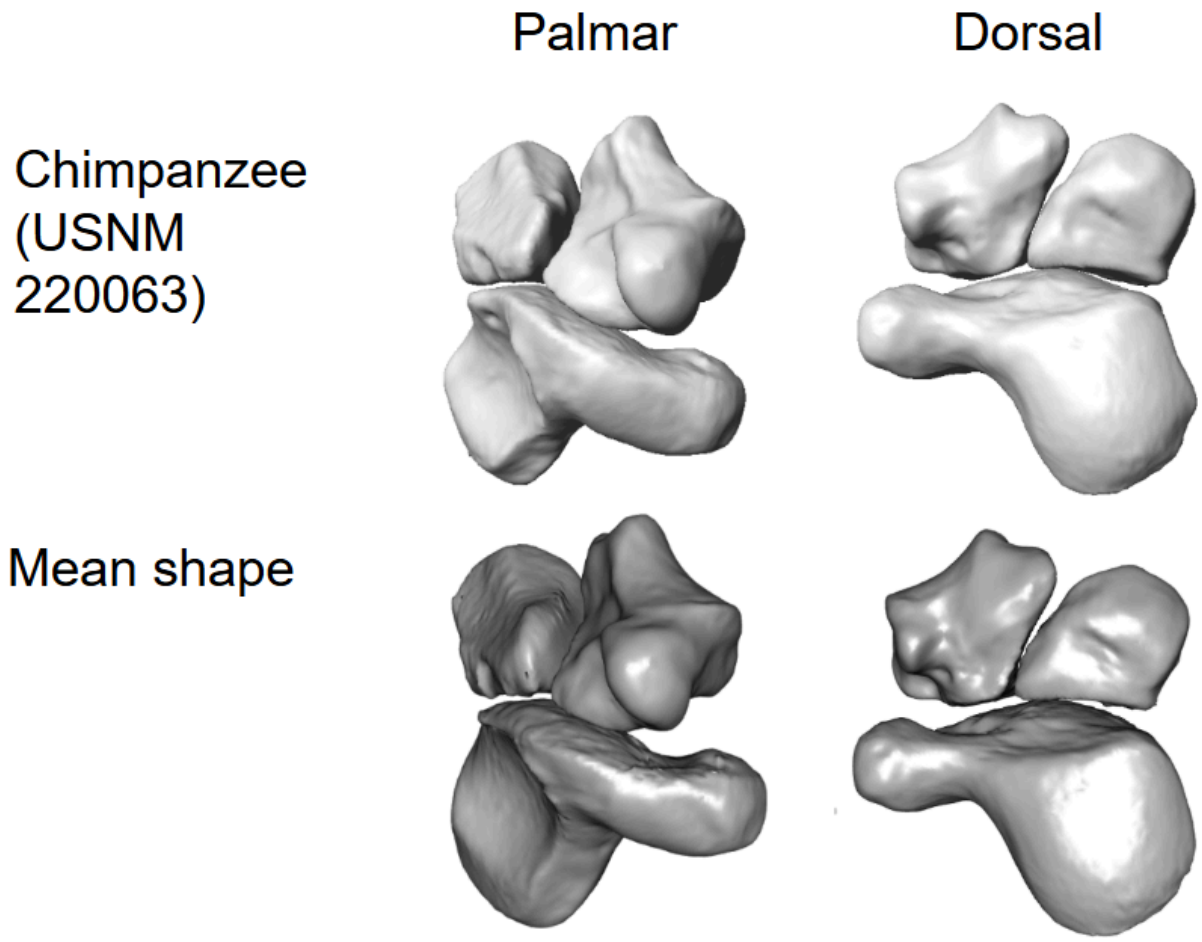

Figure 28. The chimpanzee that is most similar in overall shape to the calculated mean shape of the three-bone analysis of African apes only. Thus, the mean shape shown here is USNM 220063 warped to the estimated mean landmark configuration across all PCs. (RETURN TO TEXT) (RETURN TO DISCUSSION)

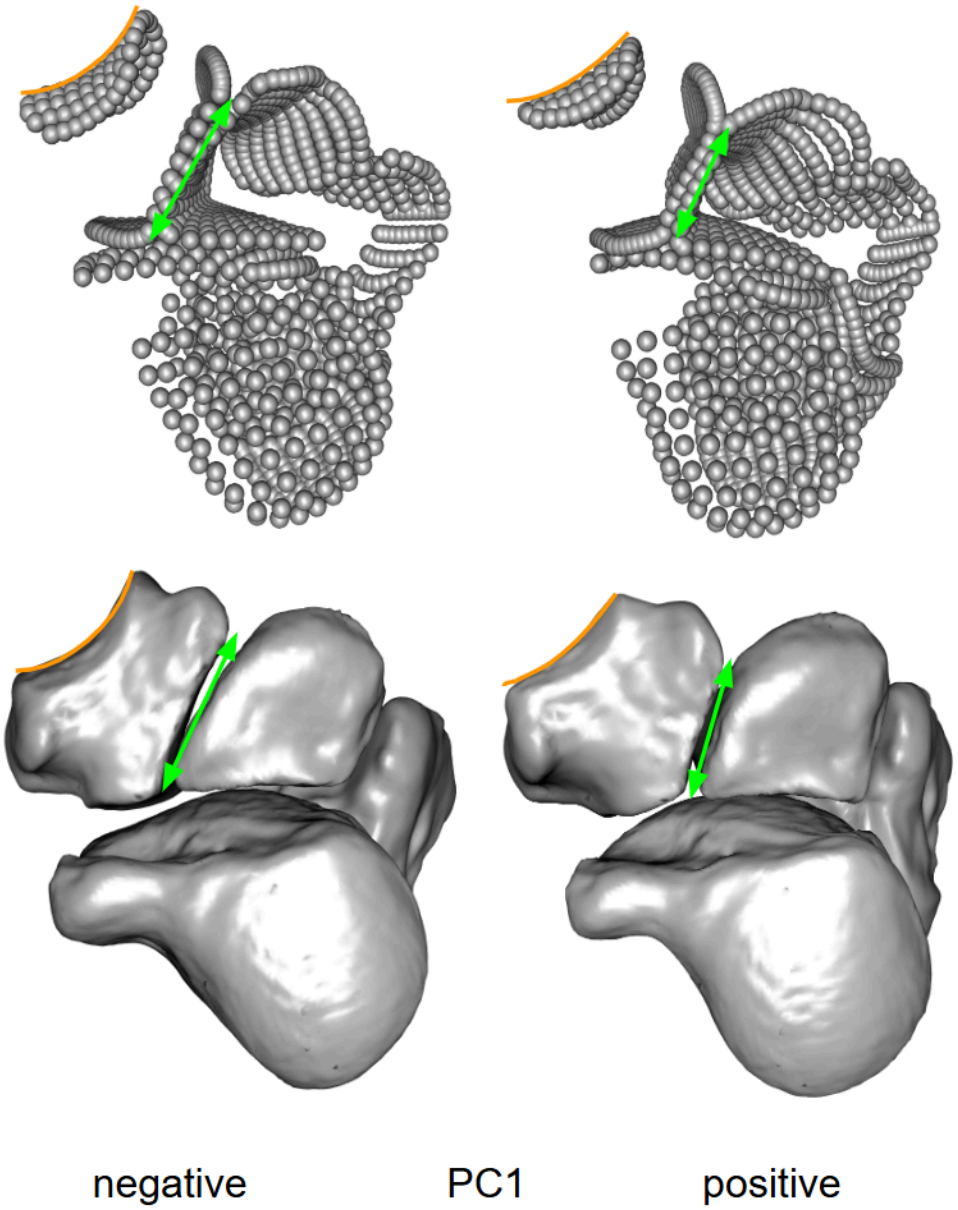

Figure 29. Dorsoradial view of the point clouds (top) and surface warps (bottom) along PC1 of mean shape (see Figure 27) for the four-bone analysis of African apes only. The annotated features differ at the positive extreme relative to the negative extreme (orange, flatter trapezium-MC1 facet; green, shorter and less tilted trapezium-trapezoid facet). (RETURN TO TEXT) (RETURN TO DISCUSSION)

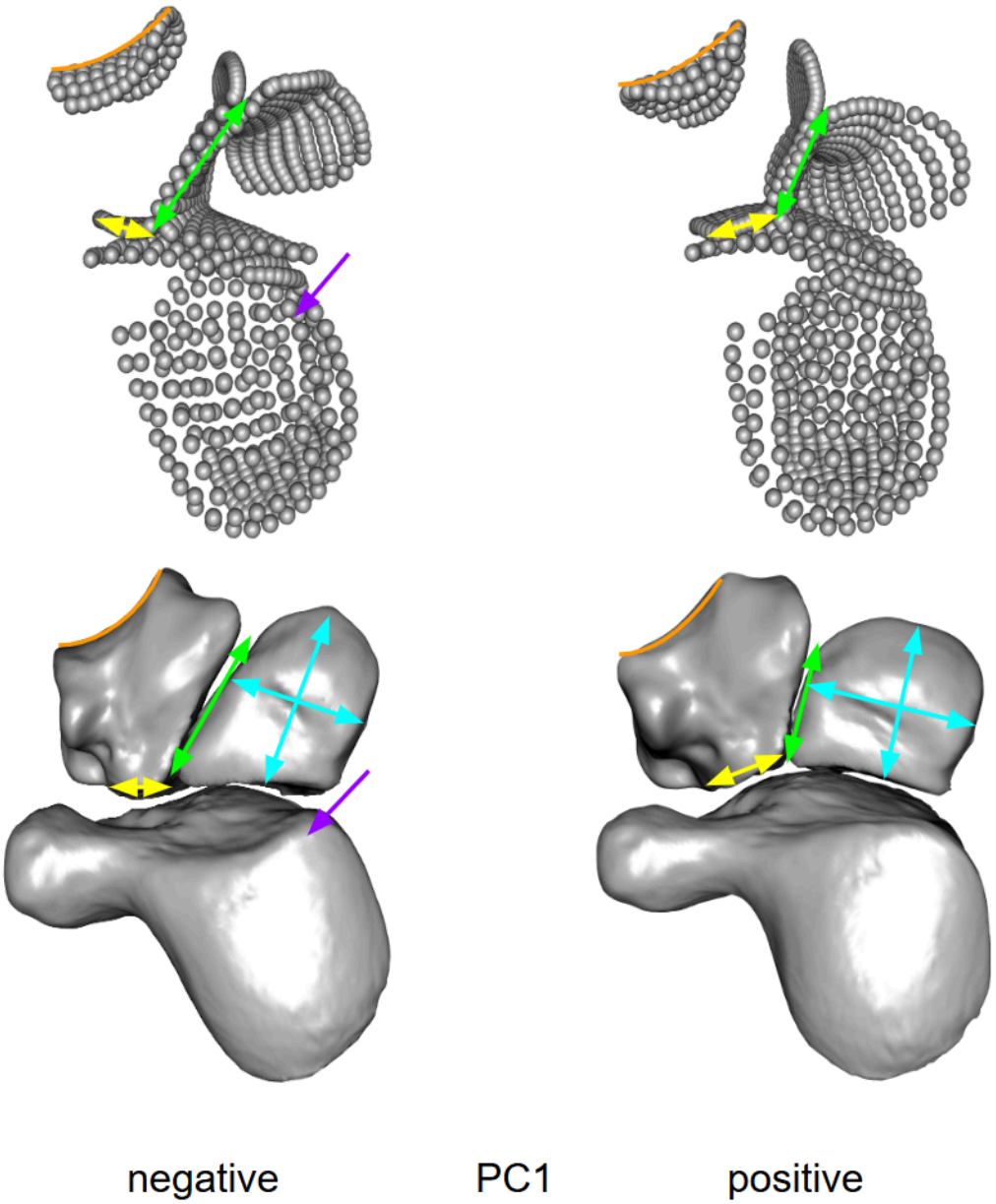

Figure 30. Dorsoradial view of the point clouds (top) and surface warps (bottom) along PC1 of the mean shape (see Figure 28) for the three-bone analysis of African apes only. The annotated features differ at the positive extreme relative to the negative extreme (orange, flatter trapezium-MC1 facet; yellow, dorsally wider trapezium-scaphoid facet; green, shorter and less tilted trapezium-trapezoid facet; light blue, taller and wider trapezoid; purple, lacks a scaphoid beak). (RETURN TO TEXT) (RETURN TO DISCUSSION)

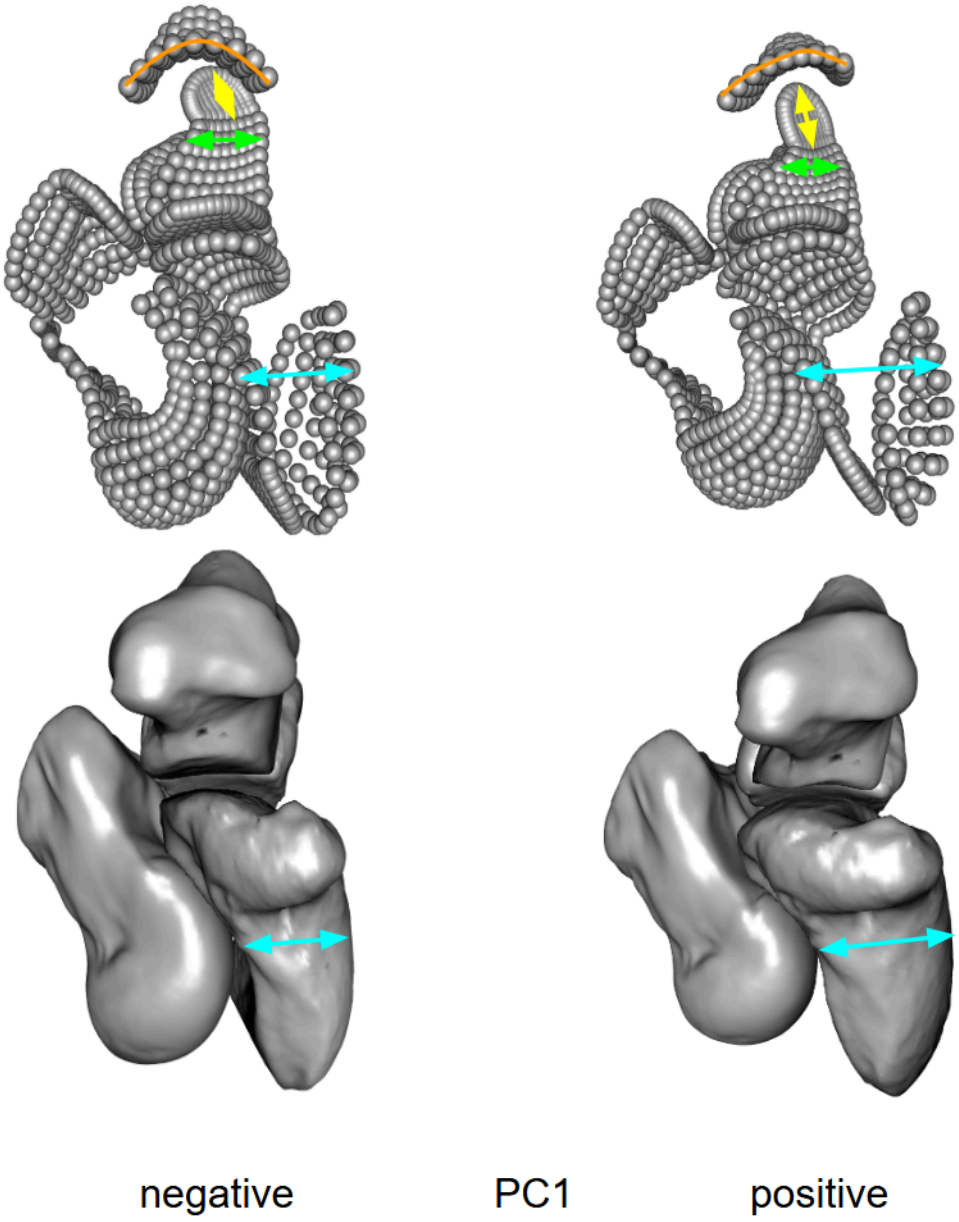

Figure 31. Radial view of the point clouds (top) and surface warps (bottom) along PC1 of the mean shape (see Figure 27) for the four-bone analysis of African apes only. The annotated features differ at the positive extreme relative to the negative extreme (orange, flatter trapezium-MC1 facet; yellow, taller trapezium-MC1 facet; green, wider trapezium-trapezoid facet; light blue, thicker scaphoid). (RETURN TO TEXT) (RETURN TO DISCUSSION)

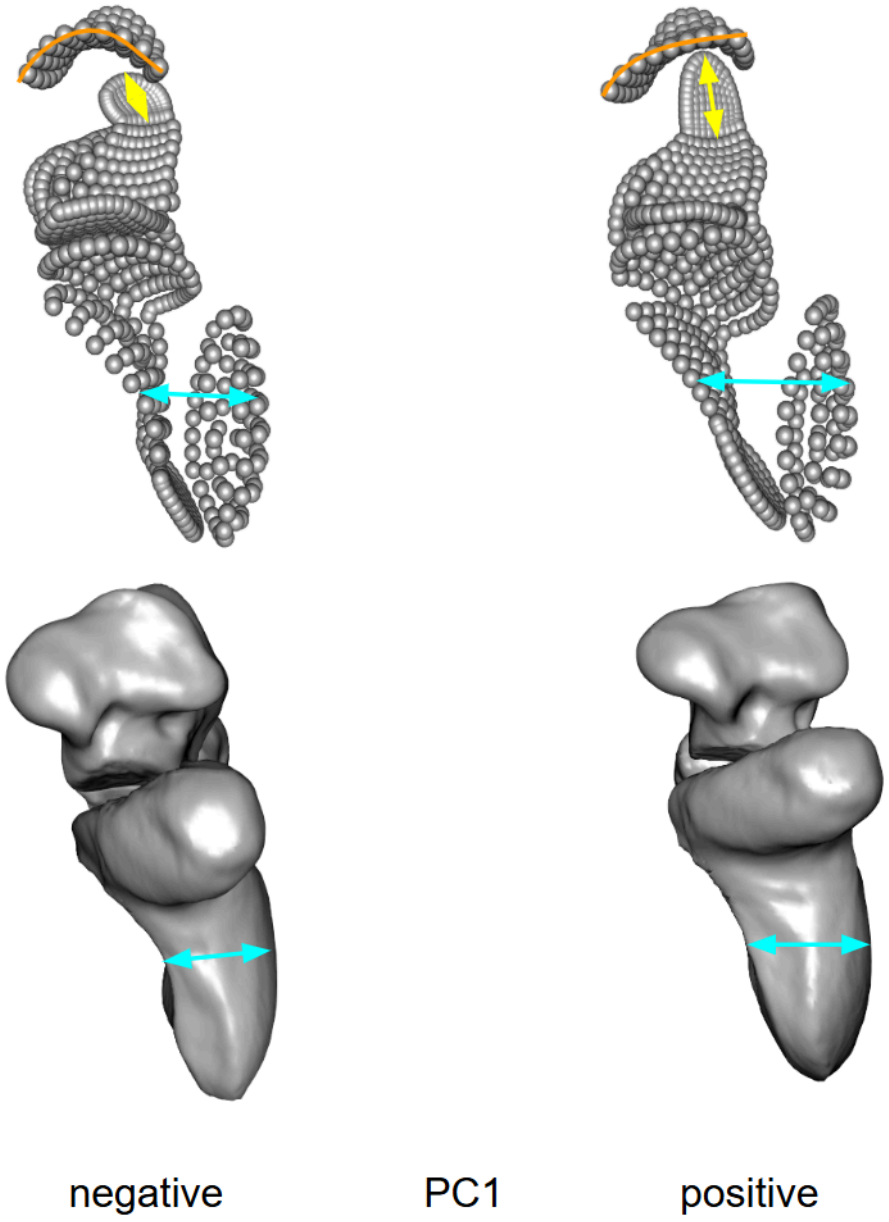

Figure 32. Radial view of the point clouds (top) and surface warps (bottom) along PC1 of the mean shape (see Figure 28) for the three-bone analysis of African apes only. The annotated features differ at the positive extreme relative to the negative extreme (orange, flatter trapezium-MC1 facet; yellow, taller trapezium-MC1 facet; light blue, thicker scaphoid). (RETURN TO TEXT) (RETURN TO DISCUSSION)

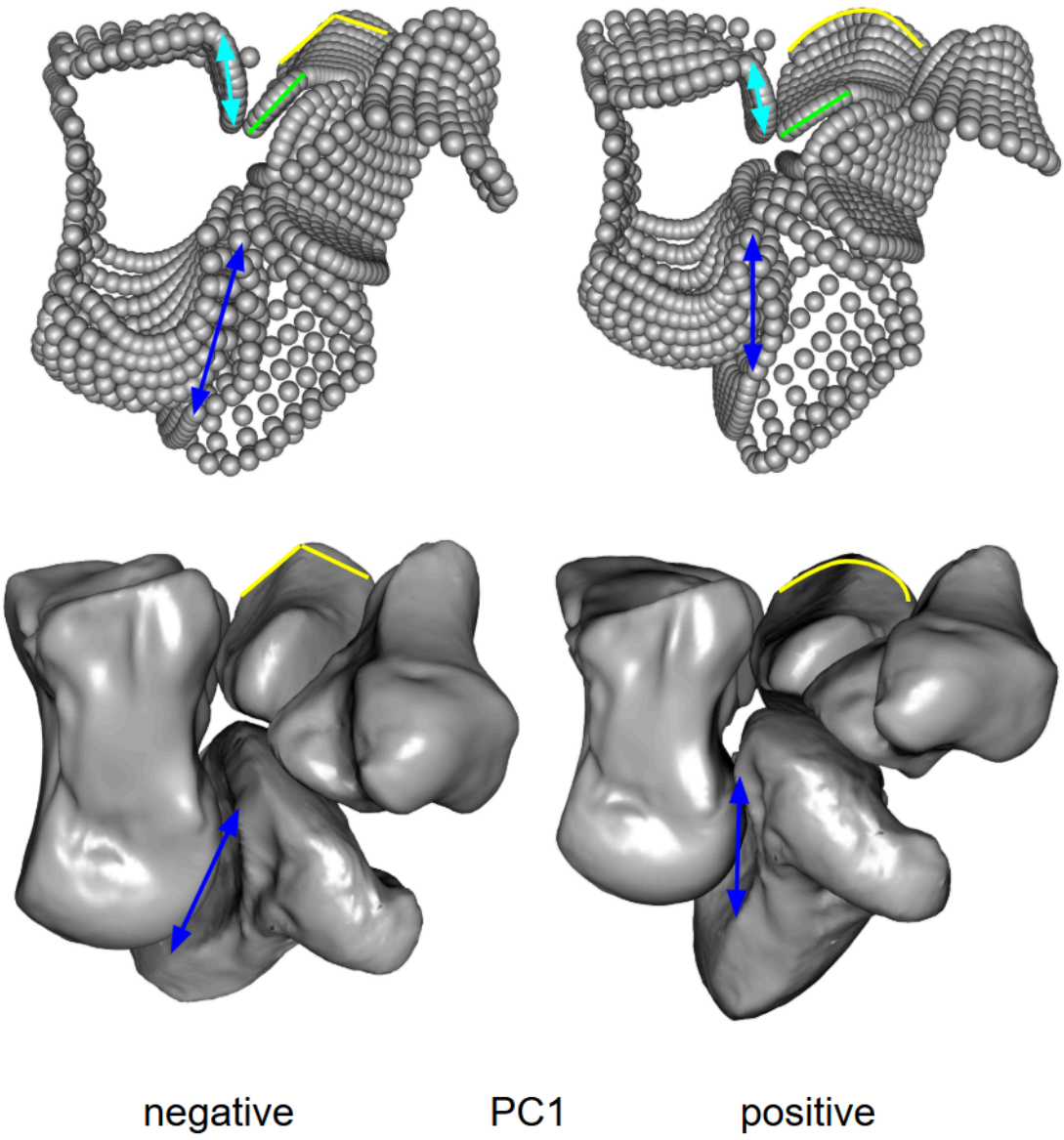

Figure 33. Palmar view of the point clouds (top) and surface warps (bottom) along PC1 of the mean shape (see Figure 27) for the four-bone analysis of African apes only. The annotated features differ at the positive extreme relative to the negative extreme (yellow, saddle-shaped trapezoid-MC2 joint; green, more proximodistally orientated trapezoid-ulnar MC2 facet; light blue, more proximodistally orientated capitate-MC2 facet; dark blue, shorter scaphoid-capitate facet). (RETURN TO TEXT) (RETURN TO DISCUSSION)

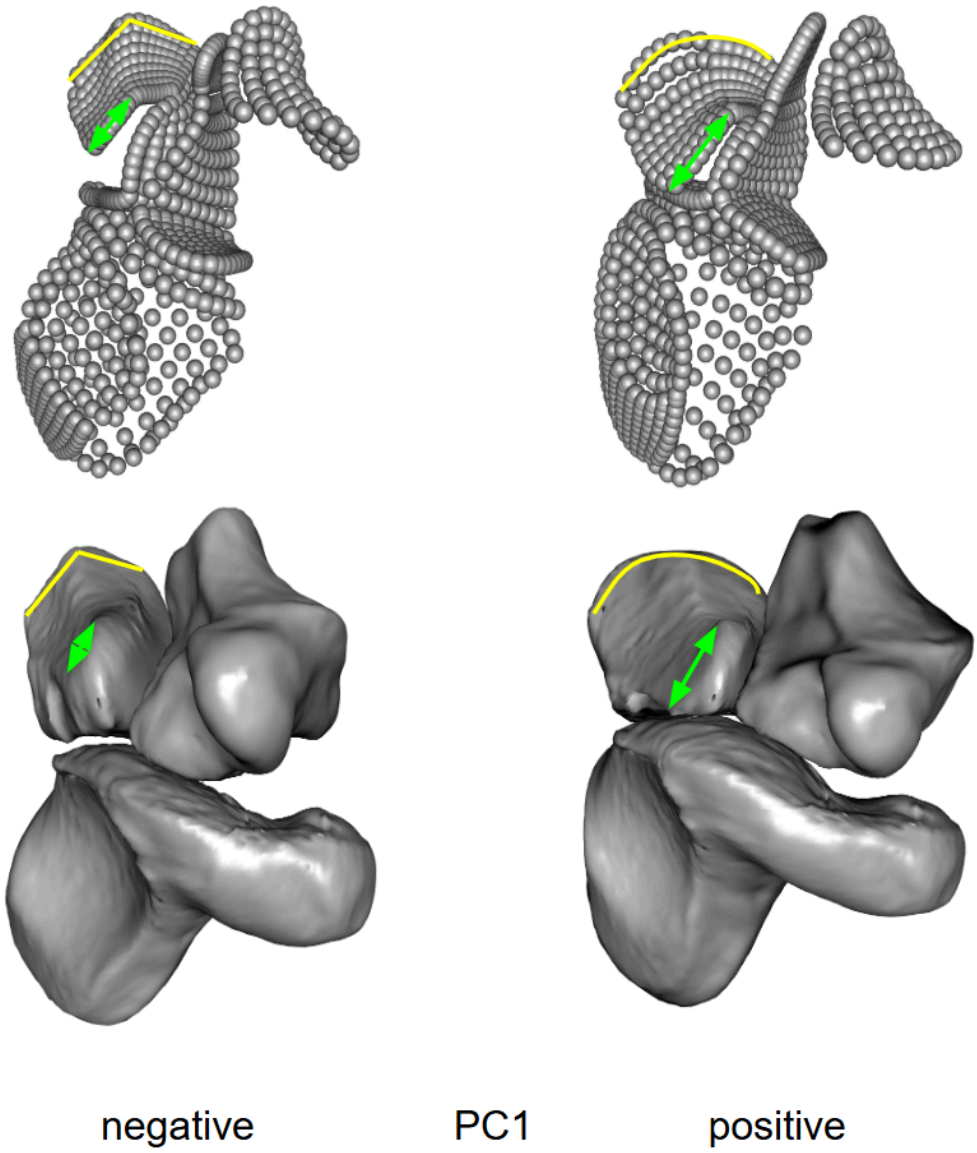

Figure 34. Palmar view of the point clouds (top) and surface warps (bottom) along PC1 of the mean shape (see Figure 28) for the three-bone analysis of African apes only. The annotated features differ at the positive extreme relative to the negative extreme (yellow, saddle-shaped trapezoid-MC2 joint; green, more proximodistally orientated trapezoid-ulnar MC2 facet). (RETURN TO TEXT) (RETURN TO DISCUSSION)

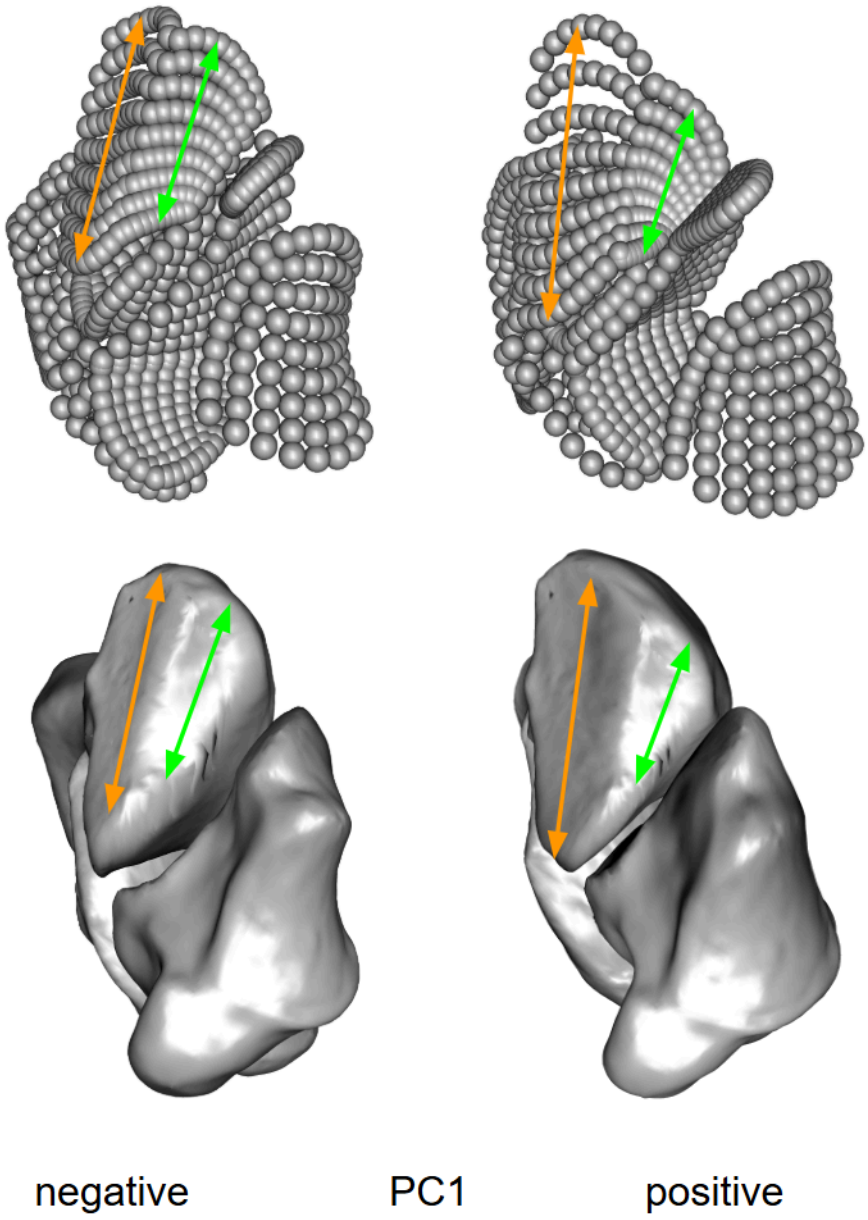

Figure 35. Distal view of the point clouds (top) and surface warps (bottom) along PC1 of the mean shape (see Figure 28) for the three-bone analysis of African apes only. The annotated features differ at the positive extreme relative to the negative extreme (orange, longer trapezoid-ulnar MC2 facet; green, shorter trapezoid-radial MC2 facet). (RETURN TO TEXT) (RETURN TO DISCUSSION)

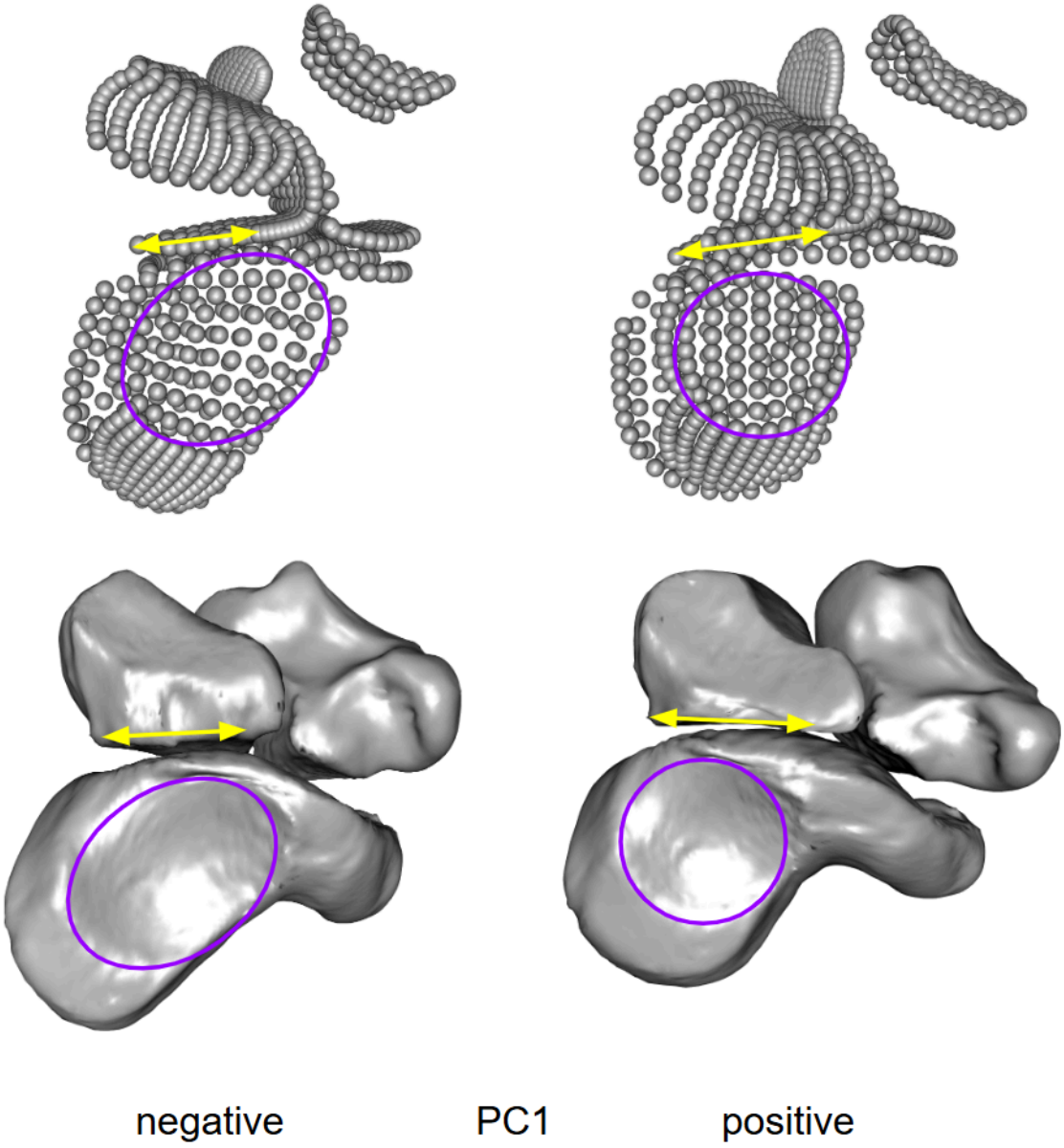

Figure 36. Ulnar view of the point clouds (top) and surface warps (bottom) along PC1 of the mean shape (see Figure 28) for the three-bone analysis of African apes only. The annotated features differ at the positive extreme relative to the negative extreme (yellow, longer trapezoid-scaphoid facet; purple, smaller and circular scaphoid-capitate facet). (RETURN TO TEXT) (RETURN TO DISCUSSION)

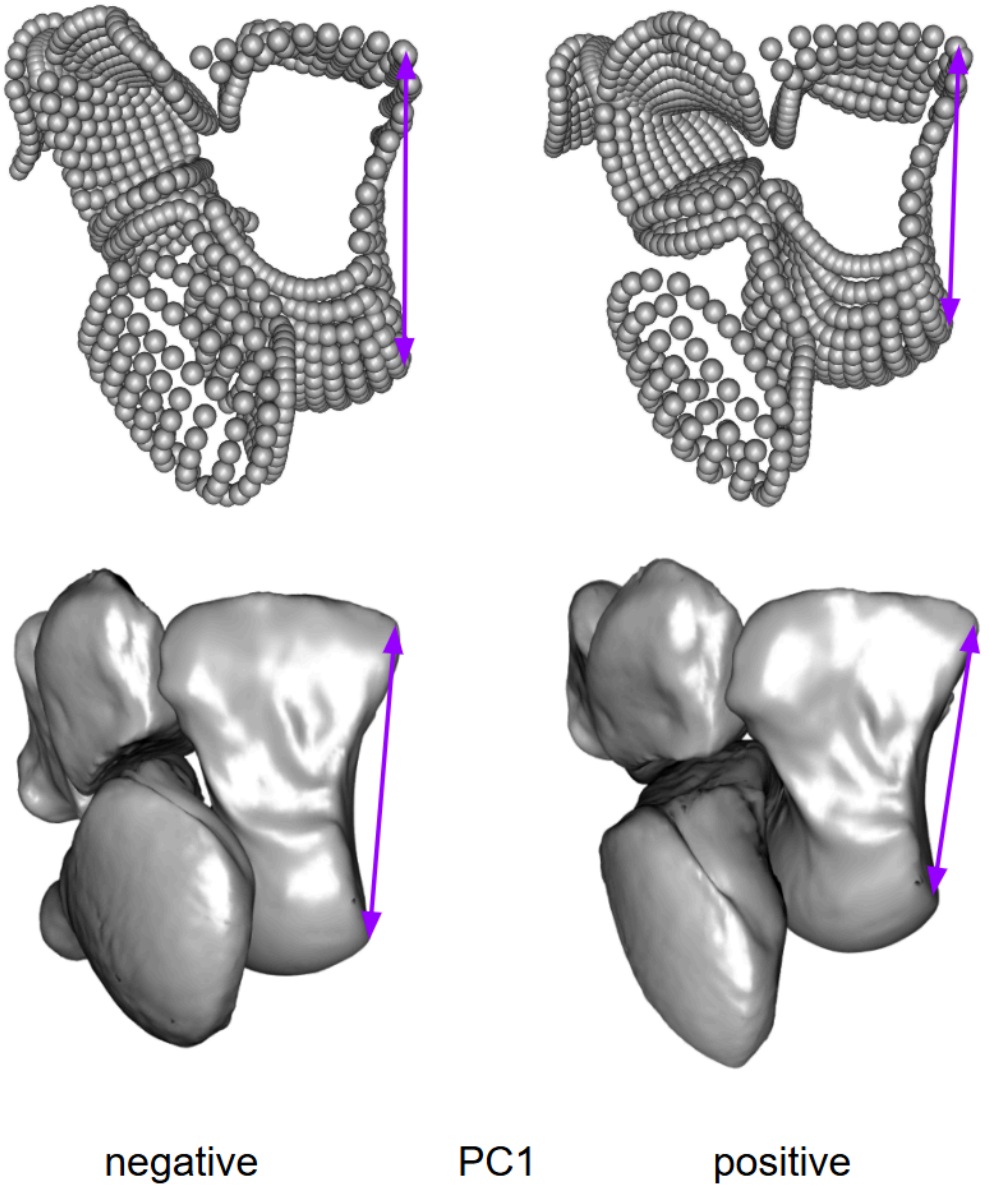

Figure 37. Dorsal view of the point clouds (top) and surface warps (bottom) along PC1 of the mean shape (see Figure 27) for the four-bone analysis of African apes only. The annotated features differ at the positive extreme relative to the negative extreme (purple, shorter capitate-hamate facet). (RETURN TO TEXT) (RETURN TO DISCUSSION)

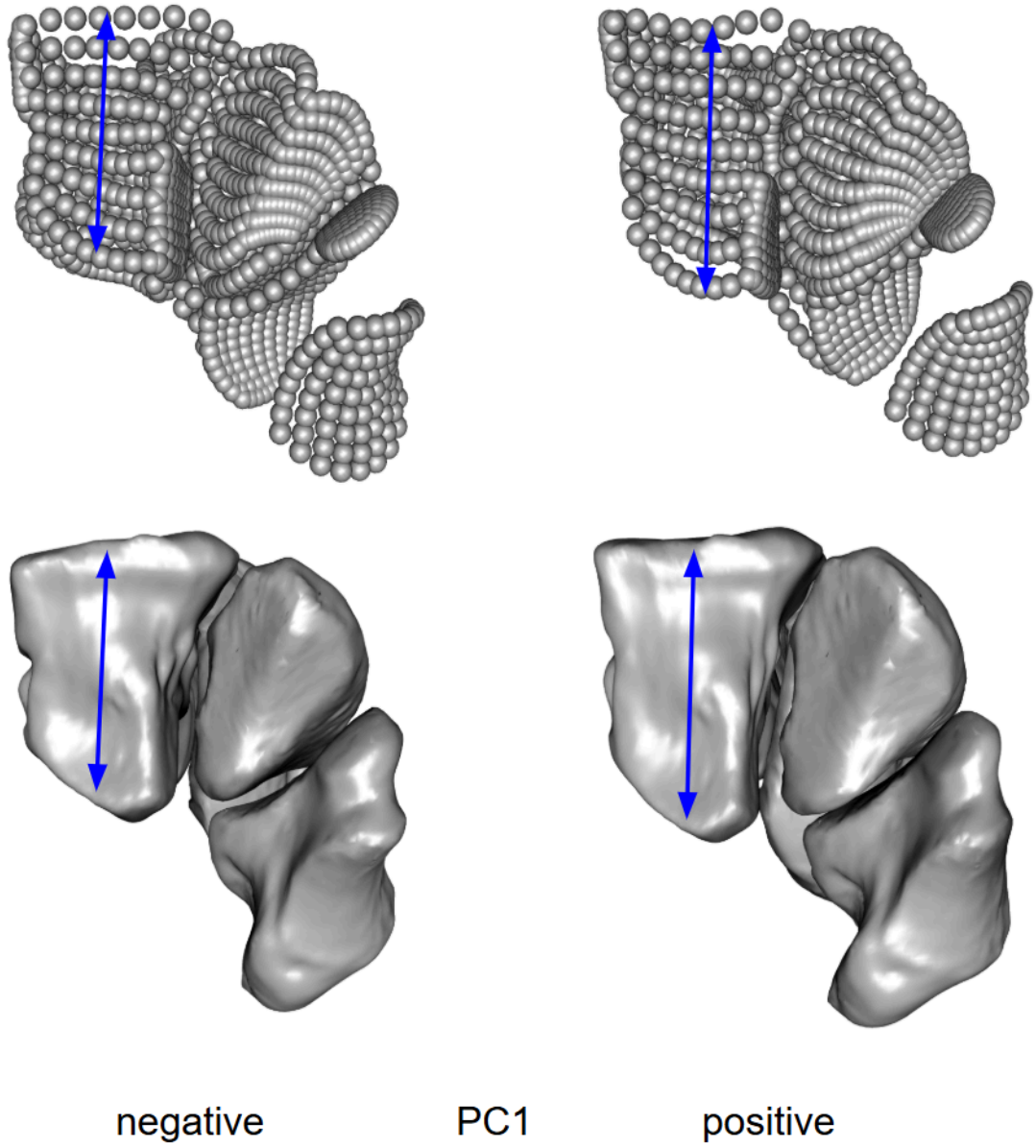

Figure 38. Distal view of the point clouds (top) and surface warps (bottom) along PC1 of the mean shape (see Figure 27) for the four-bone analysis of African apes only. The annotated features differ at the positive extreme relative to the negative extreme (dark blue, longer capitate-MC3 facet). (RETURN TO TEXT) (RETURN TO DISCUSSION)

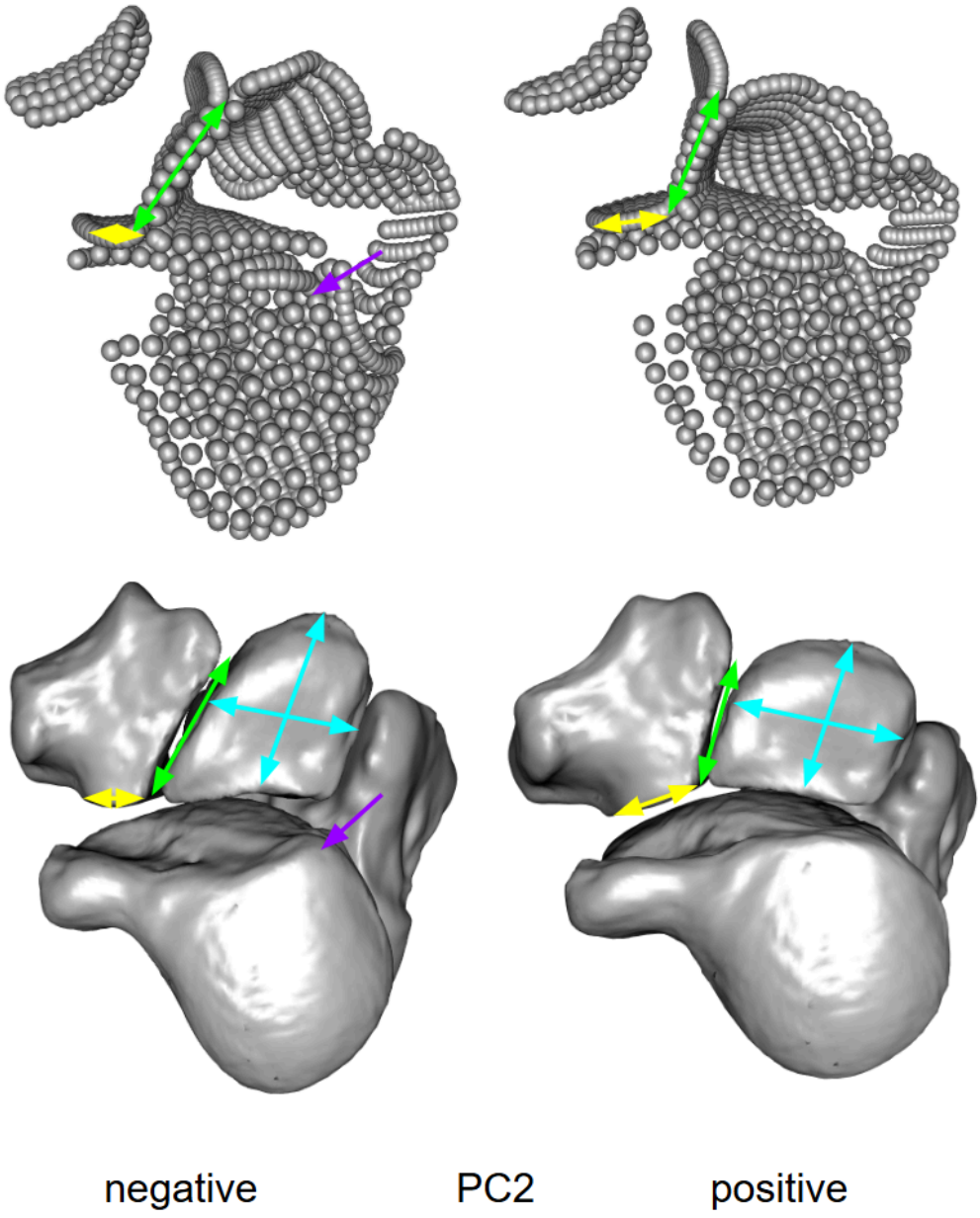

Figure 39. Dorsoradial view of the point clouds (top) and surface warps (bottom) along PC2 of the mean shape (see Figure 27) for the four-bone analysis of African apes only. The annotated features differ at the positive extreme relative to the negative extreme (yellow, dorsally wider trapezium-scaphoid facet; green, shorter and less tilted trapezium-trapezoid facet; light blue, shorter and wider trapezoid; purple, lack of a scaphoid beak). (RETURN TO TEXT) (RETURN TO DISCUSSION)

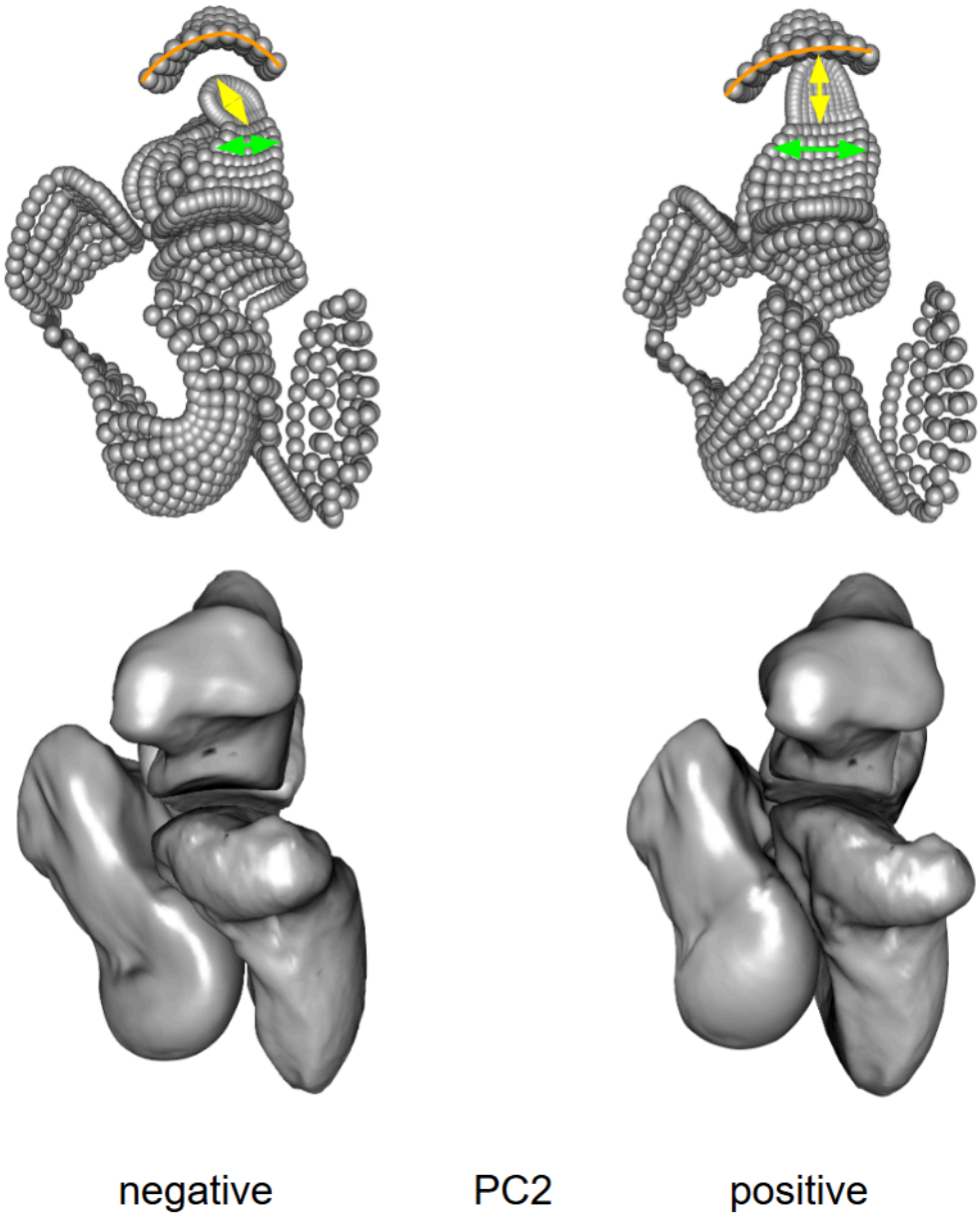

Figure 40. Radial view of the point clouds (top) and surface warps (bottom) along PC2 of the mean shape (see Figure 27) for the four-bone analysis of African apes only. The annotated features differ at the positive extreme relative to the negative extreme (orange, flatter trapezium-MC1 facet; yellow, taller trapezium-MC1 facet; green, wider trapezium-trapezoid facet). (RETURN TO TEXT) (RETURN TO DISCUSSION)

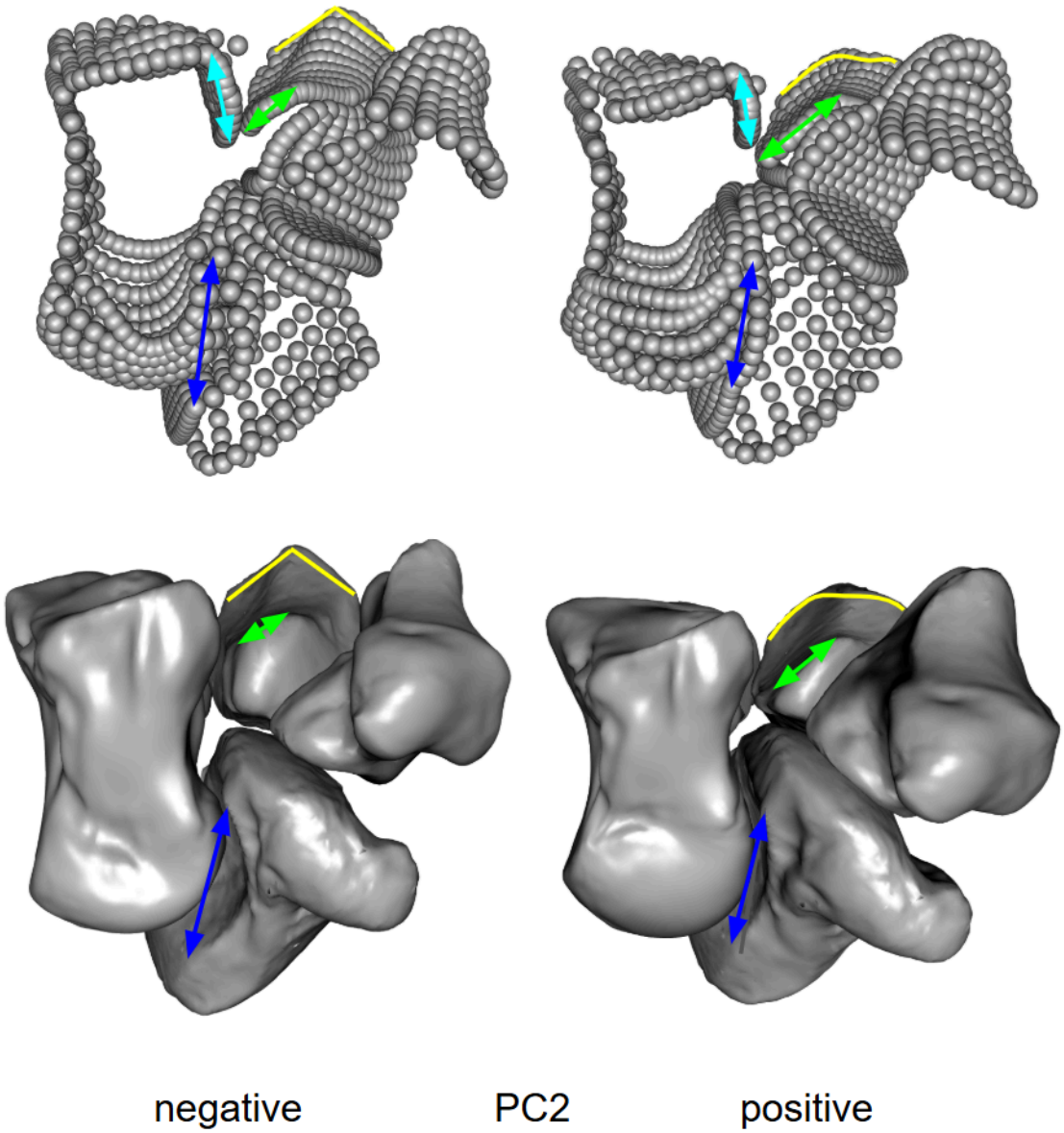

Figure 41. Palmar view of the point clouds (top) and surface warps (bottom) along PC2 of the mean shape (see Figure 27) for the four-bone analysis of African apes only. The annotated features differ at the positive extreme relative to the negative extreme (yellow, saddle-shaped trapezoid-MC2 joint; green, wider and more proximodistally orientated trapezoid-ulnar MC2 facet; light blue, shorter and more proximodistally orientated capitate-MC2 facet; dark blue, shorter scaphoid-capitate facet). (RETURN TO TEXT) (RETURN TO DISCUSSION)

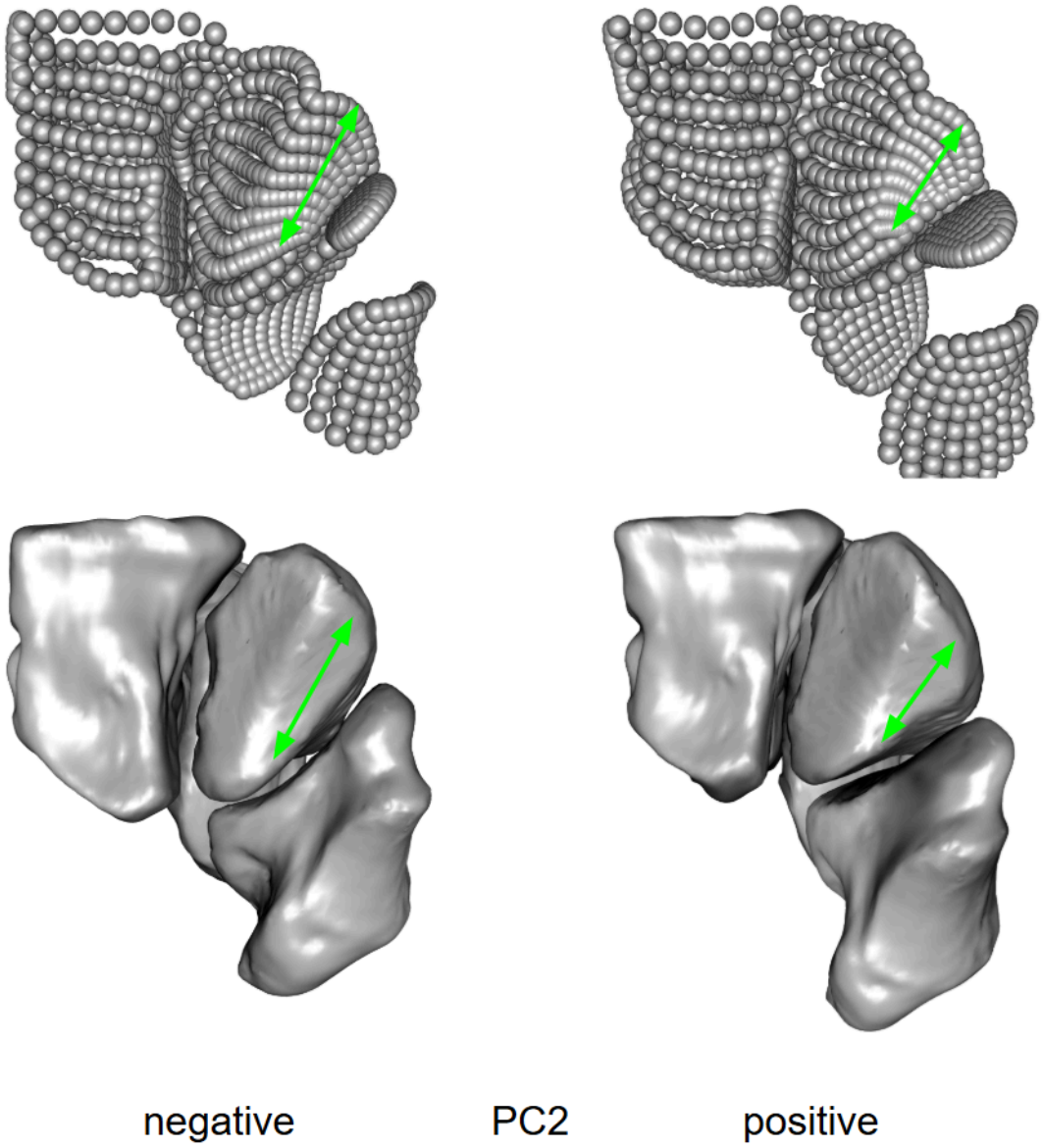

Figure 42. Distal view of the point clouds (top) and surface warps (bottom) along PC2 of the mean shape (see Figure 27) for the four-bone analysis of African apes only. The annotated features differ at the positive extreme relative to the negative extreme (green, shorter trapezoid-radial MC2 facet). (RETURN TO TEXT) (RETURN TO DISCUSSION)

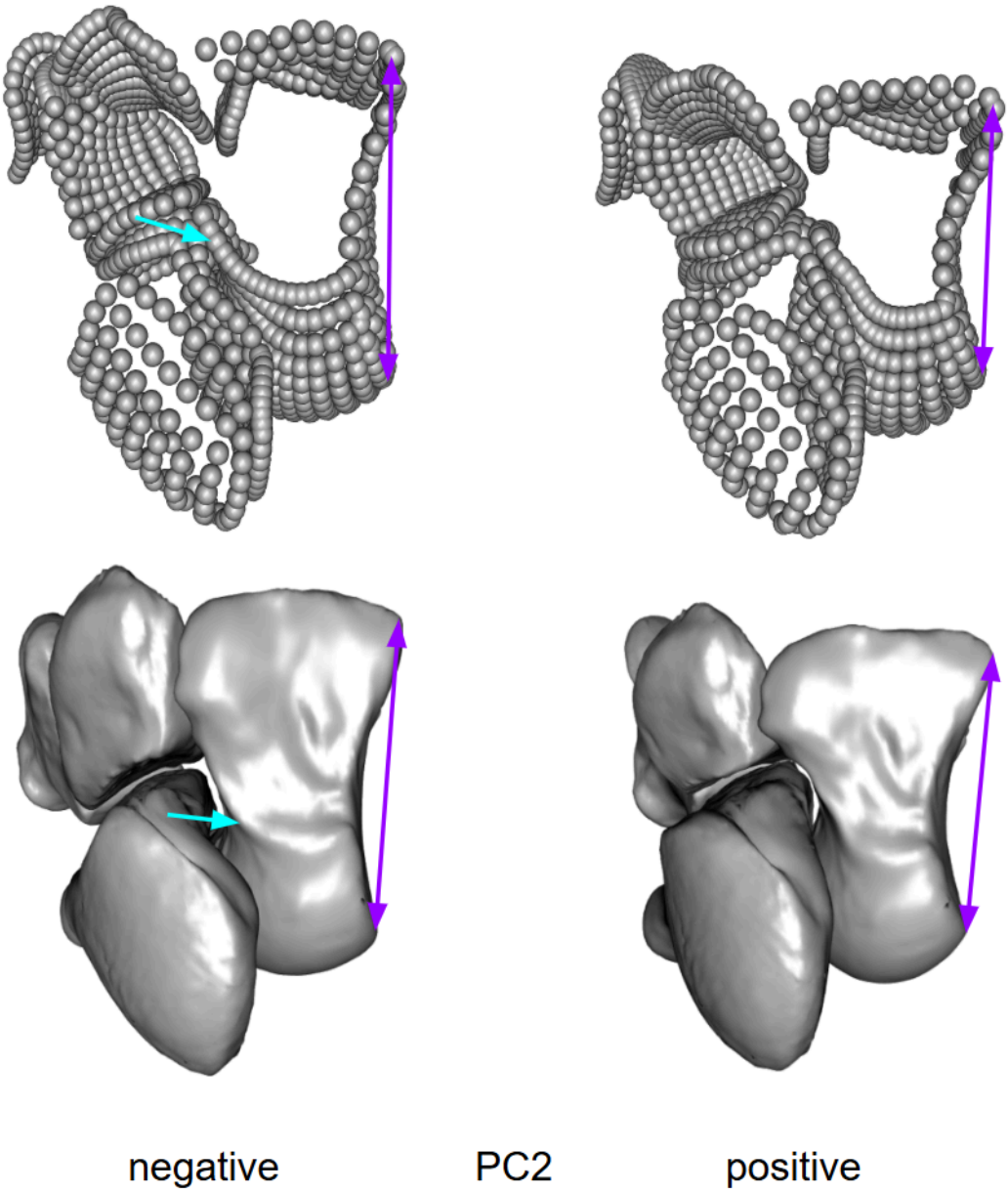

Figure 43. Dorsal view of the point clouds (top) and surface warps (bottom) along PC2 of the mean shape (see Figure 27) for the four-bone analysis of African apes only. The annotated features differ at the positive extreme relative to the negative extreme (light blue, lacks a dorsal ridge on the capitate; purple, shorter capitate-hamate facet). (RETURN TO TEXT) (RETURN TO DISCUSSION)

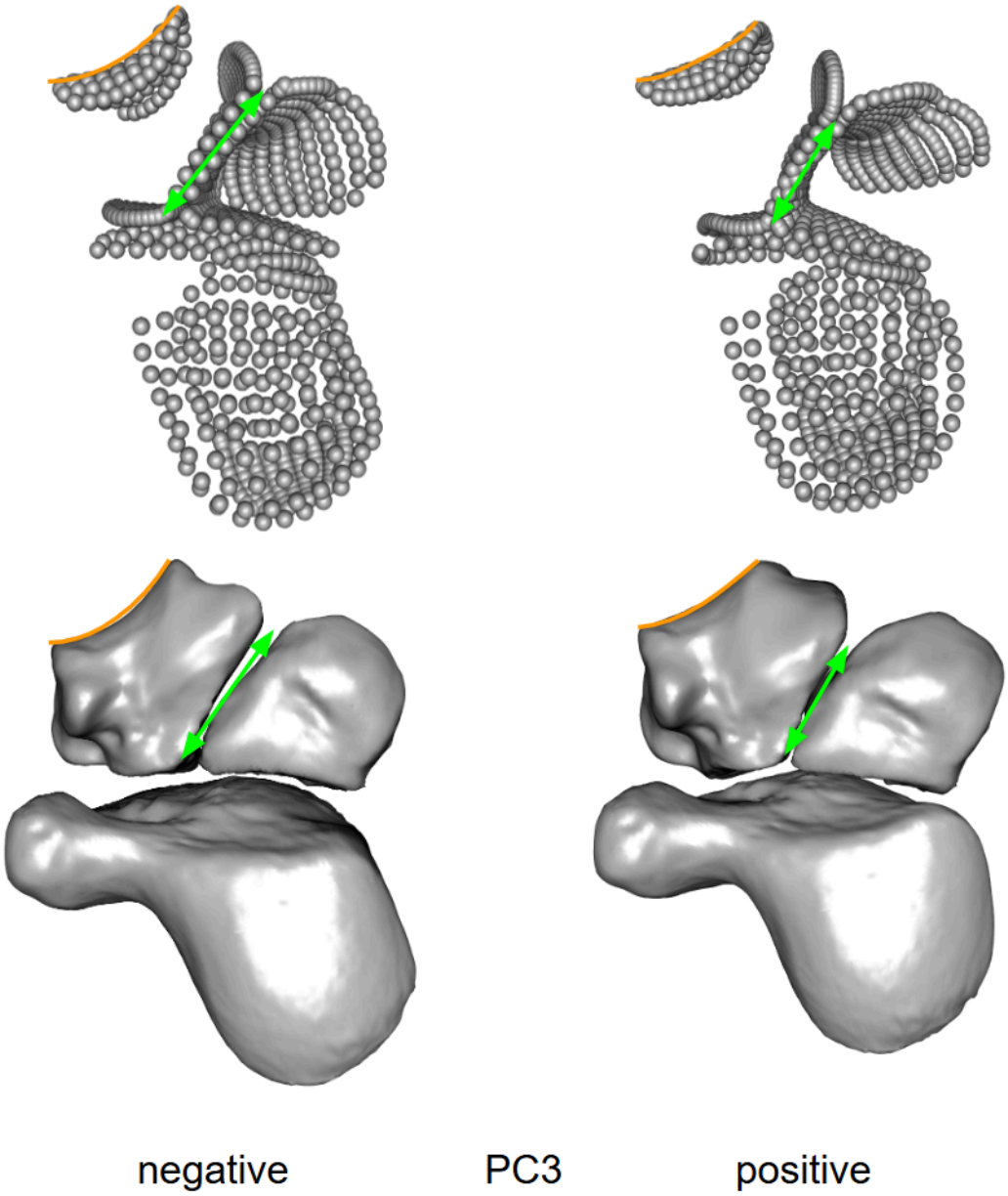

Figure 44. Dorsoradial view of the point clouds (top) and surface warps (bottom) along PC3 of the mean shape (see Figure 28) for the three-bone analysis of African apes only. The annotated features differ at the positive extreme relative to the negative extreme (orange, flatter trapezium-MC1 facet; green, shorter and less tilted trapezium-trapezoid facet). (RETURN TO TEXT) (RETURN TO DISCUSSION)

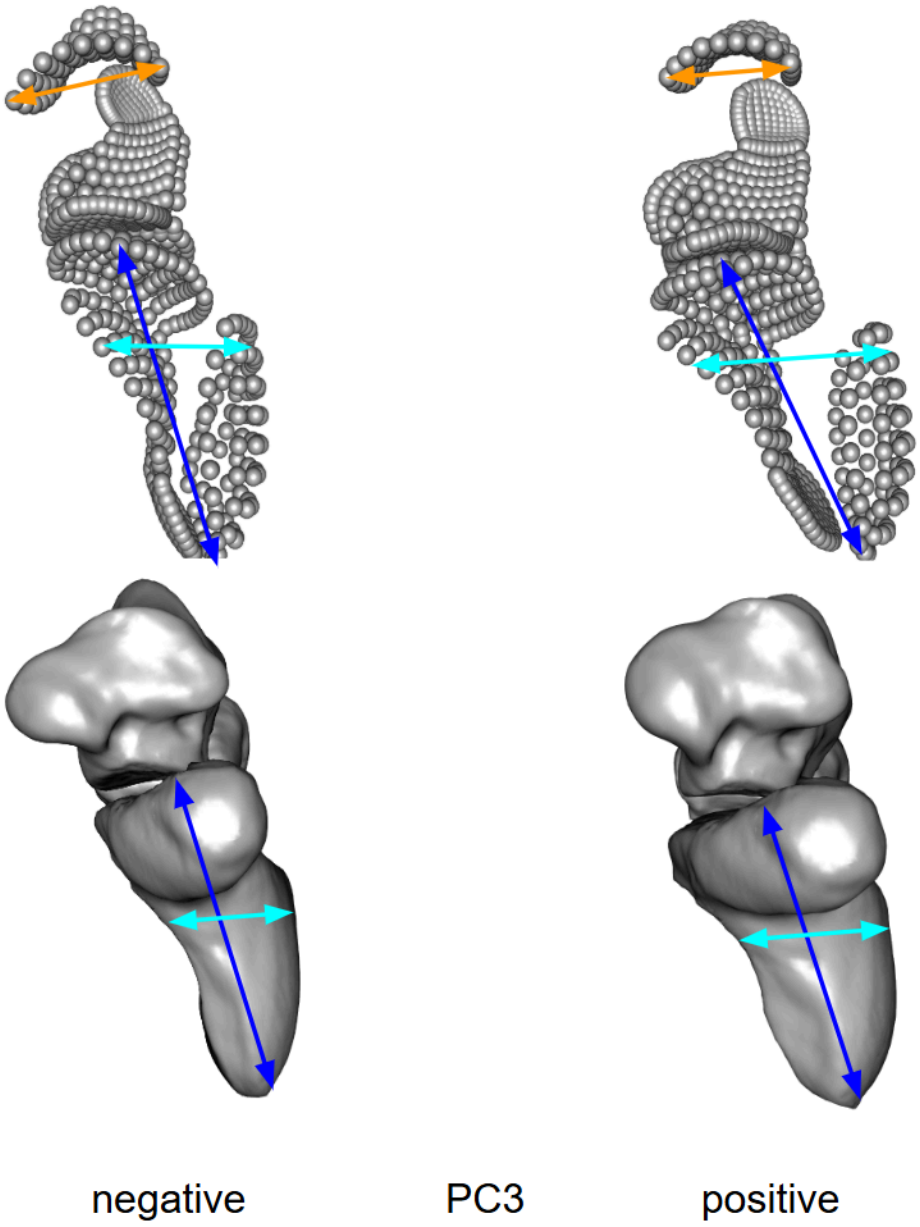

Figure 45. Radial view of the point clouds (top) and surface warps (bottom) along PC3 of the mean shape (see Figure 28) for the three-bone analysis of African apes only. The annotated features differ at the positive extreme relative to the negative extreme (orange, flatter trapezium-MC1 facet; orange, narrower trapezium-MC1 facet; light blue, thicker scaphoid; dark blue, shorter scaphoid). (RETURN TO TEXT) (RETURN TO DISCUSSION)

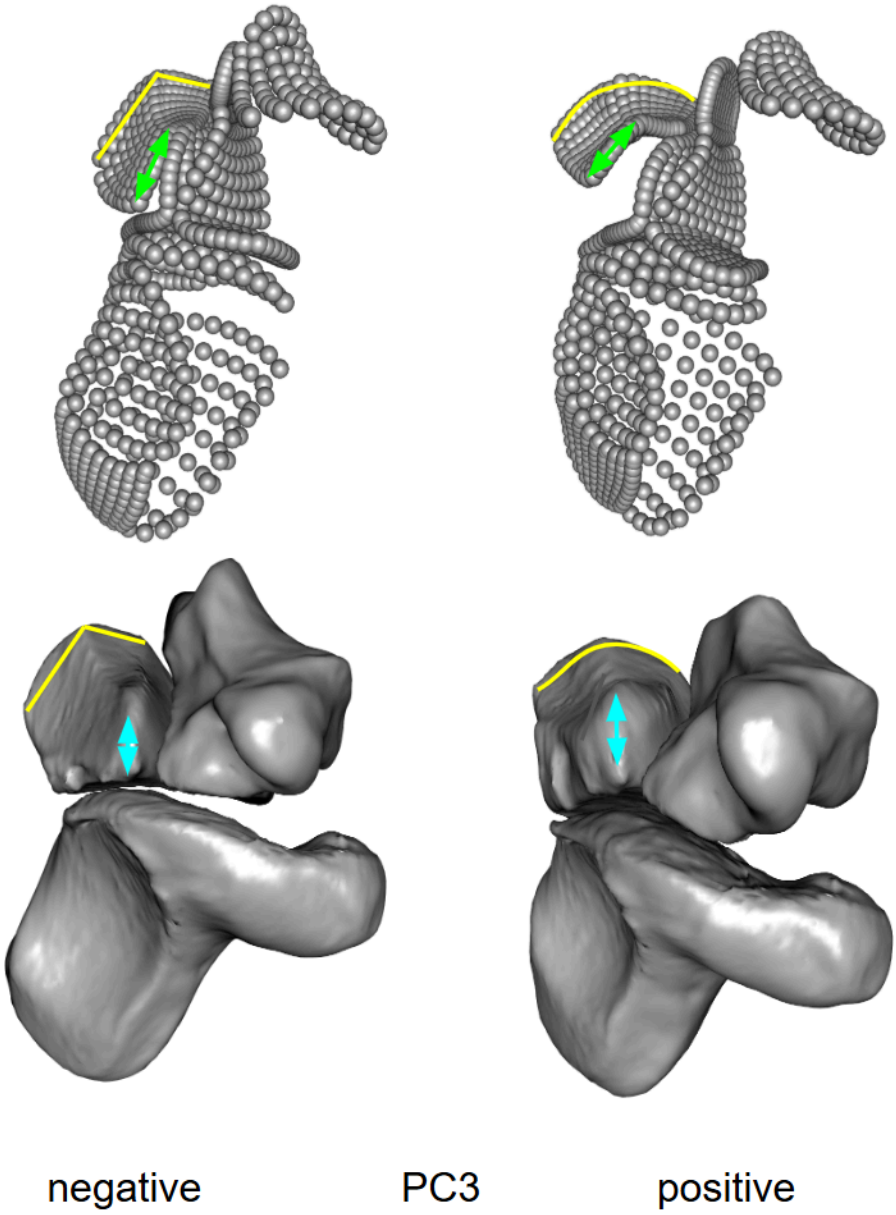

Figure 46. Palmar view of the point clouds (top) and surface warps (bottom) along PC3 of the mean shape (see Figure 28) for the three-bone analysis of African apes only. The annotated features differ at the positive extreme relative to the negative extreme (yellow, saddle-shaped trapezoid-MC2 joint; green, narrower and more proximodistally orientated trapezoid-ulnar MC2 facet; light blue, broader palmar nonarticular area on the trapezoid). (RETURN TO TEXT) (RETURN TO DISCUSSION)

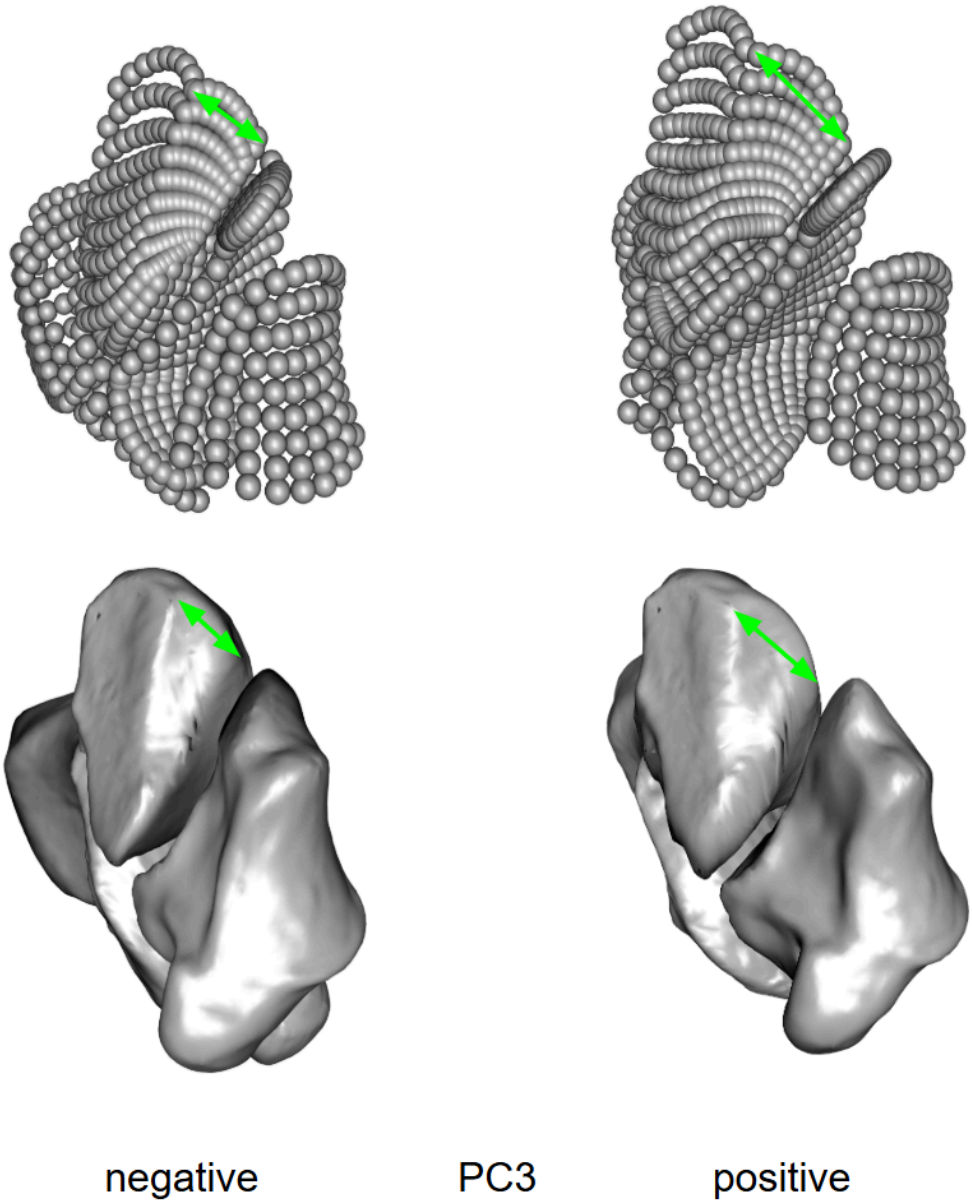

Figure 47. Distal view of the point clouds (top) and surface warps (bottom) along PC3 of the mean shape (see Figure 28) for the three-bone analysis of African apes only. The annotated features differ at the positive extreme relative to the negative extreme (green, wider trapezoid-radial MC2 facet). (RETURN TO TEXT) (RETURN TO DISCUSSION)

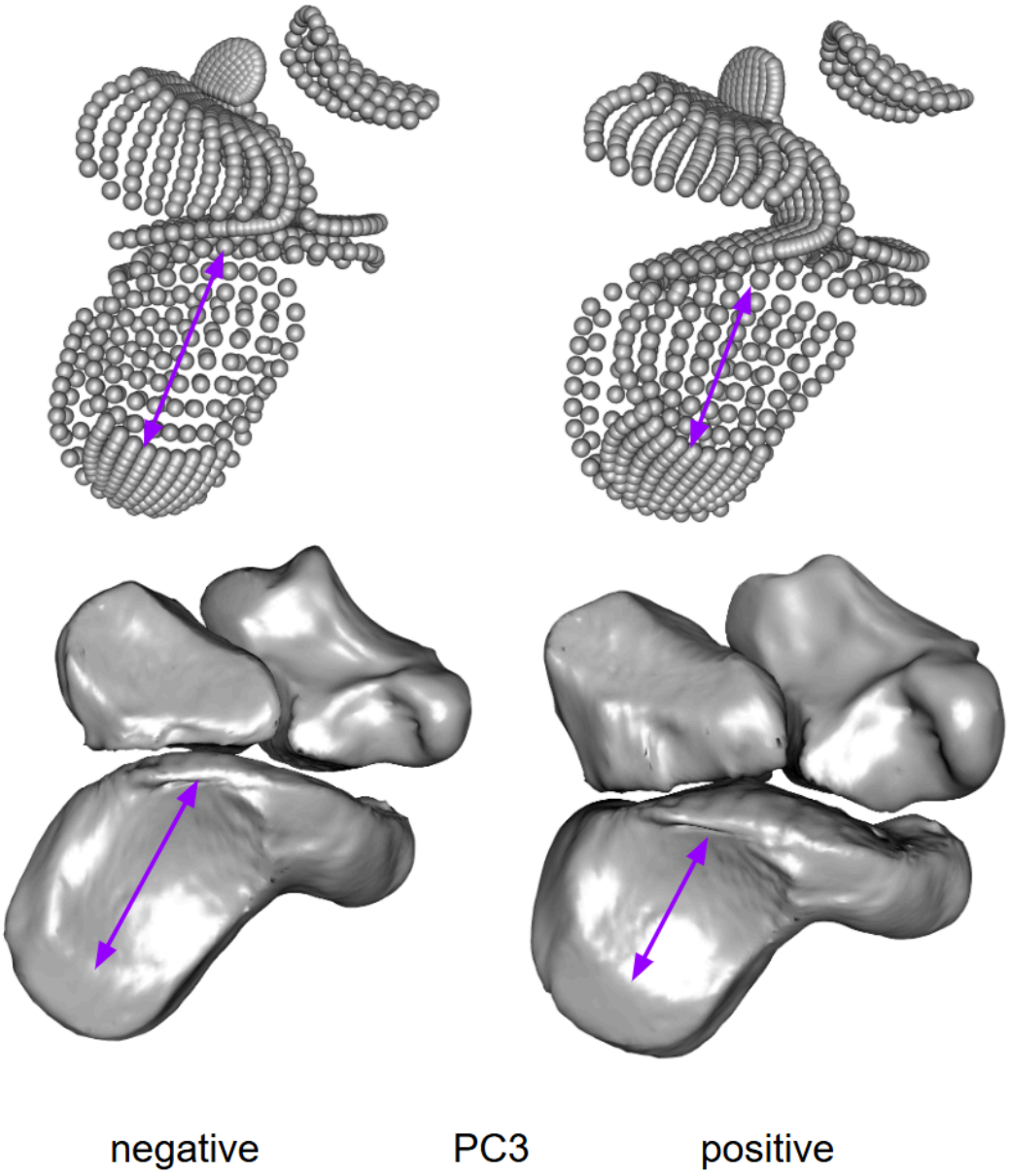

Figure 48. Ulnar view of the point clouds (top) and surface warps (bottom) along PC3 of the mean shape (see Figure 28) for the three-bone analysis of African apes only. The annotated features differ at the positive extreme relative to the negative extreme (purple, proximodistally shorter scaphoid-capitate facet). (RETURN TO TEXT) (RETURN TO DISCUSSION)

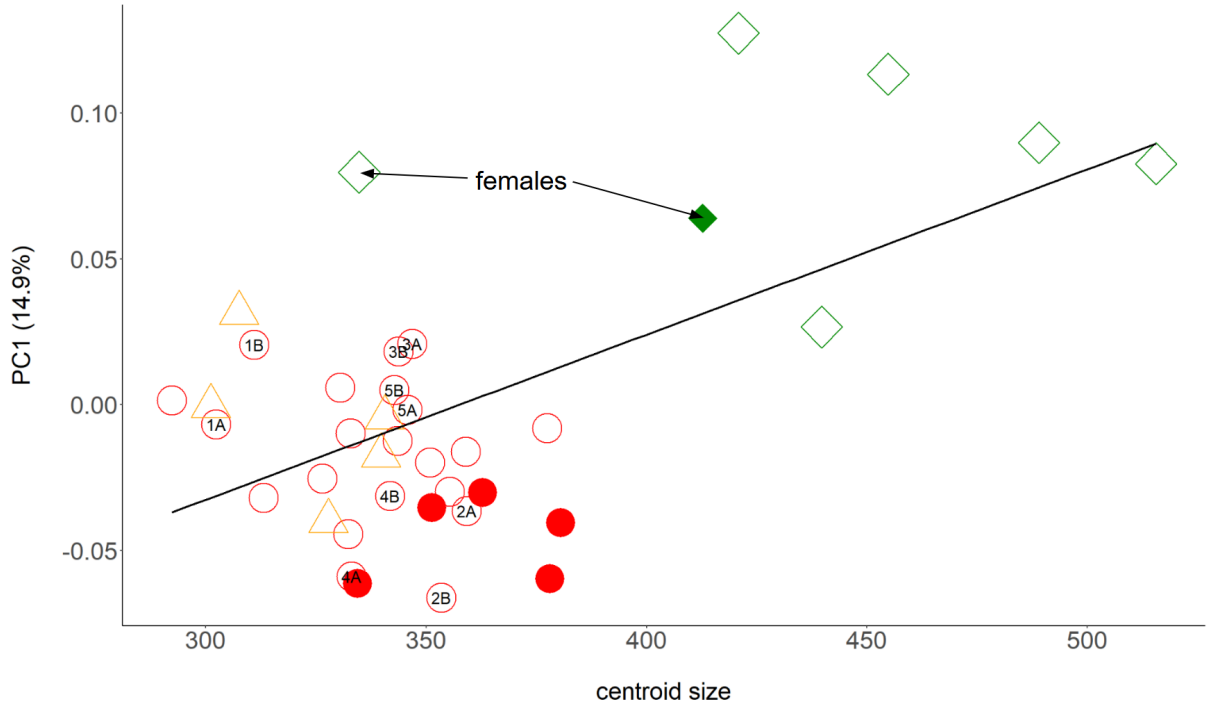

Figure 49. Centroid sizes of the articulated wrists versus PC1 of the three-bone analysis (chimpanzees = red circles, bonobos = yellow triangles, western gorillas = green diamonds). Closed and open shapes represent intact cadaver and manually articulated specimens, respectively. Symbols with the same number indicate duplicate articulations (A = OL's articulation, B = Dr. Tocheri's articulation). The line represents a linear regression and suggests a subtle trend between but not within taxa. (RETURN TO TEXT) (RETURN TO DISCUSSION)

Tables

Table 1. Sample of extant taxa used for this study. (RETURN TO TEXT)

Genus	# specimens	Bone				Bone combination	
		tpm	tzd	sca	cap	tpm, tzd, sca, cap	tpm, tzd, sca
G. g. gorilla	7	7	7	7	5	5	7
P. troglodytes	21	21	21	21	18	18	21
P. paniscus	5	5	5	5	5	5	5
H. sapiens	24	24	24	24	4	4	24
TOTAL	57	57	57	57	32	32	57

*tpm, trapezium; tzd, trapezoid; sca, scaphoid; cap, capitate

*There is one *G. g. gorilla* and five *P. troglodytes* from intact cadaver wrist

*Five *P. troglodytes* and two *H. sapiens* were articulated in duplicate (one by OL and the other by Dr. Tocheri) and are not included in table counts

Table 2. Description of anchor landmarks on the trapezium (see Figure 3). (RETURN TO TEXT)

Number	Description
1	Most proximodorsal point on the trapezoid facet
2	Most distodorsal point on the trapezoid facet
3	Most distopalmar point on the trapezoid facet
4	Most proximopalmar point on the trapezoid facet
5	Most proximodorsal point on the MC2 facet
6	Most proximopalmar point on the MC2 facet
7	Most radiopalmar point on the MC1 facet
8	Most dorsoradial point on the MC1 facet
9	Most ulnar point on the MC1 facet

Table 3. Description of anchor landmarks on the trapezoid (see Figure 4). (RETURN TO TEXT)

Number	Description
1	Most palmar point on the scaphoid facet
2	Most dorsoradial point on the scaphoid facet
3	Most dorsoulnar point on the scaphoid facet
4	Most palmar point of contact between the trapezium facet and the scaphoid facet
5	Most distal point on the trapezium facet
6	Most palmar point of contact between the trapezium facet and the scaphoid facet
7	Most palmar point on the radial portion of the MC2 facet
8	Most dorsal point of contact between the radial portion of the MC2 facet and the ulnar portion of the MC2 facet
9	Most dorsal point of contact between the radial portion of the MC2 facet and the trapezium facet
10	Most palmar-ulnar point on the ulnar portion of the MC2 facet
11	Most dorsoulnar point on the ulnar portion of the MC2 facet
12	Most dorsal point of contact between the ulnar portion of the MC2 facet and the radial portion of the MC2 facet
13	Most palmar point of contact between the ulnar portion of the MC2 facet and the radial portion of the MC2 facet

Table 4. Description of anchor landmarks on the scaphoid (see Figure 5). (RETURN TO TEXT)

Number	Description
1	Most proximoulnar point on the capitate facet
2	Most distoulnar point on the capitate facet
3	Most distoradial point on the capitate facet
4	Most proximoradial point on the capitate facet
5	Most ulnar point of contact between the lunate facet and the capitate facet
6	Most radial point of contact between the capitate facet and the lunate facet
7	Most palmar-ulnar point on the trapezium-trapezoid facet
8	Most dorsoradial point on the trapezium-trapezoid facet
9	Most radiopalmar point on the trapezium-trapezoid facet
10	Most distoradial point on the radius facet
11	Most distoulnar point on the radius facet

Table 5. Description of anchor landmarks on the capitate (see Figure 6). (RETURN TO TEXT)

Number	Description
1	Most dorsoproximal point on the hamate facet
2	Most dorsodistal point on the hamate facet
3	Most distopalmar point on the hamate facet
4	Most proximopalmar point on the hamate facet
5	Most palmar-ulnar point on the MC3 facet
6	Most dorsoulnar point on the MC3 facet
7	Most dorsoradial point on the MC3 facet
8	Most palmar point on the MC3 facet
9	Most dorsal point of contact between the MC2 facet and the MC3 facet
10	Most palmar point of contact between the MC2 facet and the MC3 facet
11	Most distopalmar point on the capitate facet
12	Most dorsodistal point on the capitate facet
13	Most distal point of contact between the dorsal portion lunate facet and the hamate facet
14	Most distal point of contact between the palmar portion lunate facet and the hamate facet

Table 6. Distinct carpal features in humans described in previous studies and/or documented in this study.

Morphology in humans	Function	Source	My study
Supinated trapezium / shallower carpal tunnel	Facilitates radioulnarly directed compressive forces	Lewis, 1989; Tocheri, 2007	Present
Relatively larger trapezium	Corresponds with a radioulnarly wider MC1 and scaphoid facet		Present
Larger trapezium-MC1 facet	Reduces radioulnarly directed compressive stress	Tocheri, 2007	Present
Larger trapezium-scaphoid facet	Reduces radioulnarly directed compressive stress	Marzke et al., 1992; Tocheri, 2007	Present
More parallel MC1 and facets on the trapezium	Reduces shear stress from radioulnarly directed forces	Tocheri, 2007	Present
Flatter MC1 facet	Increases thumb mobility / reduces stability of the trapezium-MC1 joint	Marzke et al., 2010; Tocheri, 2007	Present
Narrower trapezium palmar nonarticular area	Accommodates trapezoid expansion	Tocheri, 2007	Present
More proximodistally orientated trapezium-MC2 facet	Stabilizes the trapezium from sliding distally and facilitates mobility of index finger	Marzke, 1983; Marzke et al., 1992; Tocheri, 2007	Present
Broader palmar aspect of trapezoid	Corresponds with supinated position of the trapezium	Lewis, 1989; Tocheri, 2007	Present
Less angular trapezoid-MC2 facet	Facilitates mobility of index finger	Lewis, 1977	Present
More parallel MC2 and scaphoid facets on the trapezoid	In apes, the ulnar portion of the MC2 is slanted towards the palmar aspect of scaphoid facet, which would make the MCII facet more parallel to the scaphoid-radius joint and reduce shear stress during proximodistally directed forces	Tocheri, 2007	Present

Larger and more palmarly placed trapezoid-capitate facet	Reduces radioulnarly directed compressive stress	Lewis, 1989; Marzke et al., 1992; Tocheri, 2007	Present
More parallel capitate and trapezium facets on the trapezoid	Reduces shear stress from forces radioulnarly directed forces	Tocheri, 2007	Present
Smaller trapezoid-scaphoid facet	Corresponds with a larger trapezium-scaphoid facet	Lewis, 1989; Marzke et al., 1992; Tocheri, 2007	Present
The ulnar portion of the trapezoid-MCII facet is smaller	In apes, this facet is larger which would be more effective at reducing compressive stress from proximodistally directed forces	Tocheri, 2007	Absent
Larger trapezoid-trapezium joint	Reduces radioulnarly directed compressive stress	Marzke et al., 1992	Present
Proximodistally taller scaphoid	Corresponds with a smaller radius facet		Present
Smaller scaphoid-radius facet	In apes, the facet is larger which would reduce proximodistally directed compressive stress		Present
Reduction of bone along the distoulnar edge of the scaphoid	In apes, the additional bone provides more surface area for the trapezoid and stabalises the midcarpal joint	Tocheri, 2007	Present
The capitate is relatively shorter proximodistally	Related to shortening of the hand	McHenry, 1983	Absent
Lacks dorsal ridge on the scaphoid	More mobile radiocarpal joint. In apes, this ridge limits dorsal rotation of the scaphoid relative to the radius during wrist extension	Lewis, 1989	Absent
Thicker capitate neck	Facilitates radioulnarly directed compressive forces	Kivell and Schmitt, 2009; Lewis,	Present

		1973, 1989; Richmond et al., 2001	
Less excavated radial surface of the capitate	Corresponds with a thicker capitate neck	Lewis, 1973, 1989	Present
Flatter capitate-hamate facet	Corresponds with a thicker capitate neck		Present
Dorsopalmarly shorter capitate-MC3 facet	In apes this facet is longer, reducing proximodistally directed compressive stress		Present
More regular capitate-MC3 facet	In apes, this facet is irregular which may facilitate close-packing of the wrist for stability	McHenry, 1983	Present
Bevelled dorsoradial corner of the capitate	Stabilizes the MC3 base	Marzke and Marzke, 1987	Present
More proximodistally oriented capitate-MC2 facet	Stabilizes the capitate from sliding distally and facilitates mobility of index finger	Marzke, 1983; Marzke et al., 1992; Tocheri, 2007	Present
Lacks dorsal ridge on the capitate	The dorsal ridge limits wrist extension in *Pan*	Kivell and Schmitt, 2009	Absent

References

Adams, D., Collyer, M., Kaliontzopoulou, A., Baken, E., 2025. Geomorph: Software for geometric morphometric analyses. R package version 4.0.4.

Adams, D.C., Rohlf, F.J., Slice, D.E., 2004. Geometric morphometrics: Ten years of progress following the 'revolution.' Ital. J. Zool. 71, 5–16.

Almécija, S., Orr, C.M., Tocheri, M.W., Patel, B.A., Jungers, W.L., 2015. Exploring phylogenetic and functional signals in complex morphologies: The hamate of extant anthropoids as a test-case study. Anat. Rec. 298, 212–229.

Ateshian, G.A., Rosenwasser, M.P., Mow, V.C., 1992. Curvature characteristics and congruence of the thumb carpometacarpal joint: Differences between female and male joints. J. Biomech. 25, 591–607.

Baab, K.L., McNulty, K.P., 2009. Size, shape, and asymmetry in fossil hominins: The status of the LB1 cranium based on 3D morphometric analyses. J. Hum. Evol. 57, 608–622.

Baken, E.K., Collyer, M.L., Kaliontzopoulou, A., Adams, D.C., 2021. geomorph v4.0 and gmShiny: Enhanced analytics and a new graphical interface for a comprehensive morphometric experience. Methods Ecol. Evol. 12, 2355–2363.

Bardo, A., Moncel, M.-H., Dunmore, C.J., Kivell, T.L., Pouydebat, E., Cornette, R., 2020. The implications of thumb movements for Neanderthal and modern human manipulation. Sci. Rep. 10, 19323.

Bardua, C., Felice, R.N., Watanabe, A., Fabre, A.-C., Goswami, A., 2019. A practical guide to sliding and surface semilandmarks in morphometric analyses. Integr. Org. Biol. 1, obz016.

Berger, R.A., 1996. The anatomy and basic biomechanics of the wrist joint. J. Hand Ther. 9, 84–93.

Berger, R.A., 2001. The anatomy of the ligaments of the wrist and distal radioulnar joints. Clin. Orthop. Relat. Res. 383, 32–40.

Bettinger, P.C., Berger, R.A., 2001. Functional ligamentous anatomy of the trapezium and trapeziometacarpal joint (gross and arthroscopic). Hand Clin. 17, 151–168.

Bettinger, P.C., Linscheid, R.L., Berger, R.A., Cooney, W.P., An, K.-N., 1999. An anatomic study of the stabilizing ligaments of the trapezium and trapeziometacarpal joint. J. Hand Surg. 24, 786–798.

Bettinger, P.C., Smutz, W.P., Linscheid, R.L., Cooney, W.P., An, K.-N., 2000. Material properties of the trapezial and trapeziometacarpal ligaments. J. Hand Surg. 25, 1085–1095.

Biewener, A.A., 1989. Scaling body support in mammals: Limb posture and muscle mechanics. Science 245, 45–48.

Bird, E.E., Kivell, T.L., Dunmore, C.J., Tocheri, M.W., Skinner, M.M., 2024. Trabecular bone structure of the proximal capitate in extant hominids and fossil hominins with implications for midcarpal joint loading and the dart-thrower's motion. Am. J. Biol. Anthropol. 183, e24824.

Bird, E.E., Kivell, T.L., Skinner, M.M., 2021. Cortical and trabecular bone structure of the

hominoid capitate. J. Anat. 239, 351–373.
Bird, E.E., Kivell, T.L., Skinner, M.M., 2022. Patterns of internal bone structure and functional adaptation in the hominoid scaphoid, lunate, and triquetrum. Am. J. Biol. Anthropol. 177, 266–285.
Bishop, A.T., Gabel, G., Carmichael, S.W., 1994. Flexor carpi radialis tendinitis. Part I: Operative anatomy. J. Bone Jt. Surg. 76, 1009.
Bookstein, F.L., 1992. Morphometric Tools for Landmark Data: Geometry and Biology. Cambridge University Press, Cambridge.
Cant, J.G.H., 1987. Positional behavior of female bornean orangutans (*Pongo pygmaeus*). Am. J. Primatol. 12, 71–90.
Coolidge, H.J., Shea, B.T., 1982. External body dimensions of *Pan paniscus* and *Pan troglodytes* chimpanzees. Primates 23, 245–251.
Cooney, W.P., Linscheid, R.L., An, K.-N., 1984. Opposition of the thumb: An anatomic and biomechanical study of tendon transfers. J. Hand Surg. 9, 777–786.
Cooney, W.P., Chao, E.Y., 1977. Biomechanical analysis of static forces in the thumb during hand function. J. Bone Jt. Surg. 59, 27–36.
Corruccini, R.S., 1978. Comparative osteometrics of the hominoid wrist joint, with special reference to knuckle-walking. J. Hum. Evol. 7, 307–321.
Corruccini, R.S., Ciochon, R.L., McHenry, H.M., 1975. Osteometric shape relationships in the wrist joint of some anthropoids. Folia Primatol. 24, 250–274.
Crisco, J.J., Coburn, J.C., Moore, D.C., Akelman, E., Weiss, A.-P.C., Wolfe, S.W., 2005. In vivo radiocarpal kinematics and the dart thrower's motion. J. Bone Jt. Surg. 87, 2729.
Daver, G., Détroit, F., Berillon, G., Prat, S., Grimaud-Hervé, D., 2014. Fossil hominins, quadrupedal primates and the origin of human bipedalism: A 3D geometric morphometric analysis of the primate hamate. Bull. Mém. Soc. Anthropol. 26, 121–128.
Doran, D.M., 1992. The ontogeny of chimpanzee and pygmy chimpanzee locomotor behavior: A case study of paedomorphism and its behavioral correlates. J. Hum. Evol. 23, 139–157.
Doran, D.M., 1993. Comparative locomotor behavior of chimpanzees and bonobos: The influence of morphology on locomotion. Am. J. Phys. Anthropol. 91, 83–98.
Doran, D.M., 1996. Comparative positional behavior of the African apes. In: Marchant, L.F., Nishida, T., McGrew, W.C. (Eds.), Great Ape Societies. Cambridge University Press, Cambridge, pp. 213–224.
Doran, D.M., 1997. Ontogeny of locomotion in mountain gorillas and chimpanzees. J. Hum. Evol. 32, 323–344.
Doran, D.M., Hunt, K.D., 1994. Comparative locomotor behavior of chimpanzees and bonobos: Species and habitat differences. In: Wrangham, R.W., McGrew W.C., Heltne, P.G. (Eds.), Chimpanzee Cultures. Harvard University Press, Cambridge, pp. 93–108.
Doran, D.M., McNeilage, A., 1998. Gorilla ecology and behavior. Evol. Anthropol. 6, 120–131.
Druelle, F., Schoonaert, K., Aerts, P., Nauwelaerts, S., Stevens, J.M.G., D'Août, K., 2018. Segmental morphometrics of bonobos (*Pan paniscus*): Are they really different from

chimpanzees (*Pan troglodytes*)? J. Anat. 233, 843–853.
El-Shennawy, M., Nakamura, K., Patterson, R.M., Viegas, S.F., 2001. Three-dimensional kinematic analysis of the second through fifth carpometacarpal joints. J. Hand Surg. 26, 1030–1035.
Eschweiler, J., Li, J., Quack, V., Rath, B., Baroncini, A., Hildebrand, F., Migliorini, F., 2022. Anatomy, biomechanics, and loads of the wrist joint. Life 12, 188.
Finestone, E.M., Brown, M.H., Ross, S.R., Pontzer, H., 2018. Great ape walking kinematics: Implications for hominoid evolution. Am. J. Biol. Anthropol. 166, 43–55.
Friess, M., 2010. Calvarial shape variation among Middle Pleistocene hominins: An application of surface scanning in palaeoanthropology. C.R. Palevol. 9, 435–443.
Garcia-Elias, M., 1997. Kinetic analysis of carpal stability during grip. Hand Clin. 13, 151–158.
Godfrey, L., Sutherland, M., Boy, D., Gomberg, N., 1991. Scaling of limb joint surface areas in anthropoid primates and other mammals. J. Zool. 223, 603–625.
Godfrey, L.R., Sutherland, M.R., Paine, R.R., Williams, F.L., Boy, D.S., Vuillaume-Randriamanantena, M., 1995. Limb joint surface areas and their ratios in Malagasy lemurs and other mammals. Am. J. Phys. Anthropol. 97, 11–36.
Goldsmith, M.L., 1996. Ecological influences on the ranging and grouping behavior of western lowland gorillas at Bai Hoköu, Central African Republic. Ph.D. Dissertation, State University of New York at Stony Brook.
Goldstein, D.M., Sylvester, A.D., 2023. Carpal allometry of African apes among mammals. Am. J. Biol. Anthropol. 181, 10–28.
Groves, C.P., 1971. Distribution and place of origin of the gorilla. Man 6, 44–51.
Gunz, P., Mitteroecker, P., 2013. Semilandmarks: a method for quantifying curves and surfaces. Hystrix It. J. Mamm. 24, 103–109.
Gunz, P., Mitteroecker, P., Bookstein, F.L., 2005. Semilandmarks in three dimensions. In: Slice, D.E. (Ed.), Modern Morphometrics in Physical Anthropology, Developments in Primatology: Progress and Prospects. Springer US, Boston, pp. 73–98.
Hamrick, M.W., Churchill, S.E., Schmitt, D., Hylander, W.L., 1998. EMG of the human flexor pollicis longus muscle: Implications for the evolution of hominid tool use. J. Hum. Evol. 34, 123–136.
Hamrick, M.W., Inouye, S.E., 1995. Thumbs, tools, and early humans. Science 268, 586–587.
Hawks, J., Elliott, M., Schmid, P., Churchill, S.E., Ruiter, D.J. de, Roberts, E.M., Hilbert-Wolf, H., Garvin, H.M., Williams, S.A., Delezene, L.K., Feuerriegel, E.M., Randolph-Quinney, P., Kivell, T.L., Laird, M.F., Tawane, G., DeSilva, J.M., Bailey, S.E., Brophy, J.K., Meyer, M.R., Skinner, M.M., Tocheri, M.W., VanSickle, C., Walker, C.S., Campbell, T.L., Kuhn, B., Kruger, A., Tucker, S., Gurtov, A., Hlophe, N., Hunter, R., Morris, H., Peixotto, B., Ramalepa, M., Rooyen, D. van, Tsikoane, M., Boshoff, P., Dirks, P.H., Berger, L.R., 2017. New fossil remains of *Homo naledi* from the Lesedi Chamber, South Africa. eLife 6, e24232.
Hollister, A., Buford, W.L., Myers, L.M., Giurintano, D.J., Novick, A., 1992. The axes of

rotation of the thumb carpometacarpal joint. J. Orthop. Res. 10, 454–460.
Hollister, A., Giurintano, D.J., 1995. Thumb movements, motions, and moments. J. Hand Ther. 8, 106–114.
Hunt, K.D., 1991. Mechanical implications of chimpanzee positional behavior. Am. J. Phys. Anthropol. 86, 521–536.
Hunt, K.D., 1992. Positional behavior of *Pan troglodytes* in the Mahale Mountains and Gombe Stream National Parks, Tanzania. Am. J. Phys. Anthropol. 87, 83–105.
Hunt, K.D., 1994. The evolution of human bipedality: Ecology and functional morphology. J. Hum. Evol. 26, 183–202.
Hunt, K.D., 2016. Why are there apes? Evidence for the co-evolution of ape and monkey ecomorphology. J. Anat. 228, 630–685.
Infantolino, B.W., Challis, J.H., 2010. Architectural properties of the first dorsal interosseous muscle. J. Anat. 216, 463–469.
Inouye, S.E., 1992. Ontogeny and allometry of African ape manual rays. J. Hum. Evol. 23, 107–138.
Inouye, S.E., 1994. Ontogeny of knuckle-walking hand postures in African apes. J. Hum. Evol. 26, 459–485.
Jungers, W.L., Susman, R.L., 1984. Body size and skeletal allometry in African apes. In: Susman, R.L. (Ed.), The Pygmy Chimpanzee: Evolutionary Biology and Behavior. Springer US, Boston, pp. 131–177.
Kaufmann, R.A., Pfaeffle, H.J., Blankenhorn, B.D., Stabile, K., Robertson, D., Goitz, R., 2006. Kinematics of the midcarpal and radiocarpal joint in flexion and extension: An in vitro study. J. Hand Surg. 31, 1142–1148.
Key, A., Merritt, S.R., Kivell, T.L., 2018. Hand grip diversity and frequency during the use of Lower Palaeolithic stone cutting-tools. J. Hum. Evol. 125, 137–158.
Kijima, Y., Viegas, S.F., 2009. Wrist anatomy and biomechanics. J. Hand Surg. 34, 1555–1563.
Kivell, T.L., 2016. A review of trabecular bone functional adaptation: What have we learned from trabecular analyses in extant hominoids and what can we apply to fossils? J. Anat. 228, 569–594.
Kivell, T.L., Baraki, N., Lockwood, V., Williams-Hatala, E.M., Wood, B.A., 2023. Form, function and evolution of the human hand. Am. J. Biol. Anthropol. 181, 6–57.
Kivell, T.L., Barros, A.P., Smaers, J.B., 2013. Different evolutionary pathways underlie the morphology of wrist bones in hominoids. BMC Evol. Biol. 13, 229.
Kivell, T.L., Begun, D.R., 2006. Functional morphology of new *Dryopithecus* carpals from Rudabánya, Hungary. Am. J. Phys. Anthropol. 129, 114.
Kivell, T.L., Begun, D.R., 2007. Frequency and timing of scaphoid-centrale fusion in hominoids. J. Hum. Evol. 52, 321–340.
Kivell, T.L., Begun, D.R., 2009. New primate carpal bones from Rudabánya (late Miocene, Hungary): Taxonomic and functional implications. J. Hum. Evol. 57, 697–709.
Kivell, T.L., Deane, A.S., Tocheri, M.W., Orr, C.M., Schmid, P., Hawks, J., Berger, L.R.,

Churchill, S.E., 2015. The hand of *Homo naledi*. Nat. Commun. 6, 8431.
Kivell, T.L., Kibii, J.M., Churchill, S.E., Schmid, P., Berger, L.R., 2011. *Australopithecus sediba* hand demonstrates mosaic evolution of locomotor and manipulative abilities. Science 333, 1411–1417.
Kivell, T.L., Rosas, A., Estalrrich, A., Huguet, R., García-Tabernero, A., Ríos, L., de la Rasilla, M., 2018. New Neandertal wrist bones from El Sidrón, Spain (1994–2009). J. Hum. Evol. 114, 45–75.
Kivell, T.L., Schmitt, D., 2009. Independent evolution of knuckle-walking in African apes shows that humans did not evolve from a knuckle-walking ancestor. Proc. Natl. Acad. Sci. 106, 14241–14246.
Kobayashi, M., Garcia-Elias, M., Nagy, L., Ritt, M.J.P.F., An, K.-N., Cooney, W.P., Linscheid, R.L., 1997. Axial loading induces rotation of the proximal carpal row bones around unique screw-displacement axes. J. Biomech. 30, 1165–1167.
Landsmeer, J.M.F., 1962. Power grip and precision handling. Ann. Rheum. Dis. 21, 164–170.
Lewis, O.J., 1969. The hominoid wrist joint. Am. J. Phys. Anthropol. 30, 251–267.
Lewis, O.J., 1972. Osteological features characterizing the wrists of monkeys and apes, with a reconsideration of this region in *Dryopithecus* (*Proconsul*) *africanus*. Am. J. Phys. Anthropol. 36, 45–58.
Lewis, O.J., 1973. The hominoid os capitatum, with special reference to the fossil bones from Sterkfontein and Olduvai Gorge. J. Hum. Evol. 2, 1–11.
Lewis, O.J., 1977. Joint remodelling and the evolution of the human hand. J. Anat. 123, 157–201.
Lewis, O.J., 1989. Functional morphology of the evolving hand and foot. Clarendon Press, Oxford.
Lewis, O.J., Hamshere, R.J., Bucknill, T.M., 1970. The anatomy of the wrist joint. J. Anat. 106, 539–552.
MacConaill, M.A., 1941. The mechanical anatomy of the carpus and its bearings on some surgical problems. J. Anat. 75, 166–175.
Marzke, M.W., 1971. Origin of the human hand. Am. J. Phys. Anthropol. 34, 61–84.
Marzke, M.W., 1983. Joint functions and grips of the *Australopithecus afarensis* hand, with special reference to the region of the capitate. J. Hum. Evol. 12, 197–211.
Marzke, M.W., 1992. Evolutionary development of the human thumb. Hand Clin. 8, 1–8.
Marzke, M.W., 1997. Precision grips, hand morphology, and tools. Am. J. Phys. Anthropol. 102, 91–110.
Marzke, M.W., 2013. Tool making, hand morphology and fossil hominins. Philos. Trans. R. Soc. B 368, 20120414.
Marzke, M.W., Marzke, R.F., 1987. The third metacarpal styloid process in humans: Origin and functions. Am. J. Phys. Anthropol.73, 415–431.
Marzke, M.W., Marzke, R.F., 2000. Evolution of the human hand: Approaches to acquiring, analysing and interpreting the anatomical evidence. J. Anat. 197, 121–140.

Marzke, M.W., Shackley, M.S., 1986. Hominid hand use in the pliocene and pleistocene: Evidence from experimental archaeology and comparative morphology. J. Hum. Evol. 15, 439–460.

Marzke, M.W., Tocheri, M.W., Steinberg, B., Femiani, J.D., Reece, S.P., Linscheid, R.L., Orr, C.M., Marzke, R.F., 2010. Comparative 3D quantitative analyses of trapeziometacarpal joint surface curvatures among living catarrhines and fossil hominins. Am. J. Phys. Anthropol. 141, 38–51.

Marzke, M.W., Toth, N., Schick, K., Reece, S., Steinberg, B., Hunt, K., Linscheid, R.L., An, K.-N., 1998. EMG study of hand muscle recruitment during hard hammer percussion manufacture of Oldowan tools. Am. J. Phys. Anthropol. 105, 315–332.

Marzke, M.W., Wullstein, K.L., 1996. Chimpanzee and human grips: A new classification with a focus on evolutionary morphology. Int. J. Primatol. 17, 117–139.

Marzke, M.W., Wullstein, K.L., Viegas, S.F., 1992. Evolution of the power ("squeeze") grip and its morphological correlates in hominids. Am. J. Phys. Anthropol. 89, 283–298.

Marzke, M.W., Wullstein, K.L., Viegas, S.F., 1994. Variability at the carpometacarpal and midcarpal joints involving the fourth metacarpal, hamate, and lunate in catarrhini. Am. J. Phys. Anthropol. 93, 229–240.

Matarazzo, S., 2013. Manual pressure distribution patterns of knuckle-walking apes. Am. J. Phys. Anthropol. 152, 44–50.

Mayfield, J.K., Johnson, R.P., Kilcoyne, R.F., 1976. The ligaments of the human wrist and their functional significance. Anat. Rec. 186, 417–428.

McHenry, H.M., Corruccini, R.S., 1981. *Pan paniscus* and human evolution. Am. J. Phys. Anthropol. 54, 355–367.

McHenry, H.M., 1983. The capitate of *Australopithecus afarensis* and *A. africanus*. Am. J. Phys. Anthropol. 62, 187–198.

Momose, T., Nakatsuchi, Y., Saitoh, S., 1999. Contact area of the trapeziometacarpal joint. J. Hand Surg. 24, 491–495.

Monteiro, L.R., Bordin, B., Furtado dos Reis, S., 2000. Shape distances, shape spaces and the comparison of morphometric methods. Trends Ecol. Evol. 15, 217–220.

Monteiro, L.R., Diniz-Filho, J.A.F., Furtado dos Reis, S., Araújo, E.D., 2002. Geometric estimates of heritability in biological shape. Evolution 56, 563–572.

Moojen, T.M., Snel, J.G., Ritt, M.J.P.F., Kauer, J.M.G., Venema, H.W., Bos, K.E., 2002. Three-dimensional carpal kinematics in vivo. Clin. Biomech. 17, 506–514.

Moojen, T.M., Snel, J.G., Ritt, M.J.P.F., Venema, H.W., Kauer, J.M.G., Bos, K.E., 2003. In vivo analysis of carpal kinematics and comparative review of the literature. J. Hand Surg. 28, 81–87.

Napier, J.R., 1962. The evolution of the hand. Sci. Am. 207, 56–62.

Napier, J.R., 1955. The form and function of the carpo-metacarpal joint of the thumb. J. Anat. 89, 362–369.

Napier, J.R., 1956. The prehensile movements of the human hand. J. Bone Jt. Surg. 38-B,

902–913.
Napier, J.R., 1960. Studies of the hands of living primates. Proc. Zool. Soc. Lond. 134, 647–657.
Neufuss, J., Robbins, M.M., Baeumer, J., Humle, T., Kivell, T.L., 2017. Comparison of hand use and forelimb posture during vertical climbing in mountain gorillas (*Gorilla beringei beringei*) and chimpanzees (*Pan troglodytes*). Am. J. Phys. Anthropol. 164, 651–664.
Niewoehner, W.A., 2005. A geometric morphometric analysis of late pleistocene human metacarpal 1 base shape. In: Slice, D.E. (Ed.), Modern Morphometrics in Physical Anthropology. Springer US, Boston, pp. 285–298.
Niewoehner, W.A., Weaver, A.H., Trinkaus, E., 1997. Neandertal capitate-metacarpal articular morphology. Am. J. Phys. Anthropol. 103, 219–233.
Orr, C.M., 2008. Locomotor hand postures and the functional anatomy of the hominid wrist. FASEB J. 22, 239.3.
Orr, C.M., 2017. Locomotor hand postures, carpal kinematics during wrist extension, and associated morphology in anthropoid primates. Anat. Rec. 300, 382–401.
Orr, C.M., 2018. Kinematics of the anthropoid os centrale and the functional consequences of scaphoid-centrale fusion in African apes and hominins. J. Hum. Evol. 114, 102–117.
Orr, C.M., Atkinson, R., Ernewein, J., Tocheri, M.W., 2023. Carpal kinematics and morphological correlates of wrist ulnar deviation mobility in nonhuman anthropoid primates. Am. J. Biol. Anthropol.
Orr, C.M., Leventhal, E.L., Chivers, S.F., Marzke, M.W., Wolfe, S.W., Crisco, J.J., 2010. Studying primate carpal kinematics in three dimensions using a computed-tomography-based markerless registration method. Anat. Rec. 293, 692–709.
Orr, C.M., Tocheri, M.W., Burnett, S.E., Rokus Awe Due, Wahyu Saptomo, E., Sutikna, T., Jatmiko, Wasisto, S., Morwood, M.J., Jungers, W.L., 2013. New wrist bones of *Homo floresiensis* from Liang Bua (Flores, Indonesia). J. Hum. Evol. 64, 109–129.
Orr, C.M., Atkinson, R., Ernewein, J., Tocheri, M.W., 2024. Carpal kinematics and morphological correlates of wrist ulnar deviation mobility in nonhuman anthropoid primates. Am. J. Biol. Anthropol. 183, e24728.
Palmer, A.K., Werner, F.W., Murphy, D., Glisson, R., 1985. Functional wrist motion: A biomechanical study. J. Hand Surg. 10, 39–46.
Polk, J.D., 2004. Influences of limb proportions and body size on locomotor kinematics in terrestrial primates and fossil hominins. J. Hum. Evol. 47, 237–252.
Polk, J.D., Williams, S.A., Peterson, J.V., 2009. Body size and joint posture in primates. Am. J. Phys. Anthropol. 140, 359–367.
Preuschoft, H., Weinmann, W., 1973. Biomechanical investigations of *Limnopithecus* with special reference to the influence exerted by body weight on bone thickness. Am. J. Phys. Anthropol. 38, 241–250.
Prüfer, K., Munch, K., Hellmann, I., Akagi, K., Miller, J.R., Walenz, B., Koren, S., Sutton, G., Kodira, C., Winer, R., Knight, J.R., Mullikin, J.C., Meader, S.J., Ponting, C.P., Lunter, G., Higashino, S., Hobolth, A., Dutheil, J., Karakoç, E., Alkan, C., Sajjadian, S., Catacchio,

C.R., Ventura, M., Marques-Bonet, T., Eichler, E.E., André, C., Atencia, R., Mugisha, L., Junhold, J., Patterson, N., Siebauer, M., Good, J.M., Fischer, A., Ptak, S.E., Lachmann, M., Symer, D.E., Mailund, T., Schierup, M.H., Andrés, A.M., Kelso, J., Pääbo, S., 2012. The bonobo genome compared with the chimpanzee and human genomes. Nature 486, 527–531.

R Core Team, 2024. R: A language and environment for statistical computing. R Foundation for Statistical Computing, Vienna, Austria. URL: http://www.R-project.org/.

Ramos, G.L. III, 2014. Positional behavior in *Pan paniscus* at Lui Kotale, Democratic Republic of Congo. Ph.D. Dissertation, Indiana University.

Rein, T.R., 2019. A geometric morphometric examination of hominoid third metacarpal shape and its implications for inferring the precursor to terrestrial bipedalism. Anat. Rec. 302, 983–998.

Rein, T.R., Harvati, K., 2013. Exploring third metacarpal capitate facet shape in early hominins. Anat. Rec. 296, 240–249.

Remis, M.J., 1994. Feeding ecology and positional behavior of western lowland gorillas (*Gorilla gorilla gorilla*) in the Central African Republic. Ph.D. Dissertation, Yale University.

Richmond, B.G., 2006. Functional morphology of the midcarpal joint in knuckle-walkers and terrestrial quadrupeds. In: Ishida, H., Tuttle, R., Pickford, M., Ogihara, N., Nakatsukasa, M. (Eds.), Human Origins and Environmental Backgrounds, Developments in Primatology: Progress and Prospects. Springer US, Boston, pp. 105–122.

Richmond, B.G., 2007. Biomechanics of phalangeal curvature. J. Hum. Evol. 53, 678–690.

Richmond, B.G., Begun, D.R., Strait, D.S., 2001. Origin of human bipedalism: The knuckle-walking hypothesis revisited. Am. J. Phys. Anthropol. 116, 70–105.

Richmond, B.G., Green, D.J., Lague, M.R., Chirchir, H., Behrensmeyer, A.K., Bobe, R., Bamford, M.K., Griffin, N.L., Gunz, P., Mbua, E., Merritt, S.R., Pobiner, B., Kiura, P., Kibunjia, M., Harris, J.W.K., Braun, D.R., 2020. The upper limb of *Paranthropus boisei* from Ileret, Kenya. J. Hum. Evol. 141, 102727.

Richmond, B.G., Strait, D.S., 2000. Evidence that humans evolved from a knuckle-walking ancestor. Nature 404, 382–385.

Rohde, R.S., Crisco, J.J., Wolfe, S.W., 2010. The advantage of throwing the first stone: How understanding the evolutionary demands of *Homo sapiens* is helping us understand carpal motion. J. Am. Acad. Orthop. Surg. 18, 51–58.

Rohlf, F.J., 1990. Morphometrics. Annu. Rev. Ecol. Evol. Syst. 21, 299–316.

Rohlf, F.J., Marcus, L.F., 1993. A revolution morphometrics. Trends Ecol. Evol. 8, 129–132.

Rolian, C., Lieberman, D.E., Zermeno, J.P., 2011. Hand biomechanics during simulated stone tool use. J. Hum. Evol. 61, 26–41.

Ruby, L.K., Conney, W.P., An, K.N., Linscheid, R.L., Chao, E.Y.S., 1988. Relative motion of selected carpal bones: A kinematic analysis of the normal wrist. J. Hand Surg. 13, 1–10.

Samuel, D.S., Nauwelaerts, S., Stevens, J.M.G., Kivell, T.L., 2018. Hand pressures during arboreal locomotion in captive bonobos (*Pan paniscus*). J. Exp. Biol. 221, jeb170910.

Sarmiento, E., 1985. Functional differences in the skeleton of wild and captive orang-utans and their adaptive significance. Ph.D. Dissertation, New York University.
Sarmiento, E.E., 1988. Anatomy of the hominoid wrist joint: Its evolutionary and functional implications. Int. J. Primatol. 9, 281–345.
Sarrafian, S.K., Melamed, J.L., Goshgarian, G.M., 1977. Study of wrist motion in flexion and extension. Clin. Orthop. Relat. Res. 126, 153–159.
Sarringhaus, L.A., MacLatchy, L.M., Mitani, J.C., 2014. Locomotor and postural development of wild chimpanzees. J. Hum. Evol. 66, 29–38.
Scally, A., Dutheil, J.Y., Hillier, L.W., Jordan, G.E., Goodhead, I., Herrero, J., Hobolth, A., Lappalainen, T., Mailund, T., Marques-Bonet, T., McCarthy, S., Montgomery, S.H., Schwalie, P.C., Tang, Y.A., Ward, M.C., Xue, Y., Yngvadottir, B., Alkan, C., Andersen, L.N., Ayub, Q., Ball, E.V., Beal, K., Bradley, B.J., Chen, Y., Clee, C.M., Fitzgerald, S., Graves, T.A., Gu, Y., Heath, P., Heger, A., Karakoc, E., Kolb-Kokocinski, A., Laird, G.K., Lunter, G., Meader, S., Mort, M., Mullikin, J.C., Munch, K., O'Connor, T.D., Phillips, A.D., Prado-Martinez, J., Rogers, A.S., Sajjadian, S., Schmidt, D., Shaw, K., Simpson, J.T., Stenson, P.D., Turner, D.J., Vigilant, L., Vilella, A.J., Whitener, W., Zhu, B., Cooper, D.N., de Jong, P., Dermitzakis, E.T., Eichler, E.E., Flicek, P., Goldman, N., Mundy, N.I., Ning, Z., Odom, D.T., Ponting, C.P., Quail, M.A., Ryder, O.A., Searle, S.M., Warren, W.C., Wilson, R.K., Schierup, M.H., Rogers, J., Tyler-Smith, C., Durbin, R., 2012. Insights into hominid evolution from the gorilla genome sequence. Nature 483, 169–175.
Schaller, G.B., 1963. The Mountain Gorilla, Ecology and Behavior. The University of Chicago Press, Chicago.
Schick, K.D., Toth, N., Garufi, G., Savage-Rumbaugh, E.S., Rumbaugh, D., Sevcik, R., 1999. Continuing investigations into the stone tool-making and tool-using capabilities of a bonobo (*Pan paniscus*). J. Archaeol. Sci. 26, 821–832.
Schlager, S., 2017. Chapter 9 - Morpho and Rvcg – shape analysis in R: R-Packages for geometric morphometrics, shape analysis and surface manipulations. In: Zheng, G., Li, S., Székely, G. (Eds.), Statistical Shape and Deformation Analysis. Academic Press, Cambridge, pp. 217–256.
Schuind, F., Cooney, W.P., Linscheid, R.L., An, K.N., Chao, E.Y.S., 1995. Force and pressure transmission through the normal wrist. A theoretical two-dimensional study in the posteroanterior plane. J. Biomech. 28, 587–601.
Schultz, A.H., 1934. Some distinguishing characters of the mountain gorilla. J. Mammal. 15, 51–61.
Shea, B.T., 1981. Relative growth of the limbs and trunk in the African apes. Am. J. Phys. Anthropol. 56, 179–201.
Slice, D.E., 2005. Modern Morphometrics. In: Slice, D.E. (Ed.), Modern Morphometrics in Physical Anthropology. Springer US, Boston, pp. 1–45.
Smith, R.J., Jungers, W.L., 1997. Body mass in comparative primatology. J. Hum. Evol. 32,

523–559.
Stratovan Corporation, 2024. Stratovan Checkpoint (software), version 2024.08.01:44. https://www.stratovan.com/products/checkpoint.
Susman, R.L., Creel, N., 1979. Functional and morphological affinities of the subadult hand (O.H. 7) from Olduvai Gorge. Am. J. Phys. Anthropol. 51, 311–331.
Susman, R.L., 1984. The locomotor behavior of *Pan paniscus* in the Lomako Forest. In: Susman, R.L. (Ed.), The Pygmy Chimpanzee: Evolutionary Biology and Behavior, The Pygmy Chimpanzee. Springer US, Boston, pp. 369–393.
Susman, R.L., 1991. Who made the Oldowan tools? Fossil evidence for tool behavior in Plio-Pleistocene hominids. J. Anthropol. Res. 47, 129–151.
Susman, R.L., Badrian, N.L., Badrian, A.J., 1980. Locomotor behavior of *Pan paniscus* in Zaire. Am. J. Phys. Anthropol. 53, 69–80.
Thompson, N.E., 2020. The biomechanics of knuckle-walking: 3-D kinematics of the chimpanzee and macaque wrist, hand and fingers. J. Exp. Biol. 223, jeb224360.
Thorpe, S.K.S., Crompton, R.H., 2006. Orangutan positional behavior and the nature of arboreal locomotion in Hominoidea. Am. J. Phys. Anthropol. 131, 384–401.
Tocheri, M.W., 2007. Three-dimensional riddles of the radial wrist: Derived carpal and carpometacarpal joint morphology in the genus *Homo* and the implications for understanding the evolution of stone tool-related behaviors in hominins. Ph.D. Dissertation, Arizona State University.
Tocheri, M.W., Marzke, M.W., Liu, D., Bae, M., Jones, G.P., Williams, R.C., Razdan, A., 2003. Functional capabilities of modern and fossil hominid hands: Three-dimensional analysis of trapezia. Am. J. Phys. Anthropol. 122, 101–112.
Tocheri, M.W., Orr, C.M., Jacofsky, M.C., Marzke, M.W., 2008. The evolutionary history of the hominin hand since the last common ancestor of *Pan* and *Homo*. J. Anat. 212, 544–562.
Tocheri, M.W., Orr, C.M., Larson, S.G., Sutikna, T., Jatmiko, Wahyu Saptomo, E., Rokus Awe Due, Djubiantono, T., Morwood, M.J., Jungers, W.L., 2007. The primitive wrist of *Homo floresiensis* and its implications for hominin evolution. Science 317, 1743–1745.
Tocheri, M.W., Razdan, A., Williams, R.C., Marzke, M.W., 2005. A 3D quantitative comparison of trapezium and trapezoid relative articular and nonarticular surface areas in modern humans and great apes. J. Hum. Evol. 49, 570–586.
Toth, N., Schick, K., 2009. The Oldowan: The tool making of early hominins and chimpanzees compared. Annu. Rev. Anthropol. 38, 289–305.
Toth, N., Schick, K.D., Savage-Rumbaugh, E.S., Sevcik, R.A., Rumbaugh, D.M., 1993. *Pan* the tool-maker: Investigations into the stone tool-making and tool-using capabilities of a bonobo (*Pan paniscus*). J. Archaeol. Sci. 20, 81–91.
Tsegai, Z.J., Kivell, T.L., Gross, T., Nguyen, N.H., Pahr, D.H., Smaers, J.B., Skinner, M.M., 2013. Trabecular bone structure correlates with hand posture and use in hominoids. PLOS ONE 8, e78781.
Tutin, C.E.G., Fernandez, M., 1993. Composition of the diet of chimpanzees and comparisons

with that of sympatric lowland gorillas in the Lopé Reserve, Gabon. Am. J. Primatol. 30, 195–211.
Tuttle, R.H., 1967. Knuckle-walking and the evolution of hominoid hands. Am. J. Phys. Anthropol. 26, 171–206.
Tuttle, R.H., 1969. Quantitative and functional studies on the hands of the Anthropoidea. I. The Hominoidea. J. Morphol. 128, 309–363.
Vanhoof, M.J.M., Galletta, L., De Groote, I., Vereecke, E.E., 2021. Functional signals and covariation in triquetrum and hamate shape of extant primates using 3D geometric morphometrics. J. Morphol. 282, 1382–1401.
Vanhoof, M.J.M., Galletta, L., Matthews, H., De Groote, I., Vereecke, E.E., 2024. Ulnar shape of extant primates: Functional signals and covariation with triquetrum shape. Am. J. Biol. Anthropol. 183, e24755.
Ward, C.V., Leakey, M.G., Brown, B., Brown, F., Harris, J., Walker, A., 1999. South Turkwel: A new Pliocene hominid site in Kenya. J. Hum. Evol. 36, 69–95.
Ward, C.V., Tocheri, M.W., Plavcan, J.M., Brown, F.H., Manthi, F.K., 2014. Early Pleistocene third metacarpal from Kenya and the evolution of modern human-like hand morphology. Proc. Natl. Acad. Sci. 111, 121–124.
Watts, D.P., 1984. Composition and variability of mountain gorilla diets in the Central Virungas. Am. J. Primatol. 7, 323–356.
Wickham, H., 2016. ggplot2: Elegant Graphics for Data Analysis. Springer New York, NY.
Williams, E.M., Gordon, A.D., Richmond, B.G., 2012. Hand pressure distribution during Oldowan stone tool production. J. Hum. Evol. 62, 520–532.
Williams, E.M., Gordon, A.D., Richmond, B.G., 2014. Biomechanical strategies for accuracy and force generation during stone tool production. J. Hum. Evol. 72, 52–63.
Williams-Hatala, E.M., Hatala, K.G., Key, A., Dunmore, C.J., Kasper, M., Gordon, M., Kivell, T.L., 2021. Kinetics of stone tool production among novice and expert tool makers. Am. J. Phys. Anthropol. 174, 714–727.
Williams-Hatala, E.M., Hatala, K.G., Gordon, M., Key, A., Kasper, M., Kivell, T.L., 2018. The manual pressures of stone tool behaviors and their implications for the evolution of the human hand. J. Hum. Evol. 119, 14–26.
Wolfe, S.W., Crisco, J.J., Orr, C.M., Marzke, M.W., 2006. The dart-throwing motion of the wrist: Is it unique to humans? J. Hand Surg. 31, 1429–1437.
Wunderlich, R.E., Jungers, W. l., 2009. Manual digital pressures during knuckle-walking in chimpanzees (*Pan troglodytes*). Am. J. Phys. Anthropol. 139, 394–403.
Wuthrich, C., MacLatchy, L.M., Nengo, I.O., 2019. Wrist morphology reveals substantial locomotor diversity among early catarrhines: An analysis of capitates from the early Miocene of Tinderet (Kenya). Sci. Rep. 9, 3728.
Yalden, D.W., 1972. The form and function of the carpal bones in some arboreally adapted mammals. Acta Anat. 82, 383–406.
Yoder, A.D., Yang, Z., 2000. Estimation of primate speciation dates using local molecular clocks.

Mol. Biol. Evol. 17, 1081–1090.
Young, R.W., 2003. Evolution of the human hand: the role of throwing and clubbing. J. Anat. 202, 165–174.
Zeininger, A., Richmond, B.G., Hartman, G., 2011. Metacarpal head biomechanics: A comparative backscattered electron image analysis of trabecular bone mineral density in *Pan troglodytes*, *Pongo pygmaeus*, and *Homo sapiens*. J. Hum. Evol. 60, 703–710.
Zelditch, M.L., Swiderski, D.L., Sheets, H.D., Fink, W.L., 2004. Geometric Morphometrics for Biologists: A Primer. Academic Press, Cambridge.
Zihlman, A.L., Cramer, D.L., 2008. Skeletal differences between pygmy (*Pan paniscus*) and common chimpanzees (*Pan troglodytes*). Folia Primatol. 29, 86–94.
Zwell, M., Conroy, G.C., 1973. Multivariate analysis of the *Dryopithecus africanus* forelimb. Nature 244, 373–375.